MICROVASCULAR ENDOTHELIAL RESPONSE TO COCAETHYLENE EXPOSURE: MORPHOLOGICAL AND MOLECULAR OBSERVATIONS

by

Danyel Hermes Tacker, B.S.

Dissertation
Presented to the Faculty of the University of Texas Graduate School of
Biomedical Sciences at Galveston
in Partial Fulfillment of the Requirements
for the Degree of

Doctor of Philosophy

Approved by the Supervisory Committee

Anthony O. Okorodudu, Ph.D.
Robert Glew, Ph.D.
Kathryn Cunningham, Ph.D.
G. A. Shakeel Ansari, Ph.D.
M. Tarek Elghetany, M.D.
Hal Hawkins, M.D., Ph.D.
Norbert Herzog, Ph.D.

December 2004
Galveston, Texas

Key Words: Cocaethylene, Endothelium, Toxicity, Barrier Function, Calcium, Second Messengers, Signaling, p38 Mitogen-Activated Protein Kinase, Nuclear Factor-kappaB

To My Husband and Family For Their Endless Support

ACKNOWLEDGMENTS

I must begin my acknowledgments with my mentor, Dr. Anthony O. Okorodudu. Without his flexibility and open-mindedness, his challenges, and his willingness to foster and cultivate my independence, this work would not have been possible. He has lent his knowledge, insight, and moral character to every facet of this work.

Next, I would like to thank the members of my committee for their advice, input, criticism, availability, and support. Dr. Shakeel Ansari was a great co-mentor, always providing an open door and an encyclopedic knowledge of toxicological mechanisms and chemistry in general. Drs. Kathryn Cunningham, Robert Glew, and Hal Hawkins brought not only their expertise, but also genuine enthusiasm to this project. Dr. M. Tarek Elghetany brought his extensive clinical knowledge to the project as well.

Dr. Norbert Herzog was literally there from Day One, making me feel welcome. Over the years, he provided laboratory space, molecular techniques training, guidance, and advice, each of which was invaluable and refreshingly "Herzog".

There are a number of contributors that I must also mention here. Linda Muehlberger aided in the optimization of the silver stain method. Dr. Vsevolod Popov lent his astonishing skill with electron microscopy to Aim #2, generating all of the electron micrographs herein. John Dornak aided with maintenance of the mass spectrometer, as well as troubleshooting and technical assistance with drug identification and quantitation. Dr. Juan Olano provided the ECIS system for the resistance studies and was an indispensable reference regarding microvascular endothelial cells. His post-doctoral trainee, Dr. Paul Koo, aided with the resistance experiment in the biosafety level 3 laboratory. Dr. Gustavo Valbuena was another great source of information all-around, especially regarding the cell model. Barry Elsom and Dr. Sue Fennewald were vital to the optimization of molecular techniques, and were always welcoming and supportive.

Tom Bednarek aided in image captures, last minute banner printing, and technical assistance at seminars and the like; he makes us look like professionals at every turn. Harriet Ross is deserving of thanks because of her organization, persistence, and love for the students in Pathology. Mitch Calvin made sure our orders were placed and received, and was always a great person to visit when I just needed a break (and we all do).

My friends and colleagues in the department provided advice and understanding. Erin Scott, Bi Hung Peng, Lata Kaphalia, Barry Elsom, Sue Fennewald, Roger Vertrees, Gustavo Valbuena, Bryan Shipp, Kate McElroy, Tammy Dugas, Vicente Santa Cruz, Mitch Calvin, and Kelly Mericle – thank you all so much. You contributed more than you know.

Thanks to Dr. Mary Moslen for her love of toxicology and her instruction and guidance in grant writing. Another member of the Pathology Department that deserves many thanks on my part is Dr. Roger Vertrees. Roger took me in, showed me the basics of cell culture, and in so doing, was responsible for my basic abilities to begin this work. I would like to thank Dr. David H. Walker and the Department of Pathology for the training opportunity, the NIH for providing funding for my training (F31 DA15580), the Society of Toxicology for the 2003 Travel Award, the American Society for Investigative Pathology for the 2003 Young Pathologist Award, and the Society of Forensic

Toxicologists for the 2004 Educational Research Award. Most special thanks to Buddy and Bonnie Groff, who awarded me with the scholarship that made starting college possible.

My last thanks are my most personal. To my husband Matthew Tacker, thank you for everything. Putting up with the repercussions of late or failed experiments, and smiling despite it all, kept me here for the duration. I love and adore you. To my parents Russell and Sharlene Hermes, thank you for your unending support, moral guidance, and work ethics. Thank you for telling me that nothing was beyond my ability, and thank you even more for not just telling me that, but making me *believe* it. To Jessie Hermes, my brother, you inspire me. Your talent and outlook on life have taught me worlds.

To my extended family - Lloyd and Mary Ann Hermes, Harvey and Ella Tondre, my aunts Jan Reyes and Denene Whitmore, Bill and Donna Tacker, John and Shelley Sheridan, Steve, Jetta, Kylie, and Cole Tacker, Judge and Hallie Thrasher, Don and Eva Easterwood, Gary, Colleen, and Emma Whitehead, Chris, Rachel, and Easley Smith, and Arin Whitehead – your support and love have been invaluable. To all my other friends and extended family - you know who you are and how you have helped, and I will never forget it. You will always be with me.

MICROVASCULAR ENDOTHELIAL RESPONSE TO COCAETHYLENE EXPOSURE: MORPHOLOGICAL AND MOLECULAR OBSERVATIONS

Publication No. _____
Danyel Hermes Tacker, Ph.D.

The University of Texas Medical Branch at Galveston, December 2004

Supervisor: Anthony O. Okorodudu, Ph.D.

Cocaethylene (CE) is an active metabolite of cocaine and ethanol and is a toxicant of physiological relevance due to the high rate of cocaine and ethanol co-exposure (≥80%) in cocaine abusers. It has prolonged action and increased potency on known physiological targets relative to the effect of cocaine. Since pathology in cocaine abusers is typically chronic and systemic, and CE persists in the body three to five times longer than cocaine, a link between CE and systemic disease in cocaine abusers was proposed. Consequently, this dissertation contains the studies that were used to test the hypothesis that the microvascular endothelium is a target tissue that is central in the pathogenic mechanism of cocaine-associated systemic disease, and that endothelial injury after CE exposure would result in dysregulation and altered barrier function due to changes in intracellular second messengers and signaling. To test this hypothesis, an *in vitro* model of CE exposure in human dermal microvascular endothelial cells (HMEC-1) was developed. Four Aims were designed to compartmentalize various components of the endothelial response to CE. The Aims included an array of methods to address cellular toxicity and dysfunction, including classical cytotoxicity and viability assays (Aim One), microscopic and electrical analyses of monolayer integrity (Aim Two), molecular analysis of second messengers, signaling molecule phosphorylation, and transcription factor DNA binding activity (Aims Three and Four). Aim One experiments demonstrated a lack of overt endothelial cytotoxicity caused by CE. Aim Two morphological analysis of endothelial intercellular borders and barrier integrity showed that CE exposure in the endothelial monolayers resulted in increased permeability, and hence a decrease in barrier integrity. These changes were observed temporally with alterations in cytosolic and total cellular free calcium ion (Aim Three), inositol 1,4,5 trisphosphate, and phosphorylated p38 mitogen-activated protein kinase concentrations, as well as changes in DNA binding activity and dimer composition of nuclear factor-kappaB (Aim Four). The observed changes suggest a distinct alteration of endothelial cell and monolayer function consistent with increased vascular permeability *in vivo*. Potential pathological outcomes of such effects include inflammation, vasculitis, systemic disease, and organ failure.

TABLE OF CONTENTS

Page

LIST OF TABLES

Page

LIST OF FIGURES

Page

LIST OF ILLUSTRATIONS

Page

LIST OF ABBREVIATIONS

ABBREVIATION	DEFINITION
AP-1	Activator protein-1, a transcription factor
B, B_o	Percent of enzyme bound, and control zero-bound concentration
C	Concentration
Ca^{2+}	Free ionized calcium
CDC	Centers for Disease Control, Atlanta, GA
CE	Cocaethylene
Cl	Chloride
cpm/mm^2	Cycles per minute (of radioactivity) per square millimeter of area
DAG	Diacylglycerol
DAWN	Drug Abuse Warning Network
DEA	Drug Enforcement Agency
DTT	Dithiothreitol
ECIS	Electronic cell-substrate impedance sensing
EDTA	Ethylene diamine tetraacetic acid
EGTA	Ethylene glycol-bis(beta-aminoethyl-ether)-N,N,N',N'-tetraacetate
ELISA	Enzyme-linked immunosorbant assay
EM, TEM	Electron microscopy, transmission electron microscopy
EMSA	Electrophoretic mobility shift assay
F, F_{min}, F_{max}	Data point along a kinetic readout, minimal data point, maximal data point
FBS	Fetal bovine serum
g/L, mg/L, μg/L, U/L	Expressions of concentration in terms of mass per volume, and enzyme activity per volume
HEPES	Hydroxyethylpiperazine ethanesulfonate
HMEC-1	Human microvascular endothelial cell line 1
IP_3	Inositol-1,4,5-trisphosphate
IQ	Intelligence quotient
IV	Intravenous
k	Constant (in our case, dissociation constant of a specific ion and indicator)
λ, λ1, λ2	Lambda, lambda 1, and lambda 2, representing excitation wavelengths of fluorescent indicators
L, mL, μL	Liters, milliliters, and microliters (units of volume)
LDH	Lactate dehydrogenase
LPS	Lipopolysaccharide
m, cm, mm, μm, nm	Meters, centimeters, millimeters, micrometers, nanometers (units of measurement)

ABBREVIATION	DEFINITION
M, mM, μM, nM	Molar, millimolar, micromolar, and nanomolar (units of concentration)
MΩ	Mega-ohms
MAPK	Mitogen-activated protein kinase
MCDB131	Media formulation used in our studies
MLC	Myosin light chain
MLCK	Myosin light chain kinase
MTT	3-[4,5-dimethylthiazol-2-yl]-2,5-diphenyl tetrazolium bromide
NAD^+/NADH	Nicotinamide adenine dinucleotide, oxidized and reduced
NF-κB	Nuclear factor-κB
NIDA	National Institute on Drug Abuse
NSB	Non-specific binding
PBS	Phosphate-buffered saline
pCO_2, pO_2	Partial pressure of carbon dioxide, oxygen
PKC	Protein kinase C
PLC	Phospholipase C
PMSF	Phenylmethylsulfonyl fluoride
R, R_{min}, R_{max}	Ratio, minimal ratio, maximal ratio
SR	Sarcoplasmic reticulum
T25, T75, T150	Cell culture flask sizes, with 25, 75, and 150 square centimeters of culture area
TMB	Tetramethylbenzidine

GLOSSARY

Acute exposure – "Acute" is used in this series of studies to designate the one-hour pre-treatment experiments of Aim Three, in which cytosolic free calcium and magnesium were monitored.

Calcium "sink" – An organelle in which calcium is stored within a cell. In the case of endothelium, the primary calcium sinks are the endoplasmic reticulum and the mitochondria, and a minor calcium sink is the nucleus.

Cation flux – The movement of a cation within a compartment. In this case, the movement of calcium and magnesium within the cytosol, or between the cytosol and organelles, of endothelial cells.

Cytotoxicity/toxicity – A negative effect elicited by an endogenous or exogenous agent. In this series of studies, cytotoxicity and lethality are distinctly different outcomes, although other studies use the two terms synonymously. For example, cytotoxicity can manifest as cell membrane leakage (release of enzymes such as LDH), decreased metabolic capacity, or a number of other cellular disturbances that are not necessary lethal. However, lethality may result from overt cytotoxicity, and both are monitored in this study to determine the degree of CE effect on the microvascular endothelial cell model.

Drug "mention" – A term used by the Drug Abuse Warning Network to designate the number of times a particular drug is listed in admitting paperwork for patients in the Emergency Rooms/Departments that participate in the network. The DAWN network uses drug "mentions" to calculate annual statistics that relate to frequencies of drug abuse and drug-related hospital admissions and deaths in the United States.

ECIS – Electronic cell-substrate impedance sensing, a method used to measure trans-endothelial resistance. Since resistance is inversely proportional to monolayer permeability, increases in resistance demonstrate decreases in permeability, and vice versa.

EMSA – Electrophoretic mobility shift assay, a method used to monitor DNA binding activities of proteins, which could include inhibitors, transcription factors, and nuclear-bound complexes.

Endothelium – The cell layer lining the lumen of large- and medium-sized blood vessels, and fully composing the wall of the capillary. The endothelial cell layer is one cell layer thick in healthy blood vessels, and its tight intercellular junctions regulate the passage of various nutrients and cells through the blood vessel wall into surrounding tissues.

Gene activation – Activation of the transcription of genes as a result of cell stimulus, injury, or regular function. For gene activation to be successful, inhibitors that block gene promoter sites must be removed, and proper binding of activated transcription factors must occur.

Growth kinetics – The rates of cell division observed in a culture or other cell population. Monitoring cell numbers over time, and determining the time required for the cells in culture to divide, allows for calculation of growth rate.

Homeostasis – The "natural" state of a tissue or system. Alterations in homeostasis can have pathological outcomes, depending on the site and severity of the alteration.

Immediate exposure – "Immediate" is used in this series of studies to designate the 5-minute kinetic assay of cytosolic free calcium and magnesium after injection of CE.

Infarction – The death of an area of tissue after sustained ischemia that results in failure of that tissue to function. Depending on the site of the infarction (e.g., heart versus integument/skin), such damage can be life threatening, or localized and pathological.

Ischemia – A lack of blood flow that results in cellular damage and death if prolonged. Sustained ischemia is lethal to cells, and can cause infarction of the tissue.

Kinase – An enzyme that functions to phosphorylate its target(s).

LD50 – The dose of a compound or toxicant that is lethal to 50% of the population being studied. In recent years, the LD50 has been progressively replaced by the ED50 (effective-dose-50), which is the dose of a compound or toxicant that elicits a measurable effect in 50% of the population studied.

Macrovascular – Relating to large blood vessels, such as the aorta, vena cava, and pulmonary arteries and veins.

Microvascular – Relating to small blood vessels, such as arterioles, capillaries, and venules.

Mucosa/mucosae – Epithelial cell layers that produce mucus, as in the mouth, nose/sinuses, eyes, and respiratory, gastrointestinal, and excretory tracts.

Necrosis – The death of a cell or tissue. Necrosis was originally viewed as a sudden, disorganized death, but in recent years the process has been re-evaluated and may be considered to have organized and disorganized components that contribute to cell death.

NF-κB family of proteins – The Nuclear Factor-κB (NF-κB) family of proteins function as transcription factors that are centrally involved in cellular stress responses, as well as

the promotion of inflammation in the event of cellular injury. Release of an NF-κB dimer from its inhibitory protein, IκB, results in nuclear localization of the dimer and binding to target gene promoter regions. Common targets of NF-κB include NF-κB family protein, IκB, cytokine, cellular adhesion molecule, and fos/jun gene promoter regions, which facilitate auto-regulation, inflammation, and cell stress/survival responses.

Panarteritis – Panarteritis is widespread vascular inflammation, particularly involving small blood vessels. Panarteritis typically presents as a systemic disease, and is diagnosed by biopsy. The cause was originally thought to be autoimmune, but panarteritis has been presented in human cases showing no indications of autoimmunity (e.g., drug abusers with no auto-immune antibody titers).

Permeability/barrier integrity – The ability of a monolayer to regulate the passage of molecules and cells through its intercellular junctions. Increases in endothelial permeability, or conversely, decreases in barrier integrity, result in tissue edema and escape of blood-borne cells into surrounding tissues.

Persistence – The ability of a compound, in our case cocaethylene or media nutrients, to stay in cell culture media.

Phosphatase – An enzyme that functions to de-phosphorylate its target(s).

pKa – The point at which the major acid and base ion concentrations of a buffer are equal.

Resistance – The ability of a monolayer to resist the conductance of electricity from one surface to the other. Thus, increased resistance denotes intact barrier integrity, and decreased resistance denotes a loss of barrier integrity.

Rhabdomyolysis – A wasting disease of muscle tissue. Rhabdomyolysis can be caused by ischemia, and is associated with kidney failure, since fragments of damaged/dead myocytes become blood-borne and trapped in the glomerulus, which is the filtration unit of the kidney.

Second messengers – Typically, molecules that elicit intracellular responses that are not proteins are called second messengers. Examples include free ionized calcium (Ca^{2+}), inositol 1,4,5 trisphosphate (IP_3), and diacylglycerol (DAG).

Systemic disease – Pathology manifesting in multiple organ systems, but with a common origin, indicates systemic disease. A good example of systemic disease is the multi-organ manifestation of lupus erythmatosis, an autoimmune disease. We propose that cocaine abuse leads to systemic disease because of an effect on the vascular endothelium, which exists in all human tissues.

Thrombosis – Thrombosis is the process of platelet clotting. Normal thrombosis occurs after dermal abrasion, or other rupture of blood vessels, and serves to prevent excessive bleeding and facilitate healing. Abnormal thrombosis, however, can block blood vessels, causing ischemia and necrosis in tissues surrounding the blockage. Spontaneous intravascular thrombosis has been observed in some cocaine-related case histories with pathological outcomes.

Trans-esterification – An enzyme-mediated reaction in which a molecule containing a hydroxyl group (such as water or an alcohol) is attached to an available carbon. Cocaethylene production results in the liver when ethanol is trans-esterified to the 2-carboxy group of cocaine.

Vasculitis – The inflammation of blood vessels. Autoimmune antibodies, or chemical, biological, or endogenous agents can cause vasculitis. In this dissertation, I propose that the interaction of cocaethylene and vascular endothelium could result in vasculitis and tissue ischemia.

Xenobiotic – Any chemical from outside a system or body. Xenobiotic is a blanket term that encompasses all chemicals, independent of their exposure (intended or accidental, occupational) or benefit/harm to the host/organism.

INTRODUCTION: FACTS & FIGURES: WHY COCAINE & ETHANOL CO-ABUSE IS A PROBLEM

Pharmacological use of cocaine originated in ancient South America, where the coca plant is indigenous. The original method of self-administration was the chewing of coca leaves, which stimulated workers and gave them greater longevity in their work efforts [1]. During the Spanish conquest of Central and South America in the 16th century, cocaine was introduced to Europe and was used by the Spanish government to increase the country's revenues through trade [1].

Shortly after the Dutch began European coca cultivation in 1817, evaluation of the medicinal uses of cocaine was initiated. The anesthetic properties of cocaine led to medical use of cocaine-containing eye drops and local-acting tonics that eased the pain of surgery and infection, and Freud recommended the use of cocaine in the treatment of morphine addiction [1]. In the 1800s, European cocaine production began at the Merck Company in Darmstadt, Germany [1]. This production was central to the emergence of elixirs, tonics, and medicines containing cocaine that were available to consumers. However, in 1914, cocaine was declared an illicit drug in the United States by the Harrison Act and removal of cocaine from these "medicines" began [1]. Despite the law-making efforts of the United States government since that time, cocaine has been continuously used illegally in the United States.

Beginning in the early 1900s, the "side effects" of cocaine became of particular interest to medical professionals. Despite reports of cocaine-associated disease and the status of cocaine as an illicit drug, cocaine abuse became part of the popular culture in the 1960s, and has reached epidemic proportions in the United States. Cocaine is a stimulant of choice in all economic and racial strata [1], and as a result, its effects on the human body, as well as numerous animal and cell models, have been carefully documented in case histories and research studies. Due to its lethality, cocaine is the subject of ongoing and extensive clinical and mechanistic research.

The 2002 National Survey on Drug Use and Health (NSDUH) reported that there were 19.5 million illicit drug users (8.3% of the general population) in the United States that year. Cocaine users accounted for approximately 10% (2 million users) of this population [2]. From the years 1965 to 1967, cocaine use in youths (aged 12 to 17) was extremely low at 0.1% of the population in that age group. In the 1970s, this figure began to rise, and rose to 2.2% by the mid 1980s. After a decline in the early 1990s, this figure began to increase again, peaking at 2.7% in 2002 [2].

Young adults (aged 18 to 25) have historically had the highest rates of cocaine use. In the 1960s, the percentage of young adults that had used cocaine was 1%. However, this figure has increased markedly over the past 30 years, resulting in a cocaine use rate of 15.4% for the 18- to 25-year age group in 2002. This age group shows the greatest "initiation rate" (first-time users), with 70% of new cocaine users being aged 18 or older [2].

According to NSDUH, cocaine is the second-most-abused illicit drug, with 25.2% of cocaine users reporting dependence or abuse. This follows heroin (dependence rate 53%, 2002), and ranks above marijuana (dependence rate 16.7%, 2002) [2]. In the year 2002, nearly 200,000 (199,198) cocaine-associated hospitalizations were reported by the 21 metropolitan hospitals participating in the Drug Abuse Warning Network, DAWN [3]. This figure is up 39% from the 1994 numbers of emergency room "mentions" of cocaine use upon admission, and comprises approximately 30% of the total number of emergency department "mentions" of all major substances of abuse (including alcohol) [3].

When projected to account for the entire population of the United States (currently approximately 250 million people [4]), the figures become alarming, with an estimated 1:12 Americans abusing cocaine, and 1% or more of emergency room admissions linked to cocaine abuse [3]. Thus, cocaine abuse is a major problem that costs society, the medical community, and law enforcement agencies millions of dollars every year. Seventy-five tons of cocaine were seized by the Drug Enforcement Agency in 2002 [5], of which 8.6% (over 6 tons) was seized in the State of Texas [6].

It has been reported that prenatal cocaine exposure, occurring from maternal cocaine use and subsequent trans-placental transfer, costs the United States at least $325 million per year in expenses related to special education required for these children, who commonly have speech and IQ deficits [7, 8]. Though cocaine abuse itself is life threatening and the subject of much controversy regarding strategies to regulate its use and treat addiction, the problem is further complicated by the high frequency of co-abuse with alcohol. Over 80% of cocaine abusers in drug rehabilitation programs admit to co-abuse of cocaine and ethanol [9]. This co-abuse presents an interesting clinical problem because the population of cocaine and ethanol co-abusers has been associated with an 18-23% increased risk for sudden death when compared to emergency room admissions with only cocaine abuse listed [10, 11]. In studies of university hospital emergency room admissions related to cocaine, over 80% of blood samples revealed that cocaine and ethanol had been used in combination prior to admission [9, 12, 13]. Also, DAWN has reported that cocaine and ethanol co-abuse is the most common drug combination resulting in emergency room admissions [3].

Ethanol is commonly abused concomitantly with cocaine because it reportedly enhances the euphoria and other positive aspects of cocaine abuse, while decreasing paranoia and withdrawal symptoms [9, 14]. Patients report that ethanol consumption with cocaine abuse prolongs the time of intoxication [9, 15]. Additionally, cocaine lessens ethanol's effects on locomotor coordination and the feeling of drunkenness [15, 16]. These effects appear to be factors that reinforce co-abusive behavior in the majority of patients.

Elucidation of the causes of cocaine and other drug addiction has been held to be the key to amelioration of the problem. As a result, a significant amount of research funding is designated for the study of cocaine abuse, focused on addressing the determination of psychological and organic causes of addiction behavior, as well as the mechanistic study of acute, lethal effects of drugs-of-abuse. Since ameliorating the pathology associated with cocaine abuse would reduce resource demands in the hospital

setting, and improve the outcomes of addiction treatment programs, as well as emergency room admissions linked to drug abuse, this area of cocaine research is ever expanding.

Research focusing on the cocaine-ethanol conjugate cocaethylene (CE), as well as the mechanistic research of cocaine-associated systemic pathology, is lacking, and thus demonstrates an important gap in the cocaine-associated knowledge base. Due to the extent of cocaine and ethanol co-abuse, and the projected costs of care for systemic disease in the cocaine abusing population, these two areas of research were combined in the studies reported in this dissertation.

CHAPTER 1: BACKGROUND & SIGNIFICANCE

1.1 COCAETHYLENE (CE): A METABOLIC CONSEQUENCE OF COCAINE & ETHANOL CO-EXPOSURE

Recently, researchers have speculated that the problem with cocaine and ethanol regarding pathologic outcomes may involve more than the presence of the two drugs [14, 17-19]. When a human consumes ethanol and cocaine concomitantly, a metabolite called cocaethylene (CE) is formed [20-24]. The reaction is one of trans-esterification, catalyzed by human liver carboxylesterase-1 (hCE-1). The hCE-1 enzyme typically catalyzes the breakdown of cocaine into benzoylecgonine, a pharmacologically inactive metabolite that is quickly eliminated in the urine due to its increased hydrophilicity relative to cocaine [25, 26]. However, when ethanol is present, hCE-1 also facilitates the trans-esterification

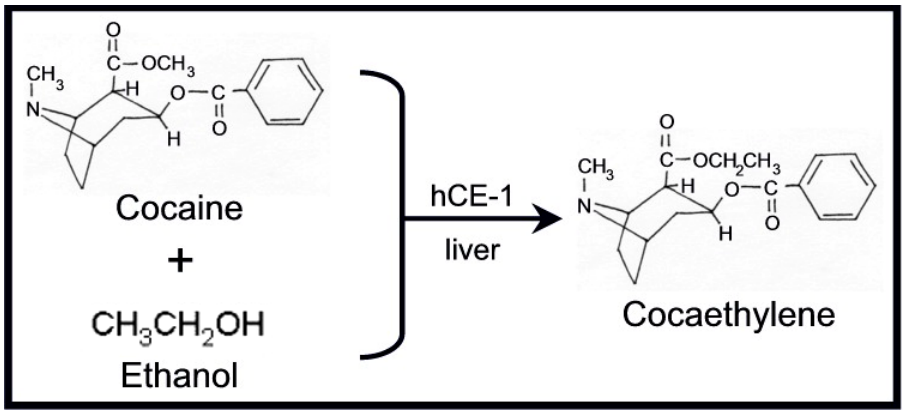

Illustration 1: The formation of cocaethylene (CE)

CE is formed in the liver when cocaine and ethanol are abused concomitantly. The reaction is a trans-esterification catalyzed by the human carboxylesterase-1 (hCE-1) enzyme, which is also the enzyme that metabolizes cocaine to the physiologically inactive elimination product benzoylecgonine.

of ethanol with cocaine. This occurs because ethanol is the preferred substrate in the hydrolysis pocket of the hCE-1 enzyme, which is the location on the enzyme where substrate localization occurs and the trans-esterification reaction is catalyzed. Thus, the water (H_2O) that is needed for cocaine de-activation to benzoylecgonine is not available, and CE is produced instead. Illustration 1 shows the formation of CE by hCE-1.

The route of cocaine administration does not appear to affect the production of CE *in vivo*, since clinical studies employing nasal insufflation and intravenous (IV) injection of cocaine caused similar serum CE levels [15, 16, 23, 27]. However, the time of peak cocaine and CE concentration in the serum occurs sooner (within minutes) with IV administration of cocaine, yielding serum cocaine peaks within minutes, and CE peaks within an hour of injection [15, 16, 23, 27].

The serum concentration of CE seen in most clinical studies is low, typically in the low nanomolar (<100 nM) range [15, 16, 23, 27]. However, CE concentrations observed in emergency departments are usually higher. For example, in 1991, Hearn *et al* detected a serum CE range of 0.03 – 0.31 mg/dL (0.9 μM to 9.8 μM, molecular weight of CE is 317) in one study of post-mortem blood [10]. In another study, serum CE concentrations up to 2.3 mg/L (7.2 μM) were reported from patients presenting to the emergency department in Dade County, Florida [10, 20]. Reports of serum CE concentrations in the 100+ μM range exist for severe overdose cases resulting in death or extreme toxicity [9]. In many cases, serum CE concentrations have been reported to be greater than serum cocaine concentrations [10, 20, 21].

Pharmacologically, CE behaves much like cocaine, binding the dopamine transporter with equal affinity, but with diminished affinity for serotonin and norepinephrine receptors [20-22, 24, 28]. Such activity prolongs the persistence of these neurotransmitters in the synaptic cleft and explains many of the behavioral effects of cocaine and CE (e.g. euphoria, reinforcement, and addiction). Also, CE binds cardiac sodium channels with greater affinity than cocaine [29], suggesting that CE may have greater influence than cocaine on the cardiac outcomes associated with abuse. This

reasoning is supported by animal studies focusing on the cardiac effects of CE [30-42]. In humans, peak serum CE levels correlate better with medical emergencies and death than peak serum cocaine levels [12, 13, 43-47]. Finally, CE has a lower half-maximal lethal dose (LD_{50}) than cocaine in mice (cocaine: female, 92.4 mg/kg, male, 93.0 mg/kg; CE: female, 60.7 mg/kg, male 63.8 mg/kg) [20, 48], thereby accounting for its greater lethality in this and other animal models [20, 22, 23, 48-52].

However, one characteristic that distinguishes CE and cocaine and may influence chronic disease development is serum half-life. The half-life of cocaine is about 40 minutes, whereas CE has been shown to have a half-life 3- to 5-times longer [27, 43, 53], or approximately 2 to 4 hours. This increase in serum half-life is accompanied by a higher bioavailability of CE (due to its increased lipophilicity relative to cocaine) and resulting slower clearance rate of both drugs. Since both cocaine and CE are inactivated by the same enzymes, namely hCE-1 and serum esterases, and cocaine is the preferred substrate for the hCE-1 enzyme, CE removal is further slowed, resulting in prolonged persistence of CE in the bloodstream and tissues [25, 26, 54, 55]. When accounting for clearance of a drug, which is typically 4 to 5 half-lives [56], CE could persist in human blood for as long as 8 to 24 hours, whereas cocaine would be cleared within 2 or 3 hours. These facts suggest that CE is not only capable of exerting greater effects on tissue targets than cocaine, but also affecting those targets for a longer period of time. Hence, given chronic co-abuse and "bingeing" behavior common to cocaine abusers, the potential for systemic effects of CE may be more important in extra-neuronal mechanistic research than cocaine itself.

1.2 SYSTEMIC DISEASE IN COCAINE ABUSERS

The primary health risks commonly associated with cocaine abuse include myocardial infarction and stroke [57-75]. Aortic dissection and rupture have also been reported [76]. From a health perspective, these outcomes are the ones most frequently associated with cocaine abuse because they present the most immediately occurring and lethal outcomes. As a result, greater emphasis has been placed on mechanistic research

surrounding cocaine abuse and cerebral and myocardial ischemia, as well as behavioral studies that probe addiction and treatment options. However, these are not the only clinically relevant outcomes regarding chronic cocaine abuse.

Patients who do not succumb to the acute effects of cocaine are still at risk for chronic disease. Although less is known about chronic disease associated with cocaine abuse than stroke and myocardial infarction, several case histories and clinical studies in cocaine literature show an association between long-term cocaine abuse and spontaneous intravascular thrombosis [77-83], rhabdomyolysis [84, 85], kidney failure [85-87], thrombocytopenia [80, 88-90], non-healing skin ulcers and rashes [80, 90-97], destruction of nasal and oral mucosae [64, 87, 91, 92, 96-105], intestinal ischemia and panarteritis [95, 100], vasculitic lesions of the skin [85, 93, 94, 106], pathologies in peripheral appendages resulting in gangrene and amputation [107], and increased serum "autoimmune" antibodies [86, 88, 92, 108-111]. The items on this impressive list of pathologies are linked by one major tissue: the vasculature.

Before discussing the microvasculature, three relevant examples of cocaine-associated systemic disease will be used to demonstrate the systemic nature of cocaine- and CE-associated pathology. These cases provide a "clinical picture" of the often-prolonged care required by cocaine abusers presenting to the hospital or emergency room. Such cases lead to clinical awareness of potential pathogenic mechanisms associated with cocaine abuse. As such, the dissemination of this new information is necessary to the development of new ideas regarding mechanistic research surrounding cocaine abuse, with focus on potential tissue and molecular targets of cocaine and CE.

1.2.1 The Mockel case report

In the case report by Mockel and colleagues in 1999 [95], a 22-year-old male who was a poly-drug user (marijuana daily, cocaine recently, ecstasy often, and LSD sometimes) presented to the emergency room with arthralgia (joint pain), erythema (redness) of the digits, and a purpuric (spotty, red, painful) rash on the back of the feet. He had a persistent cough for the previous two weeks that had cleared before admission,

and diminished sensation of touch (hypoesthesia). Upon admission, body temperature was elevated (38.1°C, normal is 37°C), as well as white cell counts (13,700/μL, normal range is 4,500-11,000/μL) and C-reactive protein (16 mg/L, normal range is 0.08 to 3.1 mg/L). After admission, body temperature, white blood cell counts, and C-reactive protein became further elevated (38.4°C, 18,300/μL, and 53 mg/dL, respectively) [95]. While these results indicate general inflammation, they provide little basis for establishing a differential diagnosis. Thus, further testing and observation were required.

The patient was admitted and various examinations performed. Chest X-ray and cardiopulmonary examinations were normal, but white blood cell counts and C-reactive protein further increased (21,500/μL and 248 mg/L, respectively) despite normal body temperature. Anti-nuclear antibodies, a general index of rheumatologic disturbance, tested positive. Drug tests were positive for marijuana and cocaine [95].

The health status of the patient began to deteriorate. He developed a progressive paralysis of his limbs, and steroids were administered to suppress suspected vasculitis. Biopsy from the nasal mucosa was unremarkable, but after the skin on the arms began to bleed, biopsy revealed “non-specific vasculitis with negative immune-histopathological study” [95]. After transfer to an intensive care unit, antibiotics were administered despite repeated negative results from microbiological investigations. In the fourth week, gastric perforation occurred and a gastric ulcer was excised. Peritonitis was noted. Biopsy of the excised ulcer showed vasculitis with immune-complex deposition [95].

One week after the surgery, infection was noted around the abdominal scar. A second surgery was required, which resulted in the re-stitching of the stomach, as well as an intestinal re-sectioning. Biopsy of these excised tissues demonstrated panarteritis (widespread inflammation of the arteries) and thrombosis, particularly in small vessels, confirming the diagnosis of vasculitis [95].

In the following weeks to months, several additional surgeries were required, including a second gastric re-sectioning in an area demonstrating the same vasculitic changes. Various bacteria were present in biopsies, but systemic bacterial infection was

not detected. Seizures occurred in the third and fourth months of the hospital stay. In the fourth month, tachycardia was consistently demonstrated, and several surgical debridements were necessary to remove necrotic skin changes on the legs. After nearly six months, the patient was transferred to a rehabilitation clinic, and follow-up one year later showed complete recovery, as well as sustained abstinence from drugs [95].

The authors discussed several potential etiologies for the patient's presentation and chronic disease. They cited methamphetamine and cocaine as etiological agents in development of vasculitis, and determined that since cocaine was the agent detected upon admission, that it was the trigger of the disease in this particular patient. Mockel and colleagues also noted that resolution of symptoms and disease usually occur once the drug is discontinued [95].

The fact that this patient's treatment was identical to that used for autoimmune panarteritis [112] is compelling, since it suggests that vasculitis caused by autoimmunity and CE may have similar clinical courses and treatments. Overall, this case provided an interesting example of chronic systemic disease associated with cocaine abuse. Previous poly-drug use could have caused damage that progressively worsened to the point where cocaine provided the final tissue insult or damage that resulted in disease. This is particularly true because there is no account to-date in the literature that cites marijuana as an etiological agent in the pathogenesis of vasculitis.

1.2.2 The Enriquez case report

In a case presented by Enriquez and co-workers in 1991, a 34-year-old male presented to the emergency room eight hours after insufflation of cocaine [85]. He denied use of ethanol or other drugs. Examination showed muscle swelling and "herpetic lesions" on the lip and arm. The following table (Table 1, below) shows the results of clinical and laboratory tests conducted upon presentation:

Table 1: Admission clinical/laboratory tests conducted in the Enriquez case report

Test	Serum, Urine	Patient Result	Clinical Range/Average*	↑, ↔, or ↓
Temperature	N/A	36.5°C	37.0°C	↔
Heart rate	N/A	102/minute	50-90/minute	↑
Blood pressure	N/A	100/60 mm Hg	120/80 mm Hg	↔
BUN (blood urea nitrogen)	S	10.5 mg/dL	7-23 mg/dL	↔
Creatinine	S	230 μM	62-115 μM	↑
Creatine kinase	S	8,930 U/L	15-105 U/L	↑
Potassium	S	4.9 mM	3.5-5.1 mM	↔
Sodium	S	140 mM	136-145	↔
Chloride	S	101 mM	98-107	↔
pH	S	6.92	7.35-7.45	↓
pO_2	S	75 mm Hg	83-108	↓
pCO_2	S	28 mm Hg	35-48 mm Hg	↓
Bicarbonate	S	5.5 mM	21-28 mM	↓
Hematocrit	S	35.2%	39%-49%	↓
Leukocytes	S	16,000/μL	4,500-11,000/μL	↑
Platelets	S	75,000/μL	150,000-400,000/μL	↔
Fibrinogen	S	2.4 g/L	2-4 g/L	↔
Prothrombin (PTT)	S	18 seconds	11-15 seconds	↑
Calcium	S	1.27 mM	4.64-5.28 mM	↓
Phosphorus	S	1.58 mM	2.7-4.5 mM	↓
Uric acid	S	1,410 μM	260-450 μM	↑

Test	**Serum, Urine**	**Patient Result**	**Clinical Range/Average***	**↑, ↔, or ↓**
Total bilirubin	S	47.6 μM	5-21 μM	↑
Alanine Aminotransferase	S	330 U/L	10-40 U/L	↑
Aspartate Aminotransferase	S	1,560 U/L	13-38 U/L	↑
Alkaline Phosphatase	S	122 U/L	38-94 U/L @ 30°C	↑
Lactate dehydrogenase	S	5,630 U/L	100-190 U/L	↑
Aldolase	S	46 U/L	1-7.5 U/L @ 30°C	↑
Sodium	U	33 mM	40-220 mM	↓
Potassium	U	57 mM	25-125 mM	↔
Blood	U	+++	-	↑
Cellularity	U	Numerous granular casts, no red cells	-	↑
Electrocardiogram	N/A	Tachycardia	N/A	↑
Abdominal ultrasound	N/A	Normal kidneys	N/A	↔

First column lists the test or analysis performed. The second column designates either serum (S) or urine (U) sample (N/A if neither). The third column lists the test result for the patient in the Enriquez case study [85]. The fourth column lists the clinical reference ranges for similar samples and adult males [113]. The fifth column denotes changes in the patient's sample relative to the clinical index (increase, no change, or decrease).

Inexplicably, drug and alcohol screens were not reported for this patient upon admission. As shown in Table 1, kidney and liver markers (enzymes, uric acid,

creatinine) were elevated, signifying dysfunction in those organ systems. The increased creatine kinase demonstrated general muscular wasting or damage. The decreased levels of pH and arterial blood gases and bicarbonate demonstrated acidosis. These test results, paired with the swollen muscles and the later anuria (lack of urination) and initial stages of renal failure led to a differential diagnosis of "acute tubular necrosis due to rhabdomyolysis", which was treated with dialysis therapy [85].

On the fourth day, the patient developed a purpuric rash on his lower limbs. Biopsy of muscle and skin confirmed the diagnosis of rhabdomyolysis, and vasculitic changes of the skin with immune and complement deposition. Tests for autoimmune markers such as anti-nuclear antibody were negative. Urine screens were positive only for cocaine. After 29 days, the patient was released with "normal blood biochemistry". However, further comment on the patient's status was not provided [85].

The authors discussed the role of cocaine as an etiological factor in the development of rhabdomyolysis. Though they had no previous knowledge of cocaine causing peripheral vasculitis, they stated that the circumstances surrounding the development of the rhabdomyolysis in this patient could have been lethal, and that cocaine could have worsened pre-existing disease that led to the emergency room presentation [85].

1.2.3 The Tapia & Schumacher case report & discussion

In 1993, Tapia and Schumacher presented a case report concerning a hypertensive 32-year-old male presenting with stroke after cocaine and ethanol ingestion [114]. This patient experienced a sudden and severe headache in the right frontal area of his head, followed by weakness on his left side. After collapsing, he was brought to the emergency room at Massachusetts General Hospital. Upon admission, the patient's noted blood pressure was 235/130 mm Hg (highly elevated, normal 120/80), and his pulse was 92 (moderately elevated, normal 50-90 beats/minute). He was lucent, but had paralysis and anesthesia of the left side of his face, as well as his left arm and leg. The patient was otherwise healthy, with no remarkable cardiovascular disruptions or skin changes [114].

Urinalysis was positive for opiates and cocaine. Further tests conducted the second day revealed decreased ventricular ejection fraction and a slight protrusion of the left ventricle (on chest X-ray) [114].

By the third day, the patient was “less alert”, with fluctuating blood pressure. Angiography demonstrated no evidence of aneurysm or vasculitis. CT scans revealed enlargement of the hemorrhage. Doppler imaging and radiography showed no change in the patient’s general status. However, the patient was steadily harder to rouse and experienced fluctuations in blood pressure. A second CT scan showed no change in the size of the hemorrhage, but instead an increase in the cerebral edema resulting from the stroke [114].

After progressive disintegration during his hospital stay, the patient was intubated, oxygen was administered, and a biopsy was obtained during evacuation of the cerebral hemorrhage. Though the diagnosis of stroke precipitated by cocaine abuse had been made (using the images captured), vasculitis was observed in biopsy specimens obtained. No aneurysm was observed. The authors stated that, “in all the cases with biopsy-proven vasculitis, angiographic examination has been negative”[114], thus demonstrating a need for further consideration of vasculitis as an underlying factor in pathological presentations associated with cocaine abuse, especially known outcomes such as stroke.

Case reports like the three above are relatively recent, and point to gaps in the current knowledge of the pathogenesis of cocaine-associated systemic disease. First, in all cases, the findings led the authors to conclude that vasculitis is a possible consequence of cocaine abuse, which could develop into systemic disease and tissue failure. This is an area of cocaine-associated disease in which mechanistic research has been lacking. Only cases such as the ones described can provide the research community with targets for its research, and expansion or re-evaluation of existing mechanistic theories. Cases such as those presented above (especially those by Enriquez and Mockel) [85, 95] demonstrate that cocaine- (and CE-) induced vasculitis deserve further investigation, with particular

emphasis on mechanism and development of treatments for patients presenting with such complications.

Second, these cases emphasize the point that more must be done to understand the full extent of cocaine's (and CE's) ability to affect the body. One clear conclusion that can be made from these three cases is cocaine's or CE's effects on organ systems have not been fully realized, and thus treatment options for patients presenting with cocaine-associated systemic disease are limited. Expansion of the existing mechanism of cocaine's activity, or the development of mechanistic theories based on the differential effects on various organs, is required for advances in prevention and treatment to occur.

Third, though the science of addiction is undoubtedly of interest to researchers because prevention of addiction would prevent lethal or pathological outcome, knowledge of the extra-neuronal targets of cocaine and CE should be regarded as equally important until the causes of addiction can be successfully treated. Until addiction can be stopped, patients will continue to die unless: 1) more is understood about the causes of their pathologies; and 2) a treatment plan has been developed for those who present with pathology. Since neither is possible without basic scientific research, clinical problems (such as these three cases) provide a starting point for mechanistic research.

1.3 THE ROLE OF MICROVASCULAR INJURY IN SYSTEMIC DISEASE

The human vasculature is complex, present in every tissue and organ in the body, and dominated in volume by the "microvasculature", which includes tissue venules, arterioles, and capillaries. These small vessels are responsible for the majority of blood-tissue transfer of vital nutrients, gases, and waste products, as well as the regulation of tissue inflammatory and allergic responses. The major component of the microvasculature that functions as the modulator of gas and nutrient exchange, as well as hemostasis and injury, is the endothelium, which lines the lumen of all blood vessels and composes the majority of the capillary wall.

The endothelium functions as a gateway to surrounding tissues. For example, the endothelium regulates the passage of blood-borne nutrients and gases to the tissues, and restricts the movement of xenobiotics and infectious agents out of the bloodstream. The endothelium also regulates the passage of immune cells to the tissues, limiting the ability of the immune cells to access tissue parenchyma. This function of the endothelium results in a regulation of inflammation when tissue parenchyma is injured, thus contributing to the maintenance of tissue homeostasis. Thus, the endothelium is responsible for the bulk of vascular and tissue equilibrium, as well as the mediation of immune function.

The endothelium is composed of individual endothelial cells, which form tight intercellular junctions that function to "seal off" the contents of the vascular lumen from the tissues surrounding the vessel. These junctions are the sites of endothelial regulation of vessel permeability, since their ability to bind to each other and the extracellular matrix around the blood vessel determine whether an endothelial layer is restrictive or permissive to movement between the blood and tissues. Researchers have only begun to understand the consequences of damage to endothelial cells in the context of tissue and organ system disease because of the complexities of endothelial cellular response to the vascular environment.

The widely accepted view is that endothelial injury and dysfunction could have devastating consequences on the tissues surrounding affected vessels (Illustration 2). Thus, widespread microvascular damage can result in systemic vascular disease, which may manifest as ischemic diseases of the heart, brain, and other vital organs, as well as the pathologies listed in Section 1.2. Microvascular damage is usually initiated in or on the vascular endothelium, and the results of endothelial injury typically involve the tight intercellular junctional complexes that compose the bonds between cells, and the cellular cytoskeleton, which maintains cell and vessel shape. While junctions are intact and the cytoskeleton is stable, permeability through the endothelial barrier is highly selective (Illustration 2, Event 1). However, if a biological or chemical agent, or physical force injures the endothelium (Illustration 2, Event 2), then cellular changes can loosen these junctions (Illustration 2, Event 3) [115]. Such disruption of endothelial cells decreases the

barrier integrity of the monolayer, allowing for free passage of molecules and cells from the vessel lumen to the tissues, where they can accumulate (Illustration 2, Event 4). When protein, serum fluids, and blood-borne cells accumulate in the tissues, oxygen delivery and exchange in the affected tissue can be impeded (Illustration 2, Event 5). Depending on the extent of accumulation and the activity of the cells, this can result in local inflammation, tissue ischemia, and necrosis [116].

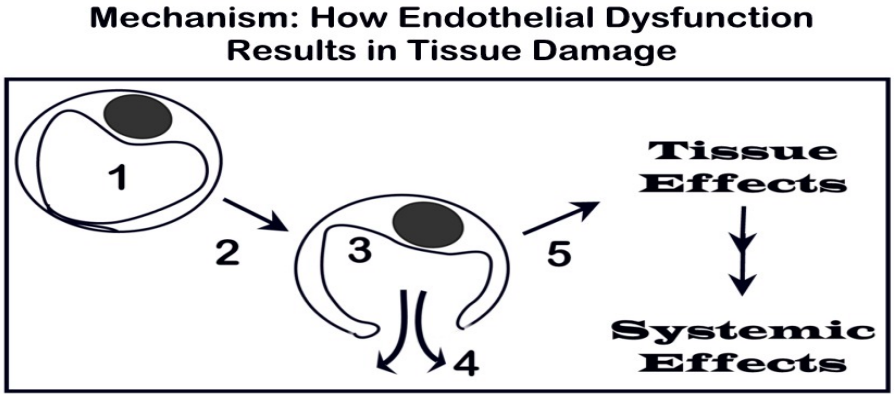

Illustration 2: Microvascular endothelial involvement in systemic disease

The numbers in the illustration represent the events described herein. Event 1: A normal microvascular endothelial cell composes the wall of the microvessel. Tight connections between endothelial cells maintain barrier integrity. Event 2: An agent or physical force affects the cell. "Agents" can be biological or chemical, and mechanical forces can be shear stress and/or altered hemodynamics. Event 3: Cellular changes occur that affect the barrier integrity of the cells and vascular wall. Event 4: As a result of altered barrier integrity, vascular permeability increases. Event 5: The accumulation of serum proteins, cells, and fluid in the tissues alters gas and nutrient exchange, and can promote inflammation. These changes can alter the function of the tissue, and depending on the function of the tissue, affect systemic function.

Since inflammation in a tissue can alter its functionality, tissue failure is possible in scenarios involving vascular disruption. Also, depending on the function of the tissue or organ involved, systemic affects may result. Thus, an otherwise small vascular change is often the source of large-scale tissue and/or organ damage or failure *in vivo*. This study

addresses the effects of CE on the microvascular endothelium, with particular emphasis on endothelial cellular function and on the barrier function of endothelial monolayers.

1.4 SIGNALING PATHWAYS RELATED TO MICROVASCULAR DISRUPTION

Many agents can act upon the microvascular endothelium and induce changes in permeability. Such agents can be intrinsic molecules (e.g., prostaglandins, thrombin), or extrinsic molecules (e.g., viral proteins, microbial glycoproteins, xenobiotics) [117-126]. A common activation pathway observed in endothelial activation involves G-protein linked receptors (GPLRs) and proteins, and subsequent activation of phospholipases (Illustration 3). However, phospholipase activation can be induced by a number of receptors or agents, and because of its versatility, the phospholipase C (PLC) signaling

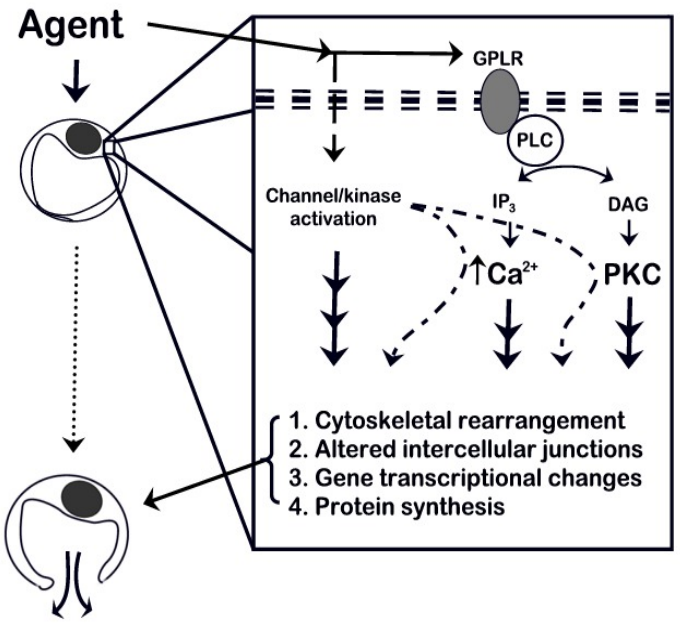

Illustration 3: Signaling pathways associated with cellular dysfunction

Redundant pathways are used in all cells injured by agents (e.g. microbiological or chemical) or mechanical forces. In endothelial cells, injury often results in altered barrier integrity and inflammation by the mechanisms listed.

cascade is ubiquitous and involves many PLC isoforms (which will not be detailed in this review). Once activated, PLC cleaves the membrane phospholipid, phosphatidylinositol

(PI), into inositol trisphosphate (IP_3) and diacylglycerol (DAG), which initiate major signaling events throughout the cell (Illustration 3) [117, 120, 127]. Both IP_3 and DAG have important roles in disruption of endothelial permeability, since they cause two major cellular events to occur (Illustration 3).

First, IP_3 binds its receptor on the surface of the endoplasmic reticulum, which serves as a calcium storage organelle, or "sink". This binding causes a conformational change in the IP_3 receptor (IP_3R), which allows the release of free calcium into the cytosol. Negative feedback by calcium causes the channel to close, and is concentration-dependent [117, 128]. This auto-regulation allows for tight cellular control of cytosolic free calcium, which is necessary due to the power and ubiquity of calcium as a cellular second messenger [117, 129]. Due to the local anesthetic affects of cocaine, CE, and related drugs, determining whether CE alters cellular calcium in the microvascular endothelium would aid in mechanistic description of the effect(s) of CE on endothelial function and permeability *in vivo*. In this study, cytosolic and cellular calcium were monitored in endothelial cells exposed to CE in an effort to address this need for mechanistic knowledge of CE.

The second event affecting endothelial permeability after PLC activation involves DAG, which functions to activate protein kinase C (PKC). PKC is a kinase with various activities in the cytosol. For example, PKC is capable of activating other kinases in a magnesium-dependent manner via phosphorylation [119, 124, 126, 130] (Illustration 3). Such kinases include myosin light chain kinase (MLCK), mitogen-activated protein kinases (MAPKs), and phosphatases that counteract kinases via dephosphorylation of kinase targets [130, 131]. These events culminate in the mobilization of the myosin light chain (MLC), the main motor protein of the cytoskeleton (Illustration 3, Event 1). Phosphorylation of MLC is mediated by MLCK, is calcium-dependent, and results in the binding of MLC to the actin framework [130]. Phosphorylation and dephosphorylation of the MLC "head" by a kinases and phosphatases (also activated by PKC) cause the myosin molecule to "walk" along actin fibers, with ATP as the fuel for the movement. The result is de-polymerization of the actin-myosin cytoskeleton, which changes cell shape and how

the cell links to neighboring cells via intercellular junctional proteins such as vascular/endothelial- (VE-) cadherin and occludins. Thus, mobilization of MLC causes cellular contraction and interrupts the ability of cells to maintain a tight barrier between the vascular lumen and surrounding tissue, and is a likely outcome in any endothelial toxicity resulting in altered morphology. [Note: Though DAG, PKC, and MLC activities are not specifically examined in this study, staining of cell-to-cell junctions and morphological assessment of endothelial monolayers after exposure to CE were performed. The morphological analysis was designed as a prelude to future studies involving DAG, PKC, and MLC.]

The second component of the increase in permeability involves intercellular junctions such as adherens junctions, which physically link endothelial cell surfaces to each other, as well as the matrix below them (Illustration 3, Event 2). The process of increased endothelial layer permeability is relevant to the present study because CE-induced, calcium-related alterations in the cytoskeleton would promote increases in monolayer permeability, which would promote tissue edema and ischemia *in vivo*. Consequently, several experiments focusing on endothelial morphological change, barrier function, and calcium balance were incorporated into this study.

Maintenance of the junctions between endothelial cells is key to selective permeability and inflammatory cell trafficking during inflammatory responses [117, 119, 130, 132-134]. Adherens junctions in endothelial cells are composed of VE-cadherin, which is an intrinsic protein expressed on the cell surface. VE-cadherin is associated with proteins of the catenin family, which link cadherin to the actin framework. Phosphorylation of the catenins (by PKC) dissociates cadherin from the actin framework, and results in disassembly of the junctional complexes, which loosens the contact between endothelial cells [117, 130, 132-134]. Though adherens junctions are not addressed in this study, their role in permeability is worthy of mention, particularly with regard to potential future studies, should CE be shown to affect endothelial layer permeability.

1.5 OTHER EFFECTS OF ENDOTHELIAL CELL DISRUPTION

When endothelial injury occurs, more than just permeability is affected. The process of inflammation that results in vasculitis involves many intersecting signaling pathways, including those of the mitogen-activated protein kinases (MAPKs, particularly p38 MAPK) and nuclear factor-κB (NF-κB) family proteins [130, 135-137]. These molecules relay signals to the nucleus that promote cell survival and transcription of mRNA (Illustration 4), which is typically translated to proteins (e.g., adhesion molecules, cytokines, transcription factors). MAPK and NF-κB (particularly p38 MAPK, and Rel-A(p65), p50, p52, Rel-B, and c-Rel) are especially important signaling molecules/transcription factors regarding cell responses to stress, and the promotion of inflammation. Thus, these targets are the focus of molecular studies in various inflammation studies [118, 136, 137], and have been included in this study for aid in studying the mechanism underlying CE-induced changes in microvascular endothelium.

Activation of most signaling molecules is achieved via phosphorylation of serine, threonine, or tyrosine residues on target proteins. Phosphorylation as a process acts as a molecular "switch", which increases or decreases the activity, stability, and/or sub-cellular localization of the target protein.

The p38 MAPK protein is generally placed near the end of signaling sequences within the cell, as it is the direct modulator of nuclear transcription factors that, when activated by kinase phosphorylation, bind DNA promoters and initiate transcription of target genes. Activated p38 MAPK signals to nuclear transcription factors such as Fos and Jun dimers, Stat1, Myc, Elk-1, MEF2, and ATF-2 (not detailed in this review), which function to activate transcription of cytokine, adhesion molecule, and regulatory proteins [138]. Fos and Jun are transcription factors that form homo- and heterodimers and bind a nuclear consensus sequence called the AP-1 binding site. When the AP-1 site is occupied by Fos and/or Jun dimers, corresponding gene transcription activity at sites containing the AP-1 site typically increases. The molecular products of Fos/Jun activation include the *fos* and *jun* genes, as well as genes encoding proteins of the NF-κB and IκB families, and

other proteins related to cell survival and inflammation [118, 139]. Thus, p38 MAPK phosphorylation was measured in this study to predict whether Fos/Jun related signaling may be activated in CE-exposed microvascular endothelium.

NF-κB transcription factors are protein dimers of the Rel/NF-κB protein family [137, 140]. Dimers of NF-κB family proteins are localized to the cytosol by inhibitory proteins belonging to the IκB protein family, or derived from the NF-κB family proteins p100 and p105. The predominant NF-κB inhibitor protein is IκBα. During cellular activation signaling, IκBα is phosphorylated by several kinases, including kinases from the MAPK family. Since phosphorylation of IκBα targets the protein for ubiquitination and degradation, the NF-κB dimer held in the cytosol by IκBα is released, allowing for localization of the NF-κB dimer to the nucleus and subsequent DNA binding and transcription of target genes. These target genes include NF-κB subunits, Fos (another important cell-survival transcription factor), and IκBα, as well as genes encoding cytokines, adhesion molecules, and other mediators of cellular response [137, 140]. Thus, the proteins of the MAPK and NF-κB signaling cascades up-regulate each other, contributing to a survival-prone and pro-inflammatory cellular state when activated. For this reason, both p38 MAPK and NF-κB were examined as potential contributors to the mechanism underlying CE-induced microvascular endothelial changes observed in this study.

The MAPK and NF-κB pathways, along with other signaling pathways, interact to create a summative “yes” or “no” signal to the nucleus to begin pro-inflammatory and survival gene expression (Illustration 4) [118, 119, 136, 137, 140], and are responsible for the production of cellular adhesion molecules, cytokines, and transcription factors that function together to ensure cell survival and promote inflammation and cell/tissue repair.

Other factors that regulate MAPK and NF-κB activation are the intracellular ion (calcium and magnesium) balances of the endothelial cell (Illustration 4, calcium shown to indicate ion changes). Generally, when intracellular calcium and/or magnesium

increase, kinase and phosphatase activities are increased in the cell, promoting increased activity of signaling molecules such as MAPK and NF-κB [117, 119, 129, 137, 140]. Thus, if cocaine or CE induces changes in intracellular calcium and magnesium, as has been shown for sodium and calcium in other cellular models [117, 119, 127, 128, 130, 132, 136, 141-147], then various intracellular signaling pathways could be up- or down regulated. These changes, in turn, could promote inflammation, and lead to the tissue ischemia, inflammation, and infarction observed in human cocaine abusers (Section 1.2).

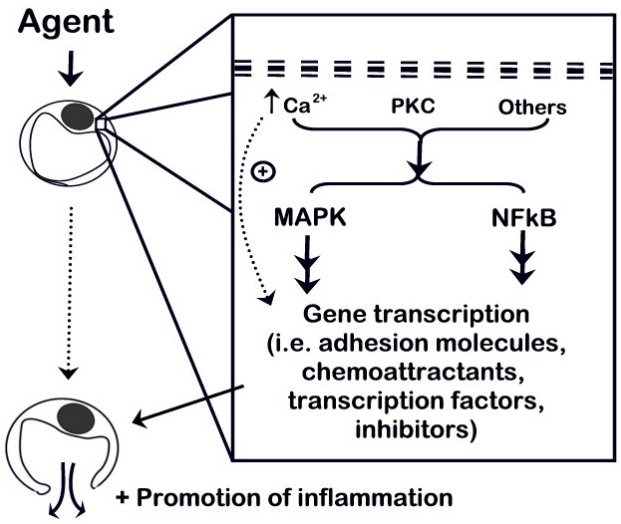

Illustration 4: Major nuclear signals in endothelial dysfunction

Second messengers such as calcium and kinases such as PKC promote the activation of other kinases (e.g. MAPK) and transcription factors (e.g. NFκB) that initiate gene activation and transcription.

1.6 RELEVANT EXPERIMENTAL EVIDENCE: TYING IT TOGETHER

Abundant case histories showing vascular disease in cocaine addicts (Section 1.2), mechanistic speculation on the part of the authors of such literature, and the current knowledge of the pharmacological activity of CE (Section 1.1), have suggested a link between CE and the vascular endothelium that has been largely under-studied. Even cocaine-associated strokes may have a stronger association with vasculitis (inflammation of blood vessels) than previously thought, as demonstrated in the case report by Tapia

and Schumacher (Section 1.2.3 [114]). Since biopsies are usually not obtained in the majority of cocaine-associated stroke cases reported in the literature [101, 148-150], the significance of vasculitis may be an under-appreciated contributor to the mechanism of stroke pathogenesis in cocaine abusers.

Cases such as the one described by Mockel and colleagues [95] have demonstrated a vascular source of tissue ischemia so severe as to require intestinal resection surgeries to prevent death in the patient. Also, kidney failure, non-healing ulcers and bruises, and thrombocytopenia are common occurrences in cocaine abusers that are largely based on microvascular disruption (Section 1.2). In the existing human case studies reporting vasculitis, cocaine is usually the suggested etiological agent, and bacterial or other potential biological agents are not suspected to have a role in disease pathogenesis. Thus, there are two summative speculations that arise from the cocaine case literature. The first is that cocaine (and/or in this case, CE) has a direct effect on the vasculature that causes disruption, tissue edema, and subsequent progression to vasculitis. The second speculation is that cocaine (and/or CE) provides an insult to already damaged tissue that exacerbates existing vasculitis and tissue damage, and leads to tissue/organ failure.

In animal models, a link to the microvascular endothelium has been established for cocaine. Scott and associates [151] injected cocaine (subcutaneous) into rats and found ulceration and tissue destruction that mimicked human cutaneous and mucosal ulceration. The authors attributed this ulceration to the direct chemical effects of the cocaine bolus on the surrounding tissues, but human cases of mucosal and nasolacrimal necrosis in abusers [96, 98, 102] have been attributed to vasculitis (possibly resulting from prolonged local effects of the drug on the tissues), thus requiring further clarification.

In 1997, Barroso-Moguel *et al* presented the results of a study they conducted in rats with chronic exposure to cocaine (30 mg/kg/day, up to 90 days). Alterations in brain capillaries were described at 7, 15, 30, 60, and 90 days after treatment. After 7 days of

cocaine treatment, capillaries were dilated and contained small thrombi. Edema was detected. As the chronicity of cocaine exposure progressed, brain capillary lesions became more complex, with increasing edema, immune cell infiltrates, decreased lumen diameter, and increased capillary wall thickness. After 90 days of cocaine exposure, blockage of capillaries due to fibrosis and thrombosis was common, as was extensive edema. These results prompted the authors to comment that, "those destructive lesions appeared to have a direct vascular basis" [152], and note that similar lesions were also noted in studies they conducted in other tissues (testicle, kidney) in rats.

The intra-vital microscopy experiments of Chang and co-workers [153] also demonstrated a microvascular link to cocaine toxicity. The authors observed increased blood-borne leukocyte numbers in mesenteric blood vessels after rats were injected with cocaine [153]. Also, using an intra-vital microscopic method to observe cellular behavior, the authors reported increased leukocyte rolling along the endothelial surface, as well as sedimentation, which occurs just before transmigration to the tissues from the vessel lumen [153]. Finally, the authors noted an increase in expression of intercellular adhesion molecule (ICAM) –1, an adhesion molecule linked with extravasation of inflammatory cells, in the mesenteric venules viewed [153]. The authors stated that the observed changes "may underlie the progressive vascular damage seen in chronic cocaine abusing individuals" [153], lending credence to the proposed mechanism of pathology in this dissertation.

In 1999, an *in vitro* experiment was conducted that addressed the vascular effects of cocaine abuse. This study by Kolodgie and colleagues [17] investigated the effects of cocaine on macrovascular (human umbilical vein, HUVEC) endothelium. CE was included in some (resistance monitoring, silver staining for gaps) of the analyses described. The authors reported that CE had equal effects on permeability and cytoskeletal mobilization when compared to the effects of cocaine in the same model, whereas neither of the other cocaine metabolites tested (benzoylecgonine and ecgonine methyl ester) had any of those effects [17]. Cocaine decreased trans-endothelial resistance, a measure of permeability, which recovered when the cocaine was removed

from the bathing solution covering the endothelial monolayers. This effect was repeated in cells treated with equimolar amounts of CE [17]. Also, silver staining of endothelial monolayers after a one-hour exposure to cocaine showed an increase in the number of intercellular gap formations [17]. Such gaps are sites of pro-inflammatory leakage *in vivo* [154, 155]. Finally, actin mobilization was noted in similarly treated monolayers [17]. Such a combination of effects is important, because together these responses clearly demonstrate disruption of barrier function in cocaine (and, peripherally, CE) –treated endothelial cells. Interestingly, these effects were observed despite minimal reported effect on cellular viability (data was not shown).

These compelling results required further study for several reasons. First, the CE group was included in only one set of experiments, and its effects were mentioned only briefly in the discussion, with no specific focus on CE itself. Second, the cell line used (HUVEC) was derived from large vessel endothelium, which has different functions and phenotype relative to microvascular endothelium *in vivo* [156]. Finally, only a single time-point (1 hour) was used. As outlined below, the series of studies in this dissertation was designed evaluate the impact of CE on microvascular endothelium, and to address the mechanism underlying the permeability change that was observed by Kolodgie and colleagues [17], with focus on temporal changes for better characterization of effect.

1.7 SUMMARY OF BACKGROUND & SIGNIFICANCE, & AIMS OF PROJECT

Cocaine abuse is widespread, and co-abuse of cocaine and ethanol is common among cocaine addicts. The pathological effects of such abuse are costly to national and local health care organizations. Deaths resulting from acute exposure to cocaine are mainly caused by stroke and myocardial infarction, but in patients that do not die immediately, more chronic illnesses closely linked to vascular toxicity and inflammation (vasculitis) emerge. Over the past decade, it has been recognized that CE, a metabolic product of cocaine and ethanol, may contribute to or dominate cocaine-associated pathology. There is a paucity of investigations concerning the mechanisms of CE-

associated pathology, as well as information regarding the microvascular effects of CE. Considering these important facts, this research study was comprised to address areas not previously addressed in the current literature.

The postulate of this study was that the interaction of CE and the microvascular endothelium contributes significantly to cocaine-associated diseases throughout the body. Thus, the principal hypothesis was that CE directly interacts with the microvascular endothelium in a manner that promotes alterations in cellular function and barrier integrity. Specifically, the hypothesis of this study is that *CE disrupts microvascular endothelial permeability and function by affecting intracellular signaling and second messenger balance and generation*. The following aims were designed to test this hypothesis.

1.7.1 Aim One – Develop a CE exposure model utilizing human microvascular endothelial cells

Immortalized human dermal microvascular endothelial cells (HMEC-1) obtained from the Centers for Disease Control provide a model of the dermal microvascular lumen, with an added benefit of extended culture life. This cell line was used to develop a model of CE exposure. Proliferating HMEC-1 were exposed to CE, and growth kinetics and viability were assessed. Media levels of CE were quantitated to confirm persistence throughout the experiment. Confluent HMEC-1 monolayers were exposed to 1mM CE, and viability and cytotoxicity were assessed. Biochemical profiling of control and CE-treated culture media was performed to characterize the global metabolic effects of CE exposure, as an added measure of injury/cytotoxicity.

1.7.2 Aim Two – Assess the morphological/barrier effects of CE exposure

Ultrastructural changes of control and treated HMEC-1 monolayers were viewed using transmission electron microscopy (TEM). Silver staining for gap formations between HMEC-1 cells was performed after monolayers were treated with CE. Electronic Cell-substrate Impedance Sensing (ECIS) was used to record alterations in barrier integrity by monitoring monolayer resistance under control and CE-treatment conditions.

1.7.3 Aim Three – Assess the effects of CE exposure on HMEC-1 intracellular cation levels

Intracellular concentrations of free calcium and magnesium were monitored kinetically in HMEC-1 monolayers treated with CE in an "immediate"/acute exposure study. The fluorescent ion indicators Fura-2 AM and Mag-Fura-2 AM were used for free ion detection and quantitation. Also, acute pre-treatment experiments were performed using the same general approach to determine the effects of CE pre-exposure on baseline cytosolic and total cellular calcium and magnesium levels in HMEC-1 monolayers.

1.7.4 Aim Four – Determine the effects of CE exposure on calcium-dependent signaling events

Cellular production of IP_3 was determined in HMEC-1 monolayers treated with CE. Also, phospho-p38 MAPK detection was performed using sandwich ELISA, to determine whether this signaling pathway was involved in the effects of CE on HMEC-1. Finally, Electrophoretic Mobility Shift Assay (EMSA) was used to analyze nuclear extracts of CE-treated HMEC-1 for DNA binding activity of the transcription factor NF-κB. Supershift analysis was used to determine which NF-κB-family proteins were present in NF-κB dimers using specific antibodies against Rel-A(p65), p50, p52, and c-Rel.

CHAPTER 2: MATERIALS & METHODS

2.1 CHEMICALS & MATERIALS

2.1.1 Cell culture & CE exposure

HMEC-1 cells were provided by the Centers for Disease Control (CDC, Atlanta, GA). The National Institute on Drug Abuse (NIDA, Bethesda, MD) provided the CE fumarate. Cell culture flasks, dishes, plates, scrapers, and serological pipettes were purchased from Corning (Corning, NY) and Falcon/Becton Dickinson (Franklin Lakes, NJ). FBS, L-glutamine, PBS, trypan blue, and trypsin-EDTA (ethylene diamine tetraacetic acid) were purchased from Gibco BRL (Grand Island, NY). Coated culture dishes and plates, human recombinant epidermal growth factor, and human fibronectin were from Becton-Dickinson (Franklin Lakes, NJ), and sodium bicarbonate solution was from Cellgro (Herndon, VA). MCDB131 media mix and water-soluble hydrocortisone were from Sigma-Aldrich (St. Louis, MO). Miscellaneous supplies for cell culture were purchased from Fisher Scientific (Houston, TX).

2.1.2 Aim One (model development) studies

Deuterated CE (CE-*d*5) was obtained from Radian International (Austin, TX), and Bond Elut Certify solid-phase extraction cartridges were purchased from Varian (Harbor City, CA). Methanol, sodium phosphate (mono- and dibasic), toluene, and HCl were purchased from Sigma in the highest quality available. MTT (3-[4,5-dimethylthiazol-2-yl]-2,5-diphenyl tetrazolium bromide) and solubilizing solution were purchased from Sigma-Aldrich.

2.1.3 Aim Two (morphology & barrier) studies

Formalin (10% v/v solution), silver nitrate, nuclear fast red, Permount® mounting medium, and Lab-Tek Chamber Slides (Nalge Nunc) were purchased from Fisher Scientific. Thermanox cover slips, Ito fixative, resin, and other reagents for Transmission Electron Microscopy (TEM) were a donation of V. Popov (UTMB, Department of

Pathology). Culture arrays with electrodes for Electronic Cell-substrate Impedance Sensing (ECIS) were purchased from Applied BioPhysics (Troy, NY). J. Olano and P. Koo (UTMB, Department of Pathology) provided the ECIS equipment (Model ECIS 1600R, Applied Biophysics).

2.1.4 Aim Three (cation) studies

Sodium chloride, potassium chloride, calcium chloride, magnesium chloride, HEPES (hydroxyethylpiperazine ethanesulfonate), and dextrose for Tyrode buffer were purchased from Fluka (supplied by Sigma-Aldrich). Fura-2 AM and Mag-Fura-2 AM were purchased from Molecular Probes (Eugene, OR). Digitonin and EGTA (ethylene glycol-bis(beta-aminoethyl-ether)-N,N,N',N'-tetraacetate) were purchased from Aldrich and Fluka (both brands supplied by Sigma-Aldrich), respectively. Custom-cut 12 mm by 13 mm glass cover slips were purchased from Erie Scientific (Portsmouth, NH). All salts and reagents were of molecular-grade.

2.1.5 Aim Four (signaling) studies

Diethyl ether and trichloroacetic acid (TCA) were purchased from Fisher Scientific. Biotrak™ Assay kits for IP_3 analysis were purchased from Amersham Biosciences (Piscataway, NJ). Benzamidine, sodium fluoride, sodium azide, β-mercaptoethanol, urea, protease and phosphatase inhibitor cocktails, phenylmethylsulfonyl fluoride (PMSF), H_2SO_4, and TMB (tetramethylbenzidine) for the kinase assays and nuclear extractions were purchased from Sigma-Aldrich (St. Louis, MO). The phospho-p38 MAPK assay kit was purchased from R&D Systems (Minneapolis, MN). N. Herzog (UTMB, Department of Pathology) provided the core buffers, dithiothreitol (DTT), labeled Igκ oligonucleotide (synthesized by Bio-Synthesis, Inc., Lewisville, TX), and materials for polyacrylamide gels and imaging used in EMSA. The Micro BCA™ Protein Assay Reagent Kit for protein quantitation was purchased from Pierce (Rockford, IL). Phosphatase inhibitors were purchased from Calbiochem (San Diego, CA). PMSF and protease inhibitor cocktail for mammalian cells was purchased from Sigma-Aldrich.

2.2 METHODS – AIM ONE: DEVELOP A CE EXPOSURE MODEL UTILIZING HUMAN MICROVASCULAR ENDOTHELIAL CELLS

2.2.1 Cell maintenance/culture

HMEC-1 were sub-cultured in MCDB131 media, supplemented with L-glutamine (10 mM), sodium bicarbonate (1.18 g/L), hydrocortisone (1 mg/L), epidermal growth factor (10 μg/L), and FBS (10% v/v) according to direction given by the CDC and Ades and colleagues [156, 157]. Sub-culture was performed in a 1:4 split every 3 to 5 days, and required rinsing with calcium- and magnesium-free PBS, and trypsinization.

2.2.2 CE stock preparation

CE fumarate ($C_{18}H_{23}NO_4 \cdot 1.5\ C_4H_4O_4$, MW of CE 317.38, MW of CE fumarate 491.49) dissolves in cell culture media and buffers. Thus, CE fumarate stock of 10 mM was prepared in MCDB 131 media in amber glass bottles to prevent photo-degradation of the CE. The stock solution was stored for up to one week at 4^oC in a tightly sealed amber glass bottle to prevent autolysis and photo-degradation.

2.2.3 Growth curve/viability of proliferating cells

The growth kinetics and viability of proliferating HMEC-1 were assessed for two reasons. First, growth curves should be performed on all cell lines to determine growth kinetics of the cells for future reference and sub-culturing. Second, since proliferating cells are sensitive to toxic insult, this assessment is a way of determining dose-response, and in confirming that the 1 mM concentration of CE previously used by Kolodgie and co-workers [17] is not lethal to the HMEC-1 cells.

A 1 mM concentration of CE presents a physiologically high *in vivo* exposure to the endothelium, but poses an important challenge to the HMEC-1 cells. Thus, if 1 mM CE concentrations are not lethal to confluent HMEC-1 cells *in vitro*, then the 1 mM concentration can be use in this study for characterization of endothelial effects, and future studies utilizing lower concentrations can be employed for dose-response evaluations. Additional, intermediate concentrations (0.1 and 0.5 mM) of CE were

included in the growth curve in this study. Should 1 mM CE prove lethal to the HMEC-1 cells, a lower concentration could be used in the remaining experiments. Also, important information about the heterogeneity of endothelial sensitivity to CE concentration could be obtained.

HMEC-1 cells were seeded onto fibronectin-coated 6-well plates at a density of 1 x 10^5 cells per well. CE stock was added to each well to a final concentration of 0, 0.1, 0.5, or 1 mM CE (0 mM CE, media only), and the volume brought to 5 mL with complete media. Cultures were incubated at 37^{o}C and 5% CO_2, 95% ambient air. On day "zero", a 5 mL aliquot of cells was prepared for each treatment group for a baseline cell count. One-milliliter aliquots from each group were kept for CE extraction and quantitation (below). Samples (10 μL) taken from remaining suspension were diluted 1:1 with trypan blue solution, mixed well, and counted with a hemacytometer. On days 1 through 7, media was sampled for CE extraction and quantitation (below), and the remaining media was aspirated. After rinsing with PBS, the HMEC-1 were trypsinized (0.5 mL) for approximately 2-3 minutes at 37^{o}C and suspended in a final volume of 1 mL with PBS (0.5 mL). A 10-μL aliquot was then taken and treated as before for cell counting. Triplicate wells were sampled at each time point, and duplicate cell counts from each sample were performed (below), resulting in 6 data points per time point per experiment. This experiment was performed 3 times, resulting in 18 data points per group per time point.

Data for each cell count was taken as follows. First, the total number of cells in each of the four corner grids of the hemacytometer were counted and noted. The average number of cells per milliliter of suspension was then calculated by averaging the number of cells per grid and multiplying by 10^4. The number of live cells (cells that did not take up the blue dye) were counted in the same grids and noted. Calculation of the average number of live cells per milliliter was the same as for the total. Dividing the number of live cells per milliliter by the total number of cells per milliliter, and multiplying by 100 determined percent viability.

2.2.4 Determination of growth kinetics

To determine the generation time of HMEC-1 cultures under control and treatment conditions, determination of the number of generations (*n*) during the trials was required, as well as the time in exponential growth (*t*), and finally the generation (doubling, *g*) time of HMEC-1 cells. Illustration 5 represents a typical growth curve, and the values used to determine growth kinetics. The control group was used as a reference for maximal cell counts per well, as well as the normal growth kinetics of HMEC-1 cells. The time the control HMEC-1 started to double (t_o) was subtracted from the time the culture reached the confluent, or plateau phase, of growth (t_f), which was represented by *t*.

Illustration 5: Ideal growth curve & values used for determination of growth kinetics

"Initial" represents the initial number of cells seeded into the chambers, which lagged for 24 to 48 hours until growth began. The value representing this seeding density was N_o. At time t_o, this seeding density began to enter exponential growth. When cell density reached a plateau, the final number of cells were recorded (N_f) at the time the cells reach maximal density (t_f). From these values, the exponential growth equation was calculated, and points along the growth curve with coordinates (N, t) were determined (equations outlined in Section 2.2.4).

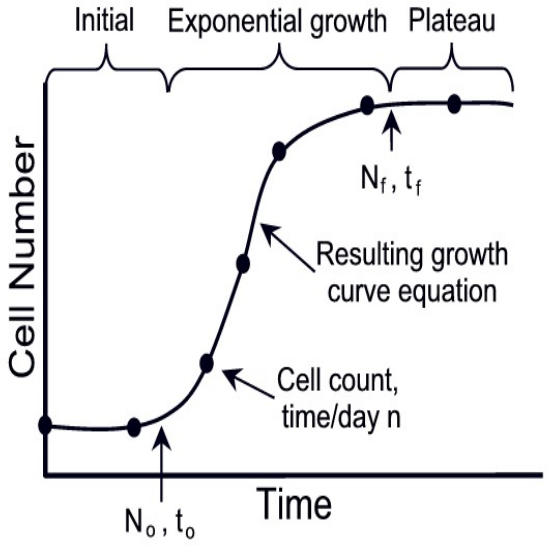

To determine the number of cell doublings (represented by *n*) during time *t* ($t = t_f - t_o$), the classic microbiology doubling equation $n = 3.3(\log N_f - \log N_o)$ was used. N_f was the final number of cells (at plateau), and N_o was the number of cells in culture when

doubling began. Using t and n, doubling time (g, representing generation time) of the control HMEC-1 was determined by using the equation $g = t/n$.

For treatment groups, t varied. To extrapolate the time at which HMEC-1 would reach confluence, the growth data was plotted in terms of cell number versus time, and regression equations for each data set were generated.

Resulting exponential equations were used to determine the time of confluence by entering the maximum number of cells observed in the control group in the place of x. The resulting y value was the time of plateau, and was used to calculate t. After t was determined, g was calculated using the equation listed above.

2.2.5 CE persistence analysis using gas chromatography-mass spectrometry

Since the spontaneous hydrolysis or metabolism of CE in culture medium was a possibility, extraction of the CE from the media of one of the growth experiments was needed for analysis (Section 2.2.3). The method of CE detection that was used was a modified version of the method reported by Burdick and colleagues [158] that was designed for efficient detection of cocaine and its metabolites in small volumes of rat blood.

During one of the growth curve trials, 1-mL samples of media (n=2 per time point, per group) were collected for the determination of CE concentration. Each sample was spiked with deuterated CE (CE-d5) in acetonitrile at a concentration of 10 μg/mL and mixed. Bond Elut Certify™ solid-phase extraction columns were placed on a vacuum chamber. Columns were conditioned by eluting 2 mL of high-grade methanol by gravity, to activate the bonded silica solid phase. Then 2 mL of phosphate buffer (0.1 M dibasic potassium phosphate, pH 6.0) was used to equilibrate the solid phase. Samples containing CE and deuterated internal standard were applied to the columns, and washed with 6 mL of reagent grade water to remove salts and impurities, followed by 3 mL of 0.1 N HCl under vacuum. Columns were washed with 9 mL of methanol and CE and internal standard trapped in the bonded phase of the column was eluted with 2 mL of methylene chloride:isopropanol (4:1, v/v) containing 2% (v/v) ammonium hydroxide.

Eluent containing CE and CE-*d*5 was dried under a slow stream of nitrogen at 40^{o}C. After drying, samples were re-suspended in 50 μL of toluene, transferred to amber glass GC vials containing glass inserts for small sample volumes. Vials were tightly capped with Teflon-lined caps, sealed with a band of Parafilm, and frozen at –20^{o}C until all samples were collected, extracted, and frozen for at least 24 hours.

Along with the media samples, a standard curve of CE was prepared in fresh MCDB131 media and similarly extracted. The standard curve included 0, 31.7, 108.5, and 317 μg/mL CE (equivalent to 0, 0.1, 0.5, and 1 mM), and was spiked with 10 μg/mL of CE-*d*5. Controls run with the standard curve and samples included an unextracted CE-*d*5 blank, and an unextracted, untreated media blank. Controls were included to confirm that untreated media did not contain CE or ions with similar properties, and that the extraction process did not significantly alter the concentration of CE-*d*5 (and hence the concentration of CE) in the samples, although a small percentage of loss was expected.

A Hewlett-Packard 5890 Series II gas chromatograph in series with a 5971 Series mass-selective detector was used to quantify the CE in the media samples. Vials were thawed and the Parafilm removed, and loaded onto auto sampler trays. One (1) mL volumes were injected using Hewlett-Packard 7673 Automatic Injection and glass syringes.

Parameters for detection were: injector temperature 280^{o}C; solvent delay 5 minutes; oven temperature 150^{o}C with increase at a rate of 20^{o} per minute until 300^{o}C; hold 10 minutes; total run time 17.5 minutes; detector interface 300^{o}C [158]. Selective ion monitoring (SIM) was used for ions m/z = 196, 201, 317, and 322 was used. Quantitative ions for CE and CE-*d*5 were 317 and 322, respectively, and the 196 and 201 ions were daughter ions used as qualifiers. Calibration of the standard curve with Chemstation 2.0 software was used to determine the CE concentration present in the media samples.

Duplicate samples per time point per group were used, and the average CE concentration was plotted versus time for statistical analysis. “Decay” rates were determined by regression analysis.

2.2.6 Viability of confluent cells

Viability of confluent HMEC-1 was of particular interest because an endothelial monolayer best represents the *in vivo* microvascular endothelium. Since treatment with 1 mM CE was reported to affect HUVEC cell monolayer permeability without causing overt cytotoxicity [17], a 1 mM CE treatment was used in the HMEC-1 model.

HMEC-1 cells were seeded onto fibronectin-coated 6-well plates at a density of $1x10^5$ cells per well. The volume was brought to 5 mL per well with complete media. Cultures were incubated for three days at 37^{o}C and 5% CO_2 to allow the cells to form stable monolayers. After two days of incubation, the media was replaced with MCDB 131, (supplemented as described in Section 2.2.1, except for a 5% (v/v) FBS concentration to prevent excess cellular stimulation). At time “zero”, three wells from each group were trypsinized (0.5 mL per well) for 2-3 minutes at 37^{o}C and suspended in a final volume of 1 mL with PBS (0.5 mL per well), after media aspiration and rinsing with PBS. A 10-µL aliquot of the cell suspension was taken, diluted 1:1 with trypan blue solution, and then counted with the aid of a hemacytometer. The remaining wells were administered CE stock or MCDB131 (with 5% FBS, control) to final CE concentrations of 0 and 1 mM. Every 24 hours for three days, three wells per group were selected, and cell counts were performed as described in Section 2.2.3. Data for each cell count was collected as described for the growth curves.

2.2.7 Biochemical analyses

As with human serum, alterations in culture media gas, electrolytes, and glucose levels, and the appearance of products of altered respiration (lactate) in the media can suggest stress and disease conditions resulting from toxic insult [113]. Gases (pO_2 and pCO_2) can be useful to toxicity assessment because of their role in aerobic metabolism [113]. Along with shifts in gas pressures, pH levels can be indicative of altered cellular

metabolism and gas consumption. Directly related to the pH of the media is the amount of HCO_3^- present in the media. HCO_3^- is used as a buffer in cell culture media to prevent rapid pH changes that result from temperature or gas changes. Thus, HCO_3^- levels may also be useful indicators of cytotoxicity caused by acidotic or hypermetabolic changes in the culture [113]. A benefit of such an analysis is that more subtle changes in cellular stasis could be detected, because biochemical monitoring allows for degrees or "shades" of toxicity, whereas viability and cytotoxicity assays often result in absolute, "black and white" or "yes/no" answers.

Electrolyte concentrations are monitored in humans because of their importance in cellular function in general. The proper operation of ion channels is pivotal to cell culture maintenance and survival. Thus, maintaining the balance of electrolytes such as ionic calcium (Ca^{2+}), or total (ionic + complexed) Mg, K, Na, and Cl is central to culture health, and an observed alteration in that balance could provide evidence of altered cellular function that results from injury [56, 113, 116, 159].

Glucose is central to cellular health because it is the main energy source to most cells in the body [56, 113, 116, 159]. Thus, confluent cell culture can be expected to consume glucose at a fairly constant rate. Increases or decreases in the rate of glucose consumption, and resulting alterations in media glucose levels, can indicate an alteration in the culture's ability to perform aerobic respiration. This is an important indicator of toxicity [56, 113]. In addition, when cultured cells are injured, affecting aerobic respiration, the cells often switch to anaerobic respiration (glycolysis), which is an inefficient pathway for glucose utilization in cells. The main product of this alternate pathway is lactate, which promotes acidosis. Lactate is produced normally in cell cultures in low levels, but an increase resulting from injury is usually indicative of cytotoxicity [113, 159].

Few recent studies have utilized basic clinical measurements to evaluate the effect(s) of potentially toxic chemicals on cells or tissues, despite their usefulness in the clinical setting, and potentially in model development. This study was conducted to

assess the basic biochemical effects of CE exposure on monolayers of HMEC-1. A limited number of common analytes were chosen to maximize the assessment of HMEC-1 function after exposure to 1 mM CE. Specifically, culture media pH/[H^+], bicarbonate (HCO_3^-), oxygen (pO_2), carbon dioxide (pCO_2), sodium (Na), potassium (K), ionized calcium (Ca^{2+}), magnesium (Mg), and chloride (Cl), glucose, and lactate levels were monitored over a period of 72 hours, using several time points (below) after treatment with 1 mM CE.

Three analytical instruments were utilized. The AVL OMNI blood gas analyzer (Roche Diagnostics, Indianapolis, IN) used with a series of gas- and ion-specific electrodes to measure levels of pH, gases, and electrolyte concentrations. Levels of HCO_3^- were determined using the Henderson-Hasselbach equation ($pH = pKa + \log [HCO_3^-]/[H_2CO_3]$, the measured pH level in the sample, and the pKa (6.1) for carbonic acid (AVL OMNI instruction manual and [113]). The HCO_3^- in the equation is calculated from $\alpha(pCO_2)$, where α (the solubility constant for CO_2) is 0.0301 (AVL OMNI instruction manual and [113]). The VITROS 250 chemistry system and the VITROS 950A chemistry system (Ortho Clinical Diagnostics, Raritan, NJ) were used for measuring the concentrations of the other electrolytes, glucose, and lactate. The VITROS analyzers utilize potentiometric and reflectance spectrophotometry to measure levels of analytes in aqueous samples.

HMEC-1 cells were seeded onto T75 flasks at a density of $1x10^5$ cells per cm^2. After allowing 20 minutes for the attachment of healthy cells, the excess was aspirated, 30 mL of MCDB131 media was added, and flasks were incubated at 37^oC and 5% CO_2 for 48 hours. The media was replaced with MCDB131 media containing 5% FBS (v/v). After additional incubation for 24 hours, triplicate baseline samples of media (1 mL per flask) were collected, and the monolayers were treated with media, CE stock, or media pH-adjusted to that of the CE stock, but not containing CE, to a final concentration of 0 or 1 mM CE. This time point was considered “time zero”. After gently mixing in the added components, another 1 mL sample of media was taken from each flask, and all

flasks were returned to the incubator. All samples were transferred in glass test tubes, capped immediately, and taken to the University of Texas Medical Branch Clinical Chemistry Laboratory for analysis.

Media pH, bicarbonate, pO_2, pCO_2, and Ca^{2+}, K, and Na were determined in each sample using the AVL OMNI blood gas analyzer. It was important that the gases be run first, since de-capping a tube to run other analyses would alter gas levels and pH. Next, 300 μL aliquots of media were placed on a VITROS 250 chemistry machine for glucose, Cl, and Mg determinations, and on a VITROS 950A (Ortho Clinical Diagnostics, Raritan, NJ) system for the determination of lactate.

All samples for each trial were taken from the same set of triplicate T75 flasks, to ensure continuity between samples. Thus, after one hour of treatment, the flasks were removed from the incubator, sampled as before, and returned as quickly as possible. All determinations were repeated after 4, 12, 24, 48, and 72 hours of CE treatment.

2.2.8 LDH release assay

Lactate dehydrogenase (LDH) is a cytosolic enzyme that is retained in healthy cells, but escapes from damaged cells [56, 113, 159]. Thus, a common test for cytotoxicity in *in vitro* toxicological testing is the LDH release assay, which is typically reported as a per-cent of cellular LDH released into the media [160]. LDH levels in media were monitored to determine the cytotoxicity of CE in the HMEC-1 model. However, since all samples in a trial were taken from one set of flasks, determination of total and final cellular LDH levels was not possible. Thus, all determinations were in terms of media LDH activity in (units of LDH activity per liter of volume, U/L), and compared as such against controls.

HMEC-1 cells were seeded onto T75 flasks, incubated, and treated as for the biochemical determinations (above). Before treatment, and at times zero, 1, 4, 12, 24, 48, and 72 hours, 1 mL samples were collected in glass tubes, capped, and taken for analysis to the UTMB Clinical Chemistry Division. LDH was determined in each sample using a VITROS 250 chemistry analyzer (Ortho Clinical Diagnostics, Raritan, NJ). The analysis

utilizes and measures the catalytic activity of the enzyme by measuring NAD^+ generated over 5 minutes in the presence of pyruvate and NADH. The rate of catalysis is expressed in U/L (VITROS handbook, and [113]).

2.2.9 MTT assay

MTT (3-[4,5-dimethylthiazol-2-yl]-2,5-diphenyl tetrazolium bromide) is reduced to a colorimetric formazan product by mitochondrial oxidases in living cells. The measurement of MTT reduction is commonly performed for cytotoxicity in confluent cultures exposed to a potentially toxic compound [161, 162], as in the HMEC-1 model. Alterations in MTT reflect average cellular oxidative capacity, since the cell number is consistent throughout the analysis [160-164]. Since MTT reduction assay enabled evaluation of another potential cytotoxic manifestation in the HMEC-1/CE exposure model (altered mitochondrial oxidative capacity), it was employed as a second measure of cytotoxicity in the HMEC-1/CE exposure model.

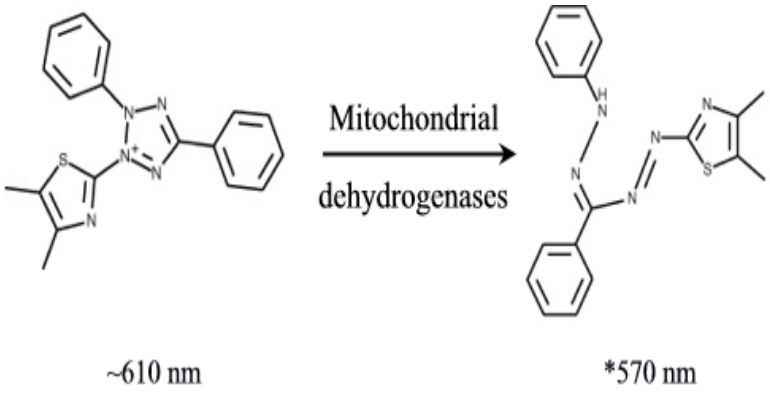

Illustration 6: MTT reduction to formazan

Mitochondrial dehydrogenases catalyze the opening of the tetrazolium ring at the center of the MTT molecule, resulting in MTT formazan production.

HMEC-1 cells were seeded onto fibronectin-coated ELISA plates at a density of $1x10^5$ cells. The top row, bottom three rows, and right half of each plate was left dry. After 20 minutes, non-adherent cells were aspirated, and 200 μL of MCDB 131 complete media was added to each well. Plates were placed in an incubator at 37°C and 5% CO_2 for 48 hours, at which time the media in each cell-containing well was replaced with 200 μL of MCDB 131 complete media. Plates were incubated for another 24 hours.

Plate layout for analysis was as follows:

Row 1 was left dry for control blank,

Row 2 contained cells only (no CE, no MTT),

Row 3 contained cells and CE (no MTT),

Row 4 contained cells and MTT (no CE),

Row 5 contained cells, CE, and MTT.

In each trial, three plates per time point (baseline, time zero, 1, 4, 12, 24, 48, and 72 hours) were prepared and analyzed.

For baseline and time-zero readings, 100 μL of the media was removed from each well containing cells. Eleven (11) μL of a 5-mg/mL suspension of MTT was added to each well of the corresponding rows, and the plates were returned to the incubator for two hours to allow for reduction of MTT to formazan. After 2 hours, 100 μL of MTT solubilization solution [10% (v/v) Triton X-100 and 0.1N HCl in anhydrous 2-propanol] was added to each well. The well contents were tapped to gently mix the contents, and the absorbance of each well was read at 570 nm using a Bio-Rad (Hercules, CA) microplate reader. The absorbance of the six wells in the top row was averaged to represent the background. This number was subtracted from all other readings to normalize the signal, and then groups were compared.

For one-hour readings, 100 μL of media was removed from each well containing cells. MTT suspension was added (11 μL, 5 mg/mL), and the plates were returned to the

incubator for one hour, at which time the corresponding wells were treated with either media or CE stock to a final concentration of 0 or 1mM CE. Plates were returned to the incubator for another hour, to allow for MTT reduction to formazan and CE exposure. Two hours after addition of MTT (one hour after CE treatment), 100 μL of solubilization solution was added to each well. Mixing, reading of absorbance, and normalization of results proceeded as before.

For the remaining time points, no media was removed from the wells at the beginning of the assay (since the media was needed for the long incubations). Corresponding wells were treated with either media or CE, and incubated for the prescribed time of treatment. For these time-points (4, 12, 24, 48, and 72-hours), 22 μL of MTT (5 mg/mL) was added to the corresponding wells at 2, 10, 22, 46, or 70 hours post-treatment, and the plates returned to the incubator for the remaining two hours of CE exposure. At the end of each time point, 100 μL of media was removed from each well and replaced with 100 μL of solubilization solution. Mixing, reading of absorbance, and normalization of results proceeded as before.

2.2.10 Statistical analysis

Triplicate results for each group from three separate trials were used for statistical analysis. One-way analysis of variance was used to determine point-to-point significance within and between groups using NCSS-PASS 2000 Dawson Edition, a student's statistical package. [This package was used for all of the statistical analysis in this dissertation.] The dependent factor tested within groups was time; for between-groups testing the dependent factor was CE treatment. All one-way ANOVA was performed versus baseline or control (0 mM) treatment. A p value of 0.05 or less was significant for either test.

2.3 METHODS – AIM TWO: ASSESS THE MORPHOLOGICAL/BARRIER EFFECTS OF CE EXPOSURE

2.3.1 Cell maintenance/culture

HMEC-1 cells were maintained as outlined in Section 2.2.1.

2.3.2 CE stock preparation

CE fumarate was prepared and stored as outlined in Section 2.2.2.

2.3.3 Transmission electron microscopy (TEM)

Ultrastructural changes in cells, as evaluated relative to the biochemical or metabolic alteration, provide compelling evidence of toxicity, as well as indicate affected targets. To further characterize the effect of CE on the morphology of HMEC-1 cells, TEM was used.

HMEC-1 cells were seeded onto round, 13 mm Thermanox cover slips (placed in the wells of 24-well culture plates) at a density of 1 x 10^5 cells per cm^2. After 20 minutes, non-adherent cells were aspirated and MCDB131 media was added. Cultures were incubated at 37^{o}C and 5% CO_2 for 48 hours, at which time the media was replaced with MCDB131 media. Cultures were then returned to the incubator for an additional 24 hours.

Baseline samples served as untreated controls, which were fixed with 1 mL per well of Ito fixative [1.25% formaldehyde (v/v), 2.5% glutaraldehyde (v/v), 0.03% $CaCl_2$ (w/v), 0.03% trinitrophenol (v/v), and 0.05 M cacodylate buffer, pH 7.3). Freshly fixed monolayers were chilled at 4^{o}C in the dark for 24 hours. Remaining monolayers were treated with 1 mM CE and incubated until the end of each time point. Each set of monolayers was similarly fixed and chilled.

All fixed monolayers were processed for TEM in the University of Texas Medical Branch Department of Pathology Electron Microscopy Laboratory. For this process, fixed cover slips were washed three times in 0.1 M cacodylate buffer and post-fixed with 1% (w/v) osmium tetroxide in 0.1 M cacodylate buffer. Samples were then washed three

more times in cacodylate buffer, once in 0.1 M maleate buffer, and stained with 1% (w/v) uranyl acetate in 0.1 M maleate buffer. Stained samples were washed four times in maleate buffer, and dehydrated stepwise in 50%, 75%, 95%, and 100% (v/v) ethanol. Dehydrated samples were then progressively infiltrated (stabilized) with stepwise ratios of propylene oxide and Poly Bed™ 812 (Polysciences, Warrington, PA), until pure Poly Bed™ was used. Samples were embedded in plastic and allowed to polymerize overnight at 60^{o}C. Polymerized sample blocks were sectioned on a Reichert-Leica Ultracut S ultramicrotome. Ultrathin sections were examined in a Philips 201 transmission electron microscope (Philips, Bothell, WA) at 60 cV (centi-Volts) after staining with lead citrate (Reynold's stain). Images were captured to Kodak film at 4,800x magnification and photographically enlarged to 14,100x magnification.

2.3.4 Silver staining

Silver staining has been used to visualize changes in monolayer permeability/barrier integrity [17, 155, 165]. This method was used to confirm the results reported by Kolodgie *et al* [17], as well as compare the results from their HUVEC model to those from the HMEC-1 model. Note: The water used for rinsing and mixing of reagents in this method was Milli-Q™ 18 MΩ reagent grade water. If chloride is present in the water used, the silver will form an silver chloride precipitate.

HMEC-1 cells were seeded in 2-chamber culture-slides at a density of 1x10^{5} cells per cm^{2}. Slides were assigned time points immediately before seeding (0/baseline, 15, and 30 minutes, and 1, 4, 12, or 24 hours) to prevent later bias. After 20 minutes, non-adherent cells were removed, and the media was replaced with fresh MCDB131 complete media. Cultures were incubated for 48 hours, at which time the media was replaced with MCDB131 complete media. Cultures were returned to the incubator for another 24 hours. On each slide, the left chamber was treated with MCDB131 complete media, and the right chamber was treated with CE stock to a final concentration of 0 and 1 mM CE, respectively. This minimized variation in handling between treatment groups.

At the end of each time point, media was aspirated and the monolayers were fixed with 10% (v/v) formalin for 20 minutes. Chambers were left on the slides until fixation was complete to prevent damage to the monolayers, and gently removed after the fixation step. Slides were then dipped ten times each in two Coplin jars containing water, then immersed in a 1% (w/v) solution of freshly prepared aqueous silver nitrate. The jars were capped and placed in the dark for a 10-minute incubation. Slides were placed in open 100 mm Petri dishes, covered with water, and exposed to 100-watt incandescent light for one hour, counterstained with Kernechtrot's nuclear fast red for 5 minutes, rinsed with water, tapped dry, and mounted with Permount™ and a cover slip. Mounting medium was allowed to set overnight. Clear nail polish was used to seal the outer edges of the cover slips.

Silver stained monolayers were viewed under a Nikon (Japan) Diaphot inverted light microscope at 100x. Images from pre-determined areas of each monolayer were captured with an attached Nikon digital camera. A scale marker was also imaged at 100x and its image captured (courtesy of T. Bednarek, UTMB, Department of Pathology), so that a scale bar could be prepared for each image.

2.3.5 Trans-endothelial resistance/electronic cell substrate impedance sensing (ECIS)

When barrier integrity of an endothelial monolayer is compromised via the formation of intercellular gaps and loosening of gap, adherens, and tight junctions, the electrical resistance across that barrier is reduced (Illustration 7, below) [17, 119, 131, 153]. Thus, the trans-endothelial resistance of a monolayer is inversely proportional to the permeability of that monolayer. Since pairing morphological results with such kinetic data would provide compelling evidence of pro-inflammatory changes in CE-treated HMEC-1, kinetic resistance measurements in the HMEC-1 model were performed using Electronic Cell-Substrate Impedance Sensing (ECIS, Applied BioPhysics, Troy, NY).

ECIS can be used to monitor trans-endothelial electrical resistance of cell monolayers, reflecting their permeability. The 10 electrodes in each chamber were

randomly dispersed so that averages could be taken from pre-determined locations, reducing bias and presenting a more representative resistance reading for the cell monolayers. The media present in the chamber provided electrolyte solution needed for resistance measurement, and resistance was fully dependent on monolayer confluence, since no-cell control chambers showed minimal resistance (Chapter 3).

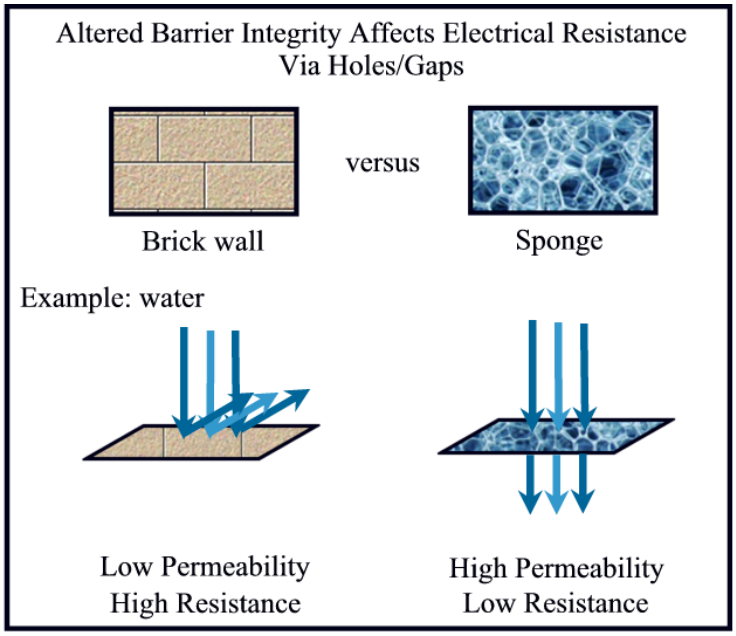

Illustration 7: Relationship between electrical resistance and permeability

HMEC-1 cells were seeded onto 6 of 8 fibronectin-coated ECIS electrode chambers on a chamber array with 10 electrodes per chamber at a density of $1x10^5$ cells per cm^2. Media in each chamber (including the two wells not containing HMEC-1 cells) was brought to 0.5 mL. The chamber array was immediately attached to the ECIS, and resistance monitoring was used to determine when confluence was reached (average was 40 hours). After at least 24 more hours of stable resistance, the monitoring was paused. To begin the analysis, a baseline resistance reading was taken (for 2 hours), and 3 of the 8 wells were treated with 10 mM CE stock to a final concentration of 1mM. Control and cell-free wells were given an equal volume of complete media. Since ECIS is capable of constant monitoring of cultures, the assay was run constantly for 72 hours. Resistance

measurements were saved to CD-ROMs, and included data spreadsheets of the run, as well as graphs resulting from the resistance readings.

2.3.6 Statistical analysis

Given the qualitative nature of the microscopic investigations, the general magnitude of effect was used as the determinant for significance. Dr. V. Popov (UTMB, Department of Pathology), who was blinded to the anticipated effects of CE on the HMEC-1 cultures, and Dr. H. Hawkins (UTMB, Department of Pathology), who had knowledge of the anticipated results, but was blinded to the treatment time for each image, provided interpretations of TEM images.

Viewing of silver stains was performed with blinding to time point to minimize bias. One viewer (D. Tacker) evaluated randomly chosen points on each slide, comparing results from the control well to the treated well based on the presence or absence of gaps. Gaps were also judged based on their general size, and whether they were continuously open through the HMEC-1 cell monolayer. At least three separate slides per CE treatment time point were viewed. Five (5) separate, random coordinates per well were chosen before viewing to minimize sampling bias.

For resistance measurements, average resistance values were taken from specific points (baseline, 0, 1, 2, 3, 4, 5, 6, 12, 24, 36, 48, 60, and 72 hours after treatment) in each database and compared between groups using paired, two-tailed student's t-test (equal variance). Point-to-point significance within groups was detected using one-way analysis of variance (ANOVA) relative to time "0" with time as the dependent factor. Significance was established at $p<0.05$. Three experiments with triplicate sampling per treatment group (duplicate sampling for background) were performed for statistical analysis.

2.4 METHODS – AIM THREE: ASSESS THE EFFECTS OF CE ON HMEC-1 INTRACELLULAR CATION LEVELS

2.4.1 Rationale for intracellular cation quantitation

Alterations in intracellular levels of calcium and magnesium are known to affect a wide range of cellular functions, and underlie an array of pathologies [113, 160, 166, 167]. Since cytosolic calcium levels are associated with mobilization of the actin cytoskeleton and signal transducers, assessment of the effects of CE treatment on HMEC-1 calcium flux was included in Aim Three. Also, since magnesium is known to counter-act calcium in such situations [167], and act as a co-factor for kinase activity [113, 129, 130], it was included in these studies.

2.4.2 Cell maintenance/culture

HMEC-1 cells were maintained as outlined in Section 2.2.1.

2.4.3 CE stock preparation

CE fumarate was prepared and stored as outlined in Section 2.2.2.

2.4.4 Preparation of monolayers & loading with indicator

HMEC-1 cells were seeded onto human fibronectin-coated, custom-cut 13 mm x 12 mm glass cover slips (placed in 60 mm culture plates) at a density of $1x10^5$ cells per slip [166]. After 20 minutes, non-adherent cells were aspirated and 5 mL of MCDB 131 media were added to each plate. Plates were prepared on stainless steel trays to prevent spilling and contamination, and prepared trays were incubated at 37^oC and 5% CO_2 for 72 hours.

Two approaches were used for calcium analysis. To explain the differences between the two approaches, Illustrations 6 and 7 (below) have been provided. Modified protocols from Faury and co-workers [166] and Okorodudu and colleagues [167] were used for intracellular ion determinations. For indicator loading, media was aspirated from the monolayers, which were rinsed twice with 5 mL of Tyrode buffer (137 mM NaCl, 2 mM KCl, 1.2 mM $CaCl_2$, 1 mM $MgCl_2$, 10 mM HEPES, and 10 mM glucose). The indicator loading buffer was composed of 4.8 mL of Tyrode buffer, 0.2 mL of 2% (v/v)

pluronic F-127 in reagent-grade water, and 25 μM of Fura-2 AM or Mag-Fura-2 AM, which were suspended in anhydrous dimethyl sulfoxide (DMSO) at a concentration of 1 μg/μL. Freshly prepared indicator loading buffer was added at 5 mL per plate. Plates were placed in a 37^{o}C water bath for 30 minutes to allow loading of the indicator (literature from Molecular Probes, and [166, 167]).

After loading was complete, plates were washed four times with 5 mL of Tyrode buffer. Another 5 mL of Tyrode buffer was added to each plate, and then plates were placed in the dark at room temperature for 1 hour. Note: This incubation was required to allow for ester cleavage to activate the indicator [167]. For pre-treatment experiments, this was the point at which CE was added to the plates at a final concentration of 1 mM.

Once the one-hour incubation was complete, slips were ready for analysis. To analyze the intracellular cation levels of each monolayer, quartz cuvettes (1 cm x 1 cm, all sides clear) were used. Each cuvette contained 2.1 mL Tyrode buffer, a small stir bar, and a "stir sleeve", which was a custom-milled Plexiglas™ square with a hole in the center to accommodate the stir bar. This sleeve allowed the stir bar to move with the cover slip positioned above it, on top of the sleeve.

Plates were removed from the dark and the Tyrode buffer was aspirated and replaced. A rubber spatula/scraper was used to lift a cover slip out of the plate (plates were promptly returned to the dark). Selected cover slips were then lightly touched to a Kimwipe (at an angle) to blot off excess Tyrode, lifted from the scraper with a pair of forceps, and positioned diagonally in the prepared cuvette (across the top left to bottom right corners). Orientation of the monolayer was to the rear of the cuvette. The cuvette was cleaned to remove fingerprints and oils on the outside surfaces, then positioned in its holder in a Hitachi (Japan) F-2000 spectrofluorimeter, which was equipped with a circulating water bath to maintain temperature (37^{o}C) in the cuvette during analysis.

2.4.5 Ion analysis programs & wavelengths

The Hitachi spectrofluorimeter contained the separate programs for ion analysis. For calcium determinations, excitation wavelengths of 342 nm and 375 nm were used. The 342 nm wavelength excited bound Fura-2, and the 375 nm wavelength excited free Fura-2, once the indicator was separated from the AM (acetoxymethyl) ester group. The spectra resulting from these excitations and the emission at 510 nm were used to determine intracellular calcium levels using a ratiometric approach, described in Section 2.4.8 (below). For intracellular magnesium experiments, excitation wavelengths were 335 nm (bound) and 370 nm (free), and the emission wavelength was 510 nm.

For "immediate exposure" experiments, run times were 700 seconds to accommodate for all treatments needed to determine concentration. Such treatments included injection of CE, injection of digitonin to stimulate maximal intracellular ion levels, and injection of EGTA to chelate ions to their minimal intracellular levels. The latter two treatments are requisite for determining maximal and minimal free ion ratios, which are essential to the final determination of intracellular ion concentration at any point in the run. This is explained in more detail below.

For 1-hour CE pre-treatment experiments, run times were 400 seconds. Treatments during a run included stimulation of maximal intracellular ion concentration with digitonin, and chelation of intracellular ions to their minimal concentration with EGTA. This is explained in more detail below.

2.4.6 "Immediate exposure" experiments

The immediate effects of CE on intracellular calcium and magnesium were observed with the following approach (Illustration 8). Samples were given approximately 200 seconds to equilibrate in the spectrofluorimeter, and then an experiment was started. The first 100 seconds was used to obtain baseline cytosolic ion levels. At 100 seconds, 21 μL of 0 or 100 mM CE stock (prepared in Tyrode buffer) was injected into the cuvette through a channel in the top of the analyzer (final CE concentration, 0 or 1 mM). Samples were given 5 minutes (300 seconds) to respond to the CE. At 400 seconds, 7.5 μL of 2%

(w/v) digitonin suspension (in absolute ethanol, final concentration 0.007% v/v) was added, and the sample was given 200 seconds to achieve maximal intracellular ion levels.

At 600 seconds, EGTA (0.5 M in water) was added in 1- to 3 μL increments until chelation was complete. The goal was to add EGTA until the graphs for bound indicator and free indicator met, but did not cross. If the graphs crossed due to excessive chelation, the time point just before crossing was determined the endpoint of the analysis, so that proper calculation of cation levels would be possible. Total time of analysis was 700 seconds per sample. Once the experiment was complete, tracings and ratio calculations were utilized for calculation of ion concentration (described below).

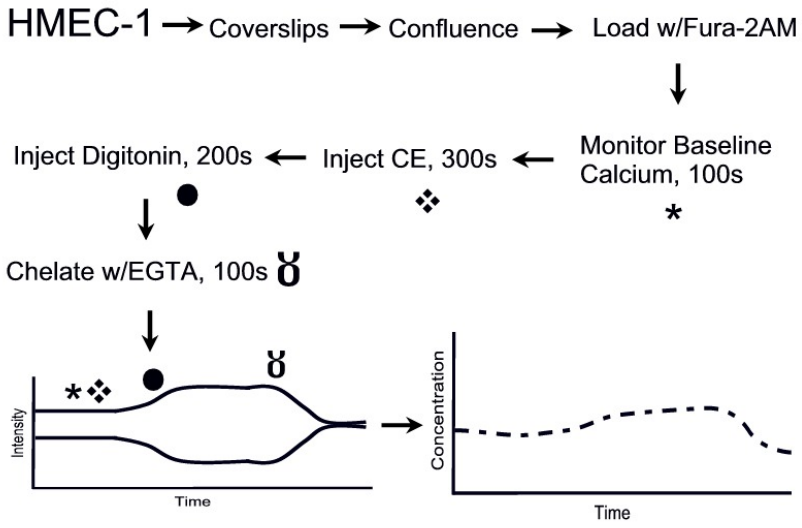

Illustration 8: Experimental design for the immediate exposure studies

This approach was used to track cytosolic calcium and magnesium in CE-treated HMEC-1 over a 5-minute exposure.

2.4.7 One-hour CE pre-treatment experiments

In this series of experiments, samples were incubated with either Tyrode buffer, or Tyrode buffer containing 1mM CE during the one-hour incubation in the dark. Preparation of cuvettes and slips was the same as before. The approach for the pre-treatment experiments is shown in Illustration 9.

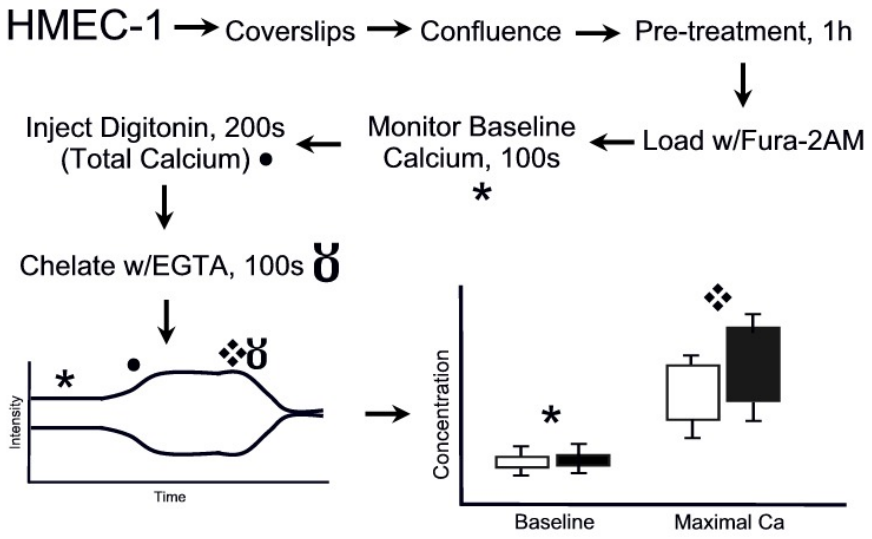

Illustration 9: Experimental design for the pre-treatment experiment

This approach was used to determine baseline cytosolic calcium, and then total cellular calcium, after a one-hour pre-treatment with CE in the HMEC-1 model.

Samples were allowed to equilibrate for 200 seconds in the spectrofluorimeter before each experiment was started. Fluorescence of free and bound indicator was tracked for 100 seconds to establish a baseline signal using software intrinsic to the F-2000 system. At 100 seconds, 7.5 μL of 2% (w/v) digitonin suspension [in absolute ethanol, final concentration 0.007% (v/v)] was added, and the sample was given 200

seconds to achieve maximal intracellular ion levels. At 300 seconds, EGTA was added in 1- to 3 μL increments until chelation was complete. The goal was to add EGTA until the graphs for bound indicator and free indicator met, but did not cross. If the graphs crossed due to excessive chelation, the time point just before crossing was determined the endpoint of the analysis, so that proper calculation of cation levels could be made. The total run time was 400 seconds per sample. Once the run was complete, tracings of the run, as well as ratio calculations, were printed and used for calculation of ion concentration (described below).

2.4.8 Data collection

Each successful experiment that reached completion with timely treatments was printed. The graphs for each excitation wavelength were traced, and the results printed for every ~25 seconds between 0 and 400, or the end of the experiment if the graphs crossed. Graphs of experiments followed a general trend, as shown in the Illustration below:

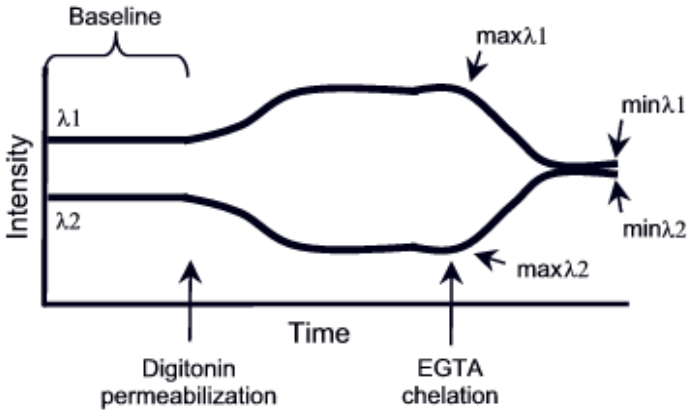

Illustration 10: Ideal cation readout on the Hitachi F2000

Intensity of excitation at each wavelength (λ1, λ2) was monitored against the time of the run (in seconds). Cell membrane and organelle permeabilization with digitonin resulted in maximal Ca^{2+} (max λ 1, 2), and minimal Ca^{2+} was obtained using EGTA chelation (min λ 1, 2).

Data printed from each experiment were used to calculate intracellular cation levels at each time point using the following calculations (F2000 Handbook and [167]):

Equation1: $R = F(\lambda 1) - Z1 / F(\lambda 2) - Z2$

Equation2: $C = K * (R - R_{min})/(R_{max} - R) * (F_{min}(\lambda 2)/F_{max}(\lambda 2));$

R represented a ratio of data results. The Z values represented auto-fluorescence measurements for each wavelength (λ), which were obtained by recording the fluorescence of a cover slip containing cells without indicator (unloaded cells). C represented free intracellular ion concentration at a given time, and K represented the K_d of the indicator (224 nM for Fura-2, 1.4 mM for Mag-Fura-2, Molecular Probes literature and [166, 167]). R_{max} and R_{min} were the highest and lowest resulting ratios from the run.

2.4.9 Calculation of intracellular cation concentrations

From the maximum and minimum excitation intensities for each sample, intracellular cation levels were calculated using the approach described above and Excel spreadsheets. Baseline and maximal values for each run and for each ion were compiled for comparison between control and treated groups. In "acute exposure" treatment groups, the intracellular ion concentrations during the 300-second CE treatment were also traced.

2.4.10 Statistical analysis

Triplicate runs from three or more separate experiments were used for analysis. Paired, two-sample Aspin-Welch t-test (unequal variance) was used to determine significance between groups at specific time points, and one-way analysis of variance was used for the detection of significance from baseline within groups, with digitonin or CE treatment as the dependent factor. Significance was achieved at $p<0.05$.

2.5 METHODS – AIM FOUR: DETERMINE THE EFFECTS OF CE EXPOSURE ON CALCIUM-DEPENDENT SIGNALING EVENTS

2.5.1 Cell maintenance/culture

HMEC-1 cells were maintained as outlined in Section 2.2.1.

2.5.2 CE stock preparation

CE fumarate stock solution was prepared and stored as outlined in Section 2.2.2, except that CE fumarate stock for EMSA analysis was prepared in calcium- and magnesium-free PBS at a concentration of 100 mM.

2.5.3 Measurement of inositol-1,4,5-trisphosphate (IP_3)

For IP_3 assays, HMEC-1 cells were seeded onto 6-well culture plates coated with fibronectin at a density of $2x10^5$ cells. Plates were incubated for 72 hours to allow the HMEC-1 to form confluent monolayers. To reduce serum sensitivity of the HMEC-1 cells during the experiment, existing culture media was replaced with fresh MCDB131 media 24 hours before the start of each experiment (48 hours after seeding).

For the analysis, monolayers of HMEC-1 cells were exposed to 1 mM CE for 0, 60, 150, 300, and 450 seconds (0, 1, 2.5, 5, and 7.5 minutes). Immediately after exposure, monolayers were placed on ice, washed with calcium- and magnesium- free PBS, and lysed with 1 mL per well of ice-cold calcium-and magnesium-free PBS containing 15% (w/v) TCA. A rubber scraper was used to scrape each well, and suspensions were transferred to chilled 1.5-mL microcentrifuge tubes and centrifuged at 2,000 x *g* for 15 minutes at 4^{o}C. Supernatants were transferred to conical tubes and washed three times with water-saturated diethyl ether (10 times the volume of the sample suspension). The aqueous fractions were transferred to fresh 1.5-mL microcentrifuge tubes on ice, and the pH of each sample adjusted to 7.5 with 10% (w/v) sodium bicarbonate (approximately 50 μL/tube). Samples were kept on ice until the IP_3 assay, which was always performed on the same day as the extraction.

The Biotrak™ IP_3 assay kit from Amersham Biosciences (Buckinghamshire, UK) was used with strict adherence to manufacturer's directions. Briefly, samples, blanks, and a standard curve were prepared. Samples were centrifuged for 15 minutes at 4°C and 2,000 x *g*, re-suspended in water and incubated for 15 minutes at room temperature. After vortexing, samples were transferred to scintillation vials, mixed with 10 mL of scintillant, and counted for 1 minute in a scintillation counter. Scintillation counts were reported in triplicate, and all samples were run in duplicate, resulting in six data points per sample. Three such experiments from separate passages of HMEC-1 cells were performed.

Since the assay is based on a competitive binding paradigm, decreases in radioactivity of the sample indicated increases in IP_3 levels in the cells studied. Radioactivity (in cpm) was converted to a "percent-bound" value for the standard curve using the following equation:

$$\%B/B_o = (\text{Standard/sample cpm} - \text{NSB cpm})/ (B_o \text{ cpm} - \text{NSB cpm}) * 100,$$

NSB cpm was the non-specific binding value (one of the blanks), and B_o cpm was the "zero-bound" value (another blank). These values were plotted against the standard concentrations to obtain a regression equation for the standard curve. The regression equation was then used to calculate the concentration of the samples obtained from the HMEC-1 treatments.

2.5.4 p38 MAP kinase assay

The Aim Four hypothesis was that calcium-dependent second messenger systems altered by CE exposure would cause downstream effects on other signaling components, such as second messengers, kinase cascades, and transcription factor activation. Since p38 MAPK is an important mediator of pro-inflammatory gene expression [130, 138, 168], phosphorylated (activated) p38 MAPK was measured in control, LPS-, and CE-treated HMEC-1 using sandwich ELISA kits obtained from R&D Systems (Minneapolis, MN). LPS treatment was a positive control [123, 124, 168]. Phospho-specific antibody included in the kit was highly specific, with a detection limit between 0 and 4000 pg/mL.

Manufacturer specifications for buffer formulations were used for all analyses, and the provided protocol was followed strictly.

For phospho-p38 MAPK assays, HMEC-1 cells were seeded in T150 culture plates (in triplicate) at a density of $5x10^6$ cells. Flasks were incubated for 72 hours to allow the HMEC-1 to form confluent monolayers of $3x10^7$ cells. To reduce reactivity of the HMEC-1 to the serum present in the media added during the experiment, media change with fresh complete media was performed 24 hours before each experiment began (48 hours after seeding).

For the analysis, HMEC-1 monolayers were exposed to 1 mM CE in complete media for 0, 1, 2, or 4 hours. Positive controls were treated with 0.1 μg/mL of *S. typhosa* endotoxin/LPS [123, 124, 168]. Negative controls were exposed to complete media containing no CE. Immediately after exposure, monolayers were returned to the incubator. At the end of each time point, the media was aspirated from each well. Monolayers were rinsed twice with calcium- and magnesium- free PBS. A cell scraper was used to remove cells from the culture plates, and one (1) mL of a lysis buffer composed of PBS, 1 mM EDTA, 0.005% (v/v) Tween 20, 0.5% (v/v) Triton X-100, 5 mM NaF, 6 M urea, Sigma protease inhibitor cocktail I (2 μL per mL of total buffer volume), Calbiochem phosphatase inhibitor cocktails I and II (10 μL per mL of total buffer volume), and PMSF (5 μL per mL of total buffer volume, stock was 1M) was added to each flask. Scraped cells in lysis buffer were transferred to 1.5 mL microcentrifuge tubes, vortexed, and aliquotted (333 μL), then frozen at –20°C until analysis.

Ninety-six-well ELISA plates were coated with capture antibody (3 μg/mL) in PBS overnight, after sealing, at room temperature. After rinsing three times with wash buffer [PBS with 0.05% (v/v) Tween 20], plates were blocked with blocking buffer [PBS with 1% (w/v) BSA, 5% (w/v) sucrose, and 0.05% (w/v) sodium azide] at room temperature for two (2) hours and rinsed with wash buffer.

Samples were centrifuged (2,000 x *g*) for 5 minutes at room temperature, transferred to fresh, pre-chilled microcentrifuge tubes, diluted to 1 mL with Diluent buffer #8 [composed of PBS, 1 mM EDTA, 0.005% (v/v) Tween 20, and 0.5% (v/v) Triton X-100], and vortexed. Prepared samples were kept on ice throughout the assays.

Eight (8) -point standard curves of phospho-p38 MAPK were prepared in duplicate for 0 to 4000 pg/mL of phospo-p38 MAPK. Blanks used in the assay included Diluent #3 [PBS with 1 mM EDTA, 0.005% (v/v) Tween 20, 0.5% (v/v) Triton X100, 5 mM sodium fluoride, and 1 M urea] and pure standard (30 ng/mL). Each blank was run in triplicate.

Blanks, standards, and samples were added to ELISA plates at 100 µL per well in duplicate. Plates were sealed and incubated on ice for 3 hours, well contents were aspirated, and plates were washed three times with wash buffer. One hundred µL of biotinylated detection antibody (250 ng/mL) was added to each well. Plates were sealed and incubated on ice for 3 hours in the dark. Well contents were aspirated and the plates were washed three times with wash buffer. Streptavidin/HRP conjugate was diluted 1:200 in PBS containing 1% (w/v) BSA and added to each well at 100 µL per well. Plates were incubated on ice for 45 minutes in the dark, and rinsed three times with wash buffer. Substrate solution, a 1:1 preparation of Sigma TMB solution and 0.03% (v/v) H_2O_2 in PBS, was added to the plates at 100 µL per well. After a 30-minute incubation at room temperature in the dark, stop solution (2 N H_2SO_4) was added to each well at 50 µL. Plates were gently tapped to mix the well contents, and immediately placed in a Bio-Rad (Hercules, CA) plate reader equipped with a 450 nm filter, with 690 nm readings serving as a background correction. Optical densities of all duplicate standards and triplicate samples were averaged.

Standard curves were established from the average optical densities of the standards run. Linear regression was used to determine the concentration of phospho-p38 in samples run with the assay. Phospho-p38 concentration in each sample was reported in picograms per 10^7 cells (pg/10^7 cells).

2.5.5 Electrophoretic Mobility Shift Assay (EMSA)

Rationale

The best way to determine whether intracellular changes are affecting gene expression is to evaluate activity in the nucleus. Transcription factors may be activated by cellular response mechanisms and resulting signaling, and migrate to the nucleus where they modulate gene expression (Illustration 11). Thus, the Electrophoretic Mobility Shift Assay (EMSA) becomes useful when trying to determine whether a particular cell stimulus results in nuclear localization and DNA binding of a given transcription factor [169, 170]. For example, the hypothesis was that CE elicits responses within HMEC-1 that result in pro-inflammatory gene (e.g., cytokine, adhesion molecule, and transcription

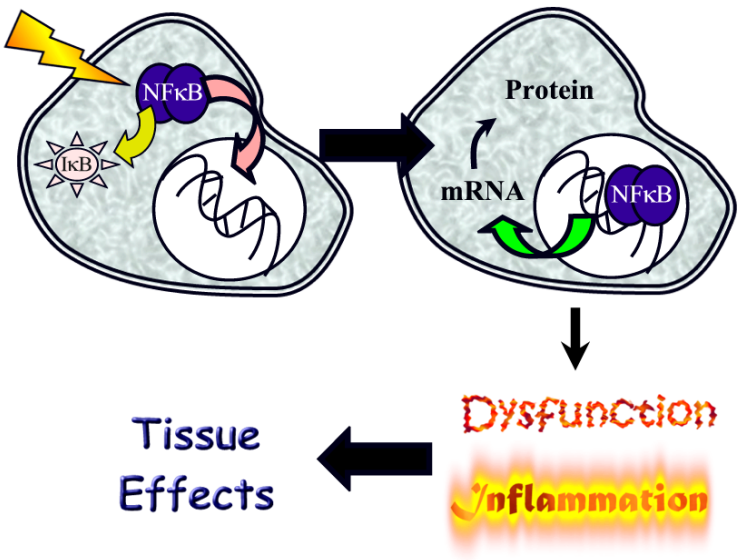

Illustration 11: Activation and effects of NF-κB DNA binding

Lightning bolt = stimulus (e.g. injury or cytokine stimulation). IκB releases the NF-κB dimer, and nuclear localization and DNA binding occur. This results in transcriptional activation of target genes that affect cellular survival and response.

factor) expression, and that NF-κB activation, nuclear localization, and DNA binding mediate this increase in expression, as shown in Illustration 10. The activation of NF-κB has been demonstrated in neurological cocaine exposure studies and is commonplace in pro-inflammatory responses of the endothelium [127, 137, 171-173], and given its

ubiquity [117, 129, 132, 137, 139, 140, 171-176], it was plausible that NF-κB could also be activated by CE exposure in the endothelium.

The principle of the EMSA is to use nuclear extracts taken from treated and control cells to determine which proteins and/or transcription factors have migrated to the nucleus [130, 132, 169, 170, 177]. Increases in DNA binding activity of transcription factors indicate two things [137, 169, 173, 177]. First, increased migration of a transcription factor to the nucleus suggests that the transcription factor has been activated, which is important in determining extra-nuclear targets for activation analysis. Second, migration of a transcription factor to the nucleus indicates that gene expression is likely to be altered (Illustration 11), since the activated transcription factor is likely to bind specific promoter regions on target genes, such as genes encoding other transcription factors, inhibitors, or cytokines [130, 132, 137, 169, 170, 173, 177]. Thus, EMSA was used to determine whether DNA binding activity of transcription factors occurred after HMEC-1 cells were exposed to CE.

Cold competition EMSA was used to establish specificity of the Ig oligonucleotide in the HMEC-1 cell extracts. Essentially, unlabeled ("cold") oligonucleotide is incubated in 50-fold molar excess with nuclear extract before addition of the labeled oligonucleotide. Specific binding of the unlabeled oligonucleotide blocks target binding sites such that the labeled oligonucleotide cannot bind, causing elimination of those bands from the EMSA. Thus, comparison of regular EMSA with a cold competition of the same extract enables identification of bands to be further analyzed using supershift assay.

Supershift assays were used to characterize specific NF-κB family proteins present in the nuclear extracts. The theory behind the supershift assay is that addition of the antibodies will result in an increased molecular weight of the transcription factor/DNA complexes being analyzed, which will cause the bands detected for specific transcription factors to supershift in the gel, or the antibody will block the binding site for the labeled oligonucleotide, thus causing the band of interest to be eliminated from of the

gel. This analysis is especially helpful when characterizing NF-κB DNA binding activity, due to the various sub-types and possible combinations of NF-κB family proteins that dimerize and bind DNA.

Extraction of nuclear protein from CE-treated HMEC-1

For nuclear protein extraction, HMEC-1 cells were seeded in five, T150 cell culture-treated flasks at a density of $5x10^6$ cells and allowed to come to confluence over 72 hours (per group). This density yielded approximately $1.5x10^8$ cells per group for nuclear extraction. Media was changed 24 hours before the experiment began (48 hours after seeding). Baseline samples were collected from untreated cells in all groups. For time-points, control HMEC-1 cells were harvested 1 or 4 hours after control media was added to the culture. Treated cultures were exposed to 100 mM CE stock in PBS (to a final dilution of 1 mM) for 1 or 4 hours. Positive controls were treated with 0.1 μg/mL of *S. typhosa* endotoxin for 1 or 4 hours [168]. At the end of treatment/exposure, cultures were rinsed with 10 mL of Ca- and Mg-free PBS. Flasks were placed on ice to halt cellular function. NOTE: After this point, all steps were performed on ice with ice-cold (0^oC) or cold (4^oC) buffers. Ten (10) mL aliquots (per flask) of ice-cold PBS were used to harvest the cells, which were scraped free from the plates with rubber scrapers. Cells were pelleted at 200 x *g* (Sorvall HS-4 rotor, RC-5B model centrifuge) for 10 minutes at 4^oC. Pellets were re-suspended in 1 mL of Ca- and Mg-free PBS and transferred to microcentrifuge tubes, and pelleted again at 200 x *g* for 5 minutes at 4^oC (1,500 rpm in a Jouan MR 14-11 microcentrifuge).

Nuclear extraction proceeded as described by Dyer and Herzog [169] and Bassett *et al* [177], with modifications. After washing, cell pellets were re-suspended in 1.0 mL of ice-cold lysis buffer. The sucrose buffer I core buffer contained 0.32 M sucrose, 3 mM $CaCl_2$, 2 mM magnesium acetate, 0.1 mM EDTA, and 10 mM Tris HCl pH 8. Reagents added just before buffer use included 1 mM DTT, 10 mM PMSF, 0.33% (v/v) Nonidet-P40, Calbiochem phosphatase inhibitor cocktails I and II (at 10 μL per mL of buffer), 40 μL of complete protease inhibitor cocktail (per mL of buffer), and 2 μL of Sigma

protease inhibitor cocktail I (per mL of buffer). Resulting cell lysates were microcentrifuged at 500 x *g* (2,800 rpm in a Jouan MR 14-11 centrifuge) for 5 minutes at 4°C.

The pellet that resulted from cell lysis and centrifugation was re-suspended in 100 µL of ice-cold low-salt buffer. The low-salt core buffer contained 20 mM HEPES pH 7.9, 25% (v/v) glycerol, 1.5 mM $MgCl_2$, 0.02 M KCl, and 0.2 mM EDTA. Reagents added just before buffer use included 1% (v/v) Nonidet P-40, 0.5 mM DTT, 0.5 mM PMSF, 10 µL each of Calbiochem phosphatase inhibitor cocktails I and II (per mL of buffer), 40 µL of complete protease inhibitor cocktail (per mL of buffer), and 1 µL of Sigma protease inhibitor cocktail (per mL of buffer). To lyse the suspended nuclei, a total of 100 µL of cold high-salt buffer was added incrementally to the suspension, with gentle mixing after each addition. The high-salt core buffer contained 20 mM HEPES, 25% (v/v) glycerol, 1.5 mM $MgCl_2$, 0.8 M KCl, and 0.2 mM EDTA. Reagents added just before buffer use included 1% (v/v) Nonidet P-40, 0.5 mM DTT, 0.5 mM PMSF, 10 µL each of Calbiochem phosphatase inhibitor cocktails I and II (per mL of buffer), 40µL of complete protease inhibitor cocktail (per mL of buffer), and 2 µL of Sigma protease inhibitor cocktail (per mL of buffer). Increased viscosity indicated nuclear lysis.

Tubes containing lysed nuclei were placed on a rocking platform at 4°C for 15 minutes. Lysates were centrifuged at 13,690 x *g* (Fisher 235B microcentrifuge) for 15 minutes at 4°C. Resulting supernatants were aliquotted (25 µL) to microcentrifuge tubes and stored at –80°C.

Nuclear extract protein quantitation

Protein concentrations of the extracts were determined using the Micro BCA™ Protein Assay Reagent Kit from Pierce (Rockford, IL). The kit used principles of the Lowry method of protein analysis, modified by Smith and co-workers for quantification [178, 179]. In short, protein was quantitated using an albumin standard curve (1.0 to 20 µg/mL) generated from kit components in a 96-well microplate. Duplicate 1:40 dilutions

of nuclear and cytoplasmic extracts were prepared with water (200 μL final volume). A series of 1:2 dilutions followed, resulting in a dilution range of 1:40 to 1:2560 for each sample. The standard was supplied from Pierce in a 2 mg/mL suspension. Dilution of the standard to 40 μg/mL in water was performed, and subsequent 1:2 dilutions with water resulted in a standard curve from 0.75 to 40 μg/mL of protein. All final volumes for dilution series were 100 μL. Working reagent was prepared [a buffer containing 4% (w/v) cupric sulfate and 4% (v/v) bicinchoninic acid], and 100 μL of the reagent was added to each well. After brief mixing, the plate was sealed and incubated for approximately 2 hours at 37^{o}C. During that time, complexation of the protein in the sample with divalent copper ions resulted in a tetradentate-Cu^{+1} complex, which produced a purple color when the bicinchoninic acid complexed with the Cu^{+1} from the complex. After the incubation, the plate was cooled to room temperature and the optical density (OD) was measured at 595 nm using a Bio-Rad microplate reader. OD of the samples was adjusted using the OD of blanks. Using the regression equation obtained from the standard curve, concentration of protein was reported in μg/mL.

Electrophoretic mobility shift assay (EMSA)

EMSA was performed as described by Dyer and Herzog and Bassett *et al* [170, 177]. A reaction cocktail containing 5 μg of nuclear extract, 1 μL of a 35 nM stock of ^{32}P-labeled Igκ oligonucleotide (recognizes NF-κB family proteins, sequence 5'-AGT TGA GGC GAC TTT CCC AGG C-3'), master mix buffer (containing 5x band-shift buffer, 20 mM DTT, poly (dI:dC), and water), and sterile deionized water (to bring final cocktail volume to 20 μL) was prepared. [Band shift buffer (5x stock) contained 100 mM HEPES, pH 7.5, 250 mM KCl, and 7.5 mM $MgCl_2$. Poly (dI:dC) stock was 4 mg/mL in reagent grade water.] After a 30-minute incubation at room temperature, 4 μL of a 5x - loading buffer [containing 80% deionized formamide, 45 mM Tris base, 45 mM boric acid, 1 mM EDTA, 0.05% (w/v) bromphenol blue, and 0.05% (w/v) xylene cyanol] was added to the samples. Samples were loaded onto a 6% polyacrylamide gel [6% (w/v) acrylamide, 0.075% (w/v) bis-acrylamide, 2.55% (v/v) glycerol, 1 x TBE (90 mM Tris

base, 90 mM boric acid, 2 mM EDTA), 0.075% (w/v) ammonium persulfate, and 34 μL TEMED/gel] and electrophoresis was conducted at 20 milliAmps (mA) per gel for approximately 2-3 hours (Fisher Biotech, Houston, TX) in 0.25 x TBE solution (22.5 mM Tris base, 22.5 M boric acid, 0.5 mM EDTA). Unused wells were loaded with 24 μL of 1x-DNA loading buffer diluted with reagent grade water. After electrophoresis, the gel was transferred to Whatman paper and dried at 75^{o}C for about 45 minutes under vacuum (Jouan GF10, San Francisco, CA).

Cold competition EMSA

Cold competition was used to distinguish bands specifically bound by the Igκ oligonucleotide from bands that were bound non-specifically. The approach was the same as for EMSA, except for addition of non-radio-labeled Igκ oligonucleotide to selected (positive controls, LPS-treated extracts) samples before addition of the ^{32}P-labeled Igκ oligonucleotide. Gel buffer addition, reactions, loading, and electrophoresis proceeded as for EMSA (above).

Supershift analysis

The approach for supershift analysis was nearly identical to EMSA as described above. However, for characterization of the specific transcription factors present in the samples imaged, specific antibodies for NF-κB-family proteins were added to the reaction cocktail for 30 minutes before the ^{32}P-labeled Igκ oligonucleotide and poly (dI:dC) were added (5x band shift buffer concentration remained the same, but DTT concentration was reduced to 2 mM). Antibodies against p65 (H-286), p50 (NLS), c-Rel (N466), and p52 (447) were the gracious donation of N. Herzog, and were used at a concentration of two μg per reaction. [Note: The donated antibodies were donated by N. Herzog (UTMB, Department of Pathology) and were purchased from Santa Cruz Biotechnology (Santa Cruz, CA).] A 30-minute incubation with ^{32}P-labeled Igκ oligonucleotide, poly (dI:dC), and reagent grade water (to bring the sample volume to 20

μL) followed antibody incubation, and gel loading and processing continued as described above.

Gel autoradiography & imaging

Cooled, dried gels were covered with plastic wrap and imaged for four or more hours using an InstantImager autoradiographer (Packard/PerkinElmer, Boston, MA), which uses a stream of gas mixture (argon, 96.5%, isobutane, 1%, and CO_2, 2.5 %, Aeriform, Texas City, TX) that is excited by the ^{32}P bound to the nuclear proteins in the gel samples. Resulting images were saved in digital (TIFF) format using accompanying software, and radiation counts were reported for bands of interest (determined using a cold-competition reaction of unlabeled Igκ oligonucleotide during preliminary studies). Band radio-intensities were reported in units of cycles per minute per square millimeter of area (cpm/mm^2). Reports were saved in text (TXT) format and compiled on Microsoft Excel spreadsheets.

For imaging of the gels, autoradiography using Kodak X OMAT autoradiography film (Eastman Kodak, Rochester, NY) was performed for one to 4 days. Developed films were scanned using a UMAX PowerLook 1000 (UMAX Technologies, Inc., Dallas TX). The PowerLook 1000 is a high-resolution scanner that produces sharp images of autoradiography films. Collected scans were saved in digital (TIFF) format and compiled with numerical data using Microsoft Photodraw V2 software.

2.5.6 Statistical Analysis

Comparison of results from the IP_3 and phospho-p38 MAPK assays included one-way analysis of variance between groups (treatment as dependent factor), and between time points (time as dependent factor) within groups. Radiometric densities from EMSA gels were compared in terms of percentage of baseline signal within groups over time, or by comparison of radiation counts between groups at each time point. Significance was achieved at $p<0.05$ or less for IP_3 or phospho-p38 MAPK results, or when changes in band density exceeded three times the reported percent error observed in autoradiography reports from the InstantImager.

CHAPTER 3: RESULTS

3.1 AIM ONE (MODEL DEVELOPMENT) RESULTS

3.1.1 Overview

The focus of Aim One was to assess the microvascular endothelial/CE exposure model in terms of lethality and cytotoxicity. Initially, growth curves were performed in proliferating HMEC-1 cell cultures using various concentrations (0, 0.1, 0.5, and 1 mM) of CE. Resulting percent viabilities and growth kinetics were used to determine the degree of CE toxicity in the model. A final experiment in this early phase of Aim One was a detection of CE concentration in media samples taken from the growth curve experiments. Thus, if CE persisted in the media throughout the growth curves, which lasted for 7 days, then CE would remain in the media for the duration of future 24- and 72-hour biochemical analyses and cytotoxicity studies planned for the second part of Aim One (as well as the remaining Aims).

After the growth experiments in proliferating HMEC-1 were complete, viability of confluent HMEC-1 after exposure to 1 mM CE was analyzed. This study was conducted to confirm that exposure to the 1 mM CE would not be lethal to the HMEC-1 monolayers, which more accurately represented the microvascular endothelium than a non-confluent/proliferating model.

Next, basic biochemical studies of cell culture media sampled at intervals (baseline, 0, 1, 4, 12, 24, 48, and 72 hours) after addition of 1 mM CE to the cultures were conducted using clinical blood gas and electrolyte/nutrient analyzers in the UTMB Clinical Chemistry Division. The goal of this set of experiments was to determine whether the HMEC-1 monolayers were being injured by the CE exposure, the supposition being that injury may result in subtle cellular alterations not detectable by LDH release or MTT reduction assays (“classical” cytotoxicity assays), which require severe cellular injury before significant change in the assay results is detectable.

Finally, LDH release and MTT reduction assays were conducted on HMEC-1 exposed to CE to determine if any changes in media biochemistry reflected severe cellular injury that could result in lethality beyond the 72-hour time point used for the HMEC-1/CE exposure model. LDH release assay was chosen because increases in LDH escape from the cytoplasm to the extracellular compartment indicate severe disruption of the cell membrane. MTT reduction assays were performed because they indicate alterations in general mitochondrial activity (below).

3.1.2 Growth & viability of proliferating HMEC-1

As stated in the Overview, this project began with a growth curve, which served two purposes. First, the growth curve for the "zero" exposure group allowed for confirmation of the known growth kinetics of standard HMEC-1 in culture. Second, since proliferating cells are sensitive to toxic insult, the assessment of whether the 1 mM concentration of CE used by Kolodgie and colleagues [17] would be lethal to the microvascular HMEC-1 cell line could be made. This was important, since the cell model used by Kolodgie and co-workers [17] was macrovascular and could have had a different sensitivity to CE than the microvascular HMEC-1 cells used in the present study. Two lower concentrations of CE (0.1 mM and 0.5 mM) were added to the growth curve in case the 1 mM exposure proved lethal.

Figure 1 shows that all CE exposure groups resulted in decreased the growth of HMEC-1 cells over the 7-day period. The 1 mM CE treatment decreased HMEC-1 cell growth to the greatest degree (~40% decrease in cell numbers, control versus 1 mM CE, $p<0.001$). Seeding density for all groups was $1.1 \times 10^5 \pm 5.5 \times 10^3$ cells. At the end of the 7-day analysis, control cell numbers had plateaued at $2.1 \times 10^6 \pm 7.5 \times 10^4$ cells/35 mm plate, and cell numbers in the 0.1 mM ($1.8 \times 10^6 \pm 8.5 \times 10^4$ cells/35 mm plate), 0.5 mM ($1.6 \times 10^6 \pm 1.1 \times 10^5$ cells/35 mm plate), and 1.0 mM ($1.2 \times 10^6 \pm 7.3 \times 10^4$ cells/35 mm plate) CE-treated groups were significantly ($p = 0.02$, 0.03, and <0.001, respectively) lower.

From the cell numbers and time periods recorded, and the exponential equations determined from the graphs of our growth curve data, the behavior of the cultures was further characterized by calculating the growth kinetics for each group. Classical growth equations (Section 2.2.4) were used to determine the time required for cells to reach

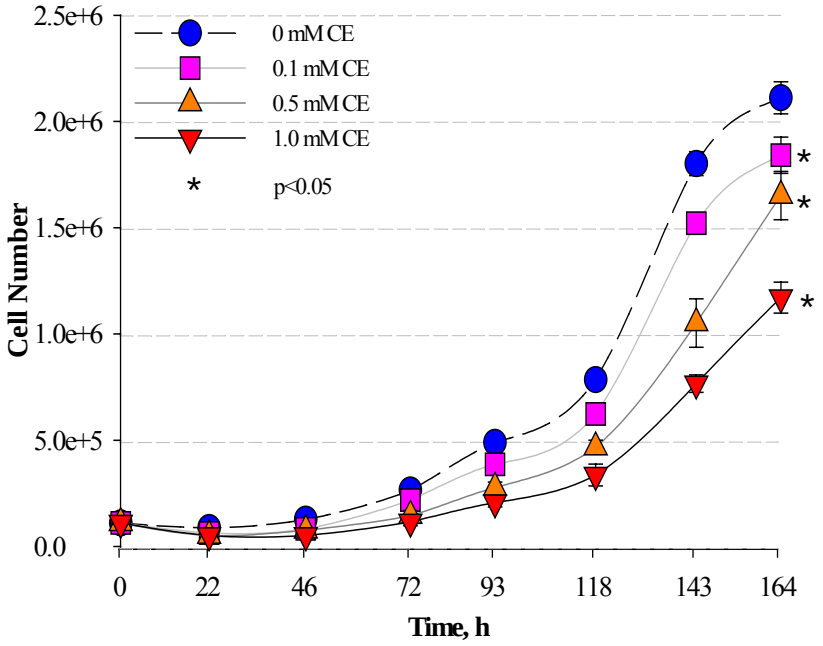

Figure 1: HMEC-1 growth curve results

HMEC-1 were exposed to 0 (blue circle), 0.1 (pink square), 0.5 (orange upright triangle), or 1.0 (red inverted triangle) mM CE and growth assessed over a period of seven days. Error bars represent standard error of mean. Asterisk (*) represents $p<0.05$ between groups during exponential growth phase by one-way ANOVA. Reprinted from *Clinica Chimica Acta*, Vol 345, D. Tacker and A. O. Okorodudu, "Evidence for injurious effect of cocaethylene in human microvascular endothelial cells," pages 69-77, Copyright 2004, with permission from Elsevier (with modifications).

maximal density (t, based on the control group plateau value), the number of doublings required to reach plateau (n, again using the control plateau value as the maximal culture density), and the doubling or generation time of the cultures (g). These values were determined for each set of data, then averaged to compose the values shown in Table 2.

Table 2: Calculated growth kinetics for HMEC-1 exposed to CE

CE	Equation	t, h	n	p-value	g, h	p-value
0.0	$y = 67757e^{0.0211x}$	124.0	4.00	---	31.3 ± 1.69	---
0.1	$y = 53524e^{0.0213x}$	132.5	4.45	0.084	29.8 ± 0.53	0.392
0.5	$y = 46600e^{0.0202x}$	148.8	4.55*	0.039	32.7 ± 0.44	0.403
1.0	$y = 43190e^{0.0183x}$	172.5	5.05*	<0.001	34.4 ± 1.57*	0.012

t = time HMEC-1 were in exponential growth

n = number of cell doublings during *t*

g = doubling/generation time HMEC-1

* = $p<0.05$, one-way ANOVA, CE treatment group versus control

As shown in Table 2, the 1 mM CE treatment group exhibited a lag in doubling time (34.4 ± 1.57 hours) that was statistically significant ($p = 0.012$) relative to controls (31.3 ± 1.69 hours generation time). The apparently faster growth rate (*g*) in the 0.1 mM group shown on the Table (29.8 ± 0.53 hours) was within the standard deviation (3.38 hours) of the control group and was thus non-significant. These effects on growth were due to a decrease in cellular viability, as shown in Figure 2.

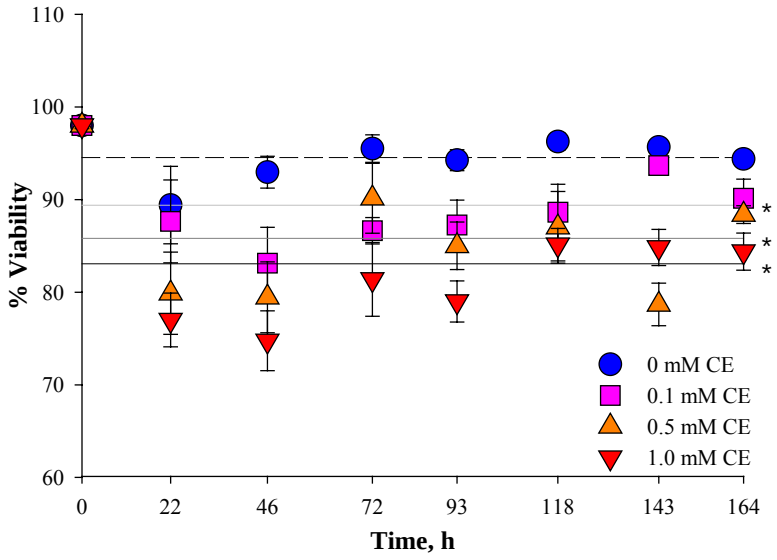

Figure 2: Viability of HMEC-1 during growth curves

Viability of control (blue circles), 0.1 mM CE (pink squares), 0.5 mM CE (orange triangles), and 1 mM CE (red inverted triangles) –treated HMEC-1. Corresponding viability averages (top to bottom: control, black dash; 0.1 mM, light gray solid; 0.5 mM, dark gray solid; 1 mM, black solid) are also shown. Asterisk (*) represents $p<0.05$ by one-way ANOVA, CE treatment versus control, mean viability.

When observing the viability data, again the 1 mM treatment group showed the most significant effect on HMEC-1 cells (Figure 2). These data demonstrated the source of the depression in cell growth, regarding numbers as well as kinetics. The control viability averaged 94.5 ± 1.4% (Figure 2, dashed line). Though the 0.1 mM (average: 89.4 ± 2.3%, light grey line) and 0.5 mM (average: 85.87 ± 2.8%, dark grey line) CE–treated groups showed significant decreases in average viability over the course of the experiment, those decreases were not consistent between time points. This result contrasted with results obtained from the 1 mM CE-treated group (average: 83.1 ± 2.3%, black line), which showed significance at each time point within the trial (*p* values

ranging from 0.015 to <0.001). The greatest decrease in viability (seen in the 1 mM CE-treated group, Figure 2) was approximately 15%. Thus, because the 1 mM CE treatment provided an acceptable viability level for proliferating cells, the 1 mM concentration was judged not to be toxic enough to kill HMEC-1 cells. Consequently, the 1 mM CE concentration was used in the remaining experiments in this study, which utilized confluent cells that were more quiescent in nature. The 0.1 mM and 0.5 mM concentrations, which showed intermediate decreases in viability, were excluded from further analysis.

In summary, the doubling times of the HMEC-1 were approximately equal in all treatment groups (Table One), yet a change was still observed in cell numbers (Figure One) and viability (Figure Two). These results demonstrate an initial cell killing potentially mediated by CE that was followed by an adaptation of the culture, after which culture growth was sustained. It is possible that HMEC-1 cells in a particular stage of growth are more susceptible to lethality when treated with CE. To demonstrate this, further study incorporating cell growth synchronization and testing with CE at various stages of the mitotic cycle would be required. Consequently, the mechanism of cell death in growing HMEC-1 exposed to CE remains unknown.

3.1.3 Persistence of CE in cell culture media

A question arose early in the study regarding the persistence of CE in the cell culture media. Would the cells metabolize the CE? Or would CE remain unaltered in culture, or hydrolyze spontaneously over time? One way to answer this question was to extract the CE from the cell culture media, quantitate the CE in the extract, and determine the resulting media concentration of CE. The growth curve experiments provided a long time line from which the persistence of CE in the cell culture media could be assessed, and under standard culture conditions required for optimal maintenance of the HMEC-1 cell line (37^{o}C, 5% CO_2, humidified). If the CE were to spontaneously hydrolyze, the rate of hydrolysis could be determined. This information would determine if further addition

of CE would be necessary during a 72-hour experiment (such as those planned for biochemistry and cytotoxicity).

Figure 3 shows that loss of approximately 50% of the CE in culture occurred within the first 72 hours of the growth curve. This slow rate of degradation suggested that the cells were not hydrolyzing the CE for two reasons. First, cell-mediated hydrolysis of

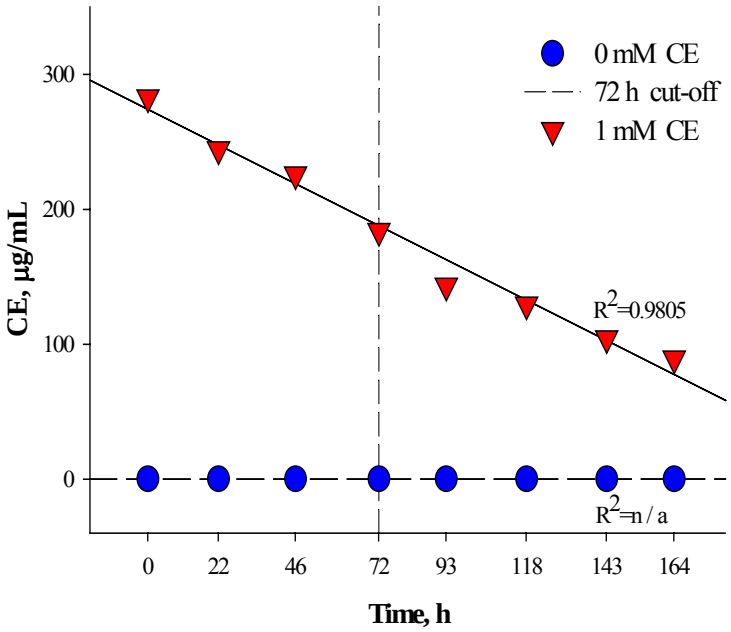

Figure 3: CE persistence in media during HMEC-1 growth curves

Plots represent CE content of media samples taken from control (blue circles) and 1 mM CE (red inverted triangles) -treated HMEC-1 over a 7-day period. Resulting regression analysis is shown for control (dashed line) and 1 mM (solid line) CE treatment. Vertical line at 72 hours denotes latest cut-off time for all future experiments. Each plot represents duplicate samples. Reprinted from *Clinica Chimica Acta*, Vol 345, D. Tacker and A. O. Okorodudu, "Evidence for injurious effect of cocaethylene in human microvascular endothelial cells," pages 69-77, Copyright 2004, with permission from Elsevier (with modifications).

CE would occur quickly due to the ability of CE to access the cellular compartment through the cell membrane. Second, endothelial cells are not known to have hCE-1 enzyme activity, which would be required to metabolize CE to cocaine or benzoylecgonine. Thus, the slow degradation was probably due to spontaneous hydrolysis occurring in the culture media due to the incubator culture conditions. A similar result has been reported by Boelsterli and colleagues [180], who did not see appreciable CE hydrolysis in cell culture (37^{o}C, 5% CO_2) conditions for up to 24 hours. Since this assay was run in duplicate during one of the growth curves, only averages and linear regressions were available for analysis. CE persistence analysis was not continued because this experiment demonstrated that the HMEC-1 cells would be exposed to CE throughout the planned 72-hour experiments, and emphasis was placed on proceeding with experiments conducted on confluent monolayers of HMEC-1 cells. However, if a future study were conducted on media samples in this exposure model, ions for cocaine (MW 300) and benzoylecgonine (MW 289) could be included in the detection parameters, and thus analyzed as products of CE breakdown.

3.1.4 Viability of confluent HMEC-1

Since a proliferating endothelial cell model was not representative of physiological endothelial tissue *in vivo*, viability testing was again conducted using the trypan blue staining technique. However, this time the viability analysis was performed using control (0 mM treatment) and 1 mM CE- treated HMEC-1 monolayers that had grown to confluence on human fibronectin. The experiments extended to 72 hours, and the data generated is shown in Figure 4.

In Figure 4, the data are presented two ways: pointwise over time to show variations in sampling, and as average/mean viability within each group (lines). There was no significant difference between control and treated monolayer viability when compared pointwise within groups (p values ranged from 0.68 at time “zero” to 0.10 at 72 hours). Considering the standard error of mean of both groups, which averaged approximately 0.9%, the difference between the control average viability (98.6 ± 0.9%)

and that of the treated group (98.5 ± 0.9%) was not significant. This finding is illustrated (Figure 4) by the inclusion of all data from both groups within the 99% confidence interval for the control group (dashed lines). This result indicated that the 1 mM treatment was not lethal to HMEC-1 cell monolayers.

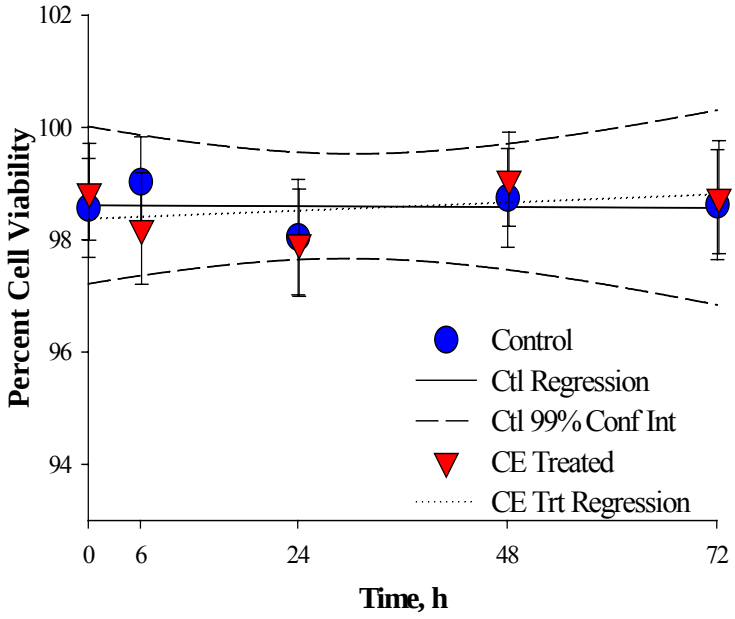

Figure 4: Viability results from confluent HMEC-1/CE exposure

Trypan blue staining was used to test the viability of HMEC-1 monolayers after control (blue circles) or 1 mM CE (inverted red triangles) treatment. Linear regressions shown: control (solid line) and 1 mM CE (dotted line). Error bars represent standard error of mean. Concave and convex dashed lines represent 99% confidence interval for 0 mM group. Significance of $p<0.05$ not achieved.

3.1.5 Biochemical studies

When a cell responds to injury, its metabolism is altered to compensate for nutrient and energy loss and facilitate repair of damaged cellular structures. The experimental hypothesis was that HMEC-1 cells injured by CE would increase their consumption of oxygen (O_2) and production of carbon dioxide (CO_2). Since concentrations of CO_2 in culture media (and blood) affect pH and bicarbonate (HCO_3^-) buffering, media pH of the CE-treated HMEC-1 cells was expected to decrease at a more rapid rate than controls (these levels steadily decline in normal culture conditions, as CO_2 production rises). Accordingly, pO_2 was expected to be lower in the CE-treated group relative to controls, since injury would require increased oxidative demand by the cells. Also, since CO_2 production in a cell is contingent upon successful oxidative phosphorylation and glucose metabolism, CE-treated HMEC-1 cells were expected to consume glucose at a greater rate than controls. Finally, since injury could cause increases in all metabolic pathways in a cell (depending on severity), and lactate is produced from glycolytic (anaerobic) metabolism, lactate should rise to greater levels in the media of CE-treated HMEC-1 compared to controls. Such results would demonstrate cellular injury from CE exposure.

To test these hypotheses, pH (H^+), HCO_3^-, pCO_2, pO_2, glucose, and lactate were measured in control and CE-treated HMEC-1 monolayers for up to 72 hours post-exposure. Also measured were concentrations of ionized calcium (Ca^{2+}), and total (ionic + protein-bound) magnesium (Mg), potassium (K), sodium (Na), and chloride (Cl), which would reflect toxicity, as injured or impaired cells become permeable to ions, resulting in loss from the media.

Figure 5 shows that HMEC-1 cell change results from exposure to CE. Figure 5A shows the marked change in media ionized hydrogen (H^+) that occurred in the CE-treated cultures (66.0 ± 0.6 nM) versus controls (45.5 ± 2.4 nM, $p<0.001$) at time "zero" relative to baseline (45.5 ± 2.2 nM for controls, 45.4 ± 2.0 nM for CE-treated). [Note: Time "zero" samples were collected immediately after the addition of CE or control media.]

The increase in H^+ was reflective of a pH decrease, due to the inverse-log relationship (H^+ in nM = 10^{-pH}) of H^+ and pH. This increase in H^+ concentration persisted for 72 hours (H^+ of CE-treated = 68.4 ± 1.8 nM versus 61.1 ± 1.0 nM for controls, p = 0.02).

The question arose as to whether the toxicity in the cells was due to the pH change alone. Consequently, the biochemistry experiments were repeated with a pH-adjusted, 0 mM CE-treated control group (not shown, HMEC-1 treated with sodium fumarate, 1 mM). This pH control showed only an alteration of pH consistent with the time "zero" CE treatment (Figure 5A). The immediate pH effect did not persist longer than the first hour, and did not affect the other analytes measured. Also, none of the other changes observed in the CE-treated group (Figures 5B-D and Figure 6) over time were seen after alteration of media pH. Thus, the remaining changes observed were attributed to CE treatment, rather than a pH-dependent mechanism.

In Figure 5B, alterations in bicarbonate concentration resulting from CE exposure are shown. Since HCO_3^- varies with pH as part of the buffering system in the media, the decrease in HCO_3^- levels over time relative to baseline (12.8 ± 0.1 mM for controls, 12.8 ± 0.2 mM for treated) was expected. Beginning 1 hour post-exposure, declines in the HCO_3^- concentrations of the CE-treated group were observed relative to controls that contributed to a decreasing trend for media over 72 hours of sampling. This effect persisted, resulting in a trend for lower media HCO_3^- in CE-treated HMEC-1 cells versus controls. Together, the H^+ and HCO_3^- data indicate increased acid production in the HMEC-1 culture model, a finding that could demonstrate altered HMEC-1 cellular function after exposure to CE.

The spike in pCO_2 (Figure 5C) upon addition of the CE to the culture media was unexpected considering the lack of overt change in HCO_3^- concentration at time "0" (Figures 5B and 5C). From the baseline values of 23 ± 1.2 and 23.2 ± 1.3 mm Hg of pCO_2 for control and CE-treated groups, respectively, the CE-treated group showed a significant increase in pCO_2 in the "zero" time point sampling (35 ± 0.6 mm Hg,

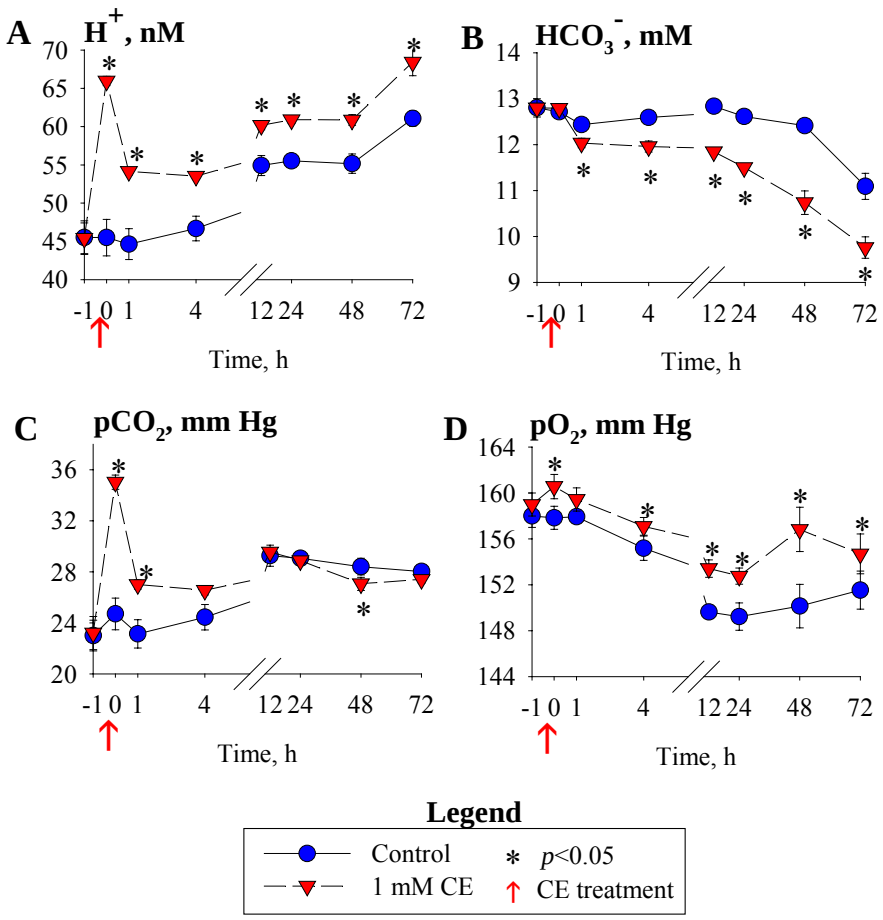

Figure 5: Biochemistry results (I) from media sampling of treated HMEC-1 cells

Media taken from control (blue circles) and CE-treated (red inverted triangles) HMEC-1 was monitored for changes in H^+ (A), HCO_3^- (B), pCO_2 (C), and pO_2 (D). Asterisk (*) represents $p<0.05$ by one-way ANOVA between control and CE-treated samples at each time point. Error bars represent standard error of mean for $n = 9$ individual data points per time point and group.

$p<0.001$), whereas the control group showed only a slight change (24.7 mm Hg, $p>0.05$). As time progressed in the trials, the pCO_2 levels in the control group steadily increased (to 28.4 ± 0.65 mm Hg), while pCO_2 for the CE-treated cultures fluctuated. At the 1-hour sampling point, the CE-treated group (27 ± 0.4 mm Hg) showed higher pCO_2 concentrations than controls (23.1 ± 1.1 mm Hg, p = 0.01). However, at 48 hours post-exposure, CE-treated pCO_2 (27.1 ± 0.5 mm Hg) averaged *lower* than controls (28.4 ± 0.6 mm Hg, $p = 0.01$). Time points in between showed intermediate pCO_2 concentrations without statistical significance ($p>0.05$) relative to controls. Thus, after the initial, abrupt increase in pCO_2 (which was related to the pH change observed), there was no change in the trend for media pCO_2 production in CE-treated HMEC-1 relative to controls.

Though pCO_2 showed no significant physiological change in the 72 hours after CE addition to the media, the results of the pO_2 analyses reflected a potential alteration in cellular function over time when HMEC-1 cells were exposed to 1 mM CE (Figure 5D). Average baseline pO_2 for control and CE-treated HMEC-1 cells was 158 ± 1.0 mm Hg, and the mean pO_2 for controls was 159 ± 1.0 mm Hg. A trend of decreasing pO_2 was expected in the CE-treated group relative to controls. However, immediately after addition of CE to the treated-group media, an increase in media pO_2 (to 160.6 ± 1.1 mm Hg) was observed relative to controls (157.8 ± 1.0 mm Hg, $p = 0.03$). This increase was generally maintained during the trial, with significant differences between groups observed from 12 hours (149.6 ± 0.3 mm Hg for controls versus 153.4 ± 0.8 mm Hg for treated, $p = 0.004$) to 72 hours (151.5 ± 1.7 mm Hg for controls versus 154.7 ± 1.7 mm Hg for treated, $p = 0.02$) post-exposure. Thus, a trend for increased media pO_2 was observed in CE-treated HMEC-1 cells relative to controls. Such a trend could indicate increased cellular utilization of anaerobic metabolism, but only if concomitant decreases in media glucose and increases in media lactate are also observed.

Remaining media analytes apparently affected by CE treatment were glucose (Figure 6A), lactate (Figure 6B), and Ca^{2+} (Figure 7). The results of biochemical analysis

of glucose and lactate are shown in Figure 6. As shown in Figure 6A, changes in media glucose concentration were observed that were statistically significant from 12 hours to 72 hours after CE treatment. A baseline average of 5.9 ± 0.0 mM was observed for both

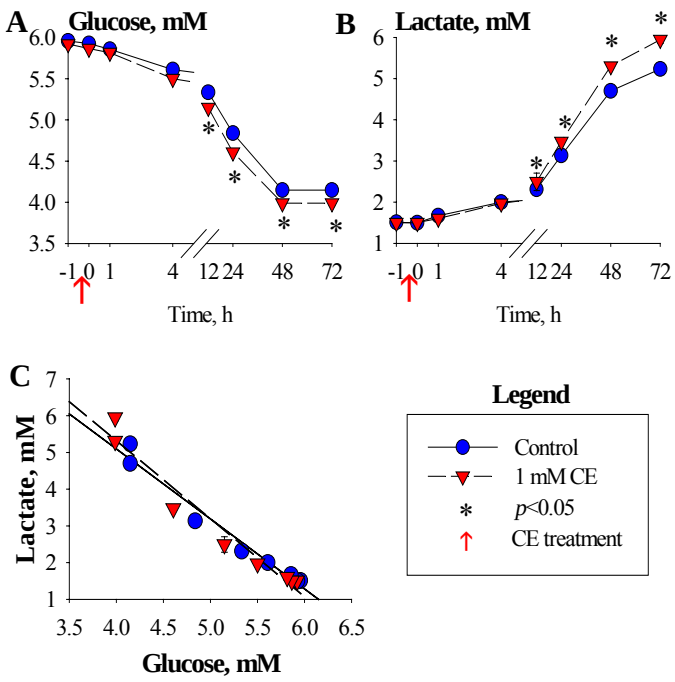

Figure 6: Biochemistry results (II) from media sampling of treated HMEC-1 cells

Media taken from control (blue circles) and CE-treated (red inverted triangles) HMEC-1 cells was monitored for changes in glucose (A) and lactate (B). Asterisk (*) represents $p<0.05$ by one-way ANOVA between groups at each time point. In (C), the association between glucose and lactate was compared between groups. Resulting linear regressions showed that the changes in (A) and (B) were not associated with significant physiological effects on the HMEC-1 cells.

groups. Final average media concentrations were 4.15 ± 0.03 mM (control) and 3.99 ± 0.03 mM (CE-treated) at 72 hours, indicating a decreasing trend for glucose in the cell culture media for both groups. This decrease in glucose over time is to be expected from live cell cultures without media change. Statistical significance between groups was established at 12 hours post-exposure, when the glucose concentration in treated media declined to 5.3 ± 0.0 mM (versus 5.15 ± 0.0 mM for control, $p = 0.02$), and persisted at the 24, 48, and 72-hour time points.

The decrease in glucose co-varied with lactate (Figure 6B) production, which started with a baseline average of 1.53 ± 0.03 mM (control, 1.50 ± 0.01 for CE-treated), and ended with significantly higher mean values of 5.23 ± 0.03 mM (control, $p<0.001$) and 5.93 ± 0.09 mM (treated, $p<0.001$). This trend reflects increased cellular demand as HMEC-1 attempt to utilize decreasing concentrations of media nutrients over the 72 hours observed.

The question arising from the glucose and lactate results is: Are the statistically significant changes between the groups from 12- to 24 hours post-treatment *physiologically* relevant? In this case, the answer is no. The trends observed in glucose consumption and lactate production were not altered significantly in the CE-treated group relative to controls (Figure 6C). Plotting of lactate concentration on the y-axis, and glucose concentration on the x-axis resulted in slopes of –2.12 for controls and –2.39 for CE-treated HMEC-1 cells. This signifies that approximately 2 millimoles of lactate were formed for every 1 millimole of glucose consumed, and links the glucose consumption in both groups over time to cellular glycolytic activity. Also, R-values for controls (0.994) and CE-treated HMEC-1 (0.995) were derived from the linear regressions of these data. Thus, the association between glucose and lactate was equally significant in both groups and there is no appreciable alteration of glucose consumption or lactate production in CE-treated HMEC-1. These results do not support the assumption that CE treatment results in metabolic changes within the HMEC-1 cells. Thus, there is no evidence that CE alters the metabolism of HMEC-1, despite an alteration of media acid concentration and buffering.

One final result from the biochemical analysis of media collected from control and CE-treated HMEC-1 cells demonstrates a potential cellular change after CE treatment. Figure 7 demonstrates a decrease in media ionized calcium over time, from a baseline average of 6.03 ± 0.01 mg/dL to averages of 5.90 ± 0.05 mg/dL ($p = 0.002$) and 5.79 ± 0.09 mg/dL ($p<0.001$) for control and treated samples, respectively at 72 hours. Additionally, there was a significant decrease in media ionized calcium in the CE-treated samples (5.86 ± 0.12 mg/dL) relative to controls (5.96 ± 0.09 mg/dL, $p = 0.03$) beginning

at 48 hours that continued to the 72-hour sampling. These changes increase the rate of Ca^{2+} loss from the media in the CE-treated HMEC-1 cells, a finding that reflects significant physiological effect. Such a change could have been due to several factors, none of which was clearly supported by the data.

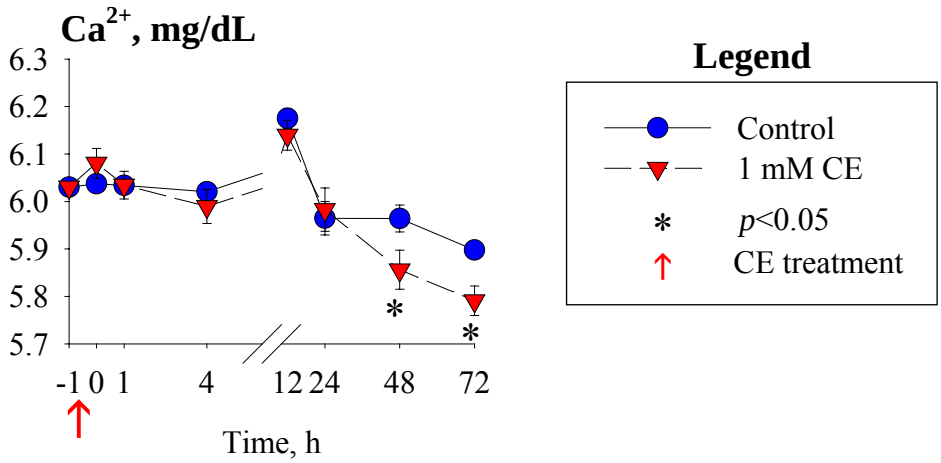

Figure 7: Biochemistry results (III) from media sampling of treated HMEC-1 cells

Media taken from control (blue circles) and CE-treated (red inverted triangles) HMEC-1 cells was monitored for changes in Ca^{2+}. Asterisk (*) represents $p<0.05$ by one-way ANOVA between groups at each time point. Error bars represent standard error of mean.

Analytes unaffected by the CE treatment ($p>0.05$) were total Mg, Cl, Na, and K.

3.1.6 Cytotoxicity assays

Having determined that HMEC-1 showed minimal changes in metabolism after treatment with CE, and that the CE exposure did not kill the cells, two cytotoxicity experiments were designed to determine the extent of any injury occurring in the exposure model. The first assay was an LDH quantitation in media samples collected

from control and CE-treated HMEC-1 monolayers after various times of exposure to CE. Since LDH is released from cells injured irreversibly and in the early stages of death [56, 113, 116], LDH activity levels indicating cytotoxicity should be significantly higher in media taken from treated cells that are compromised.

Figure 8 shows the results of these two analyses. LDH activity (Figure 8A) in culture media was the same in both groups, suggesting a lack of cytotoxicity in the culture system. Statistical analysis yielded *p* values ranging from 0.1 (at 72 hours) to 0.98 (at 4 hours). All LDH activities were contained within the 95% confidence interval for

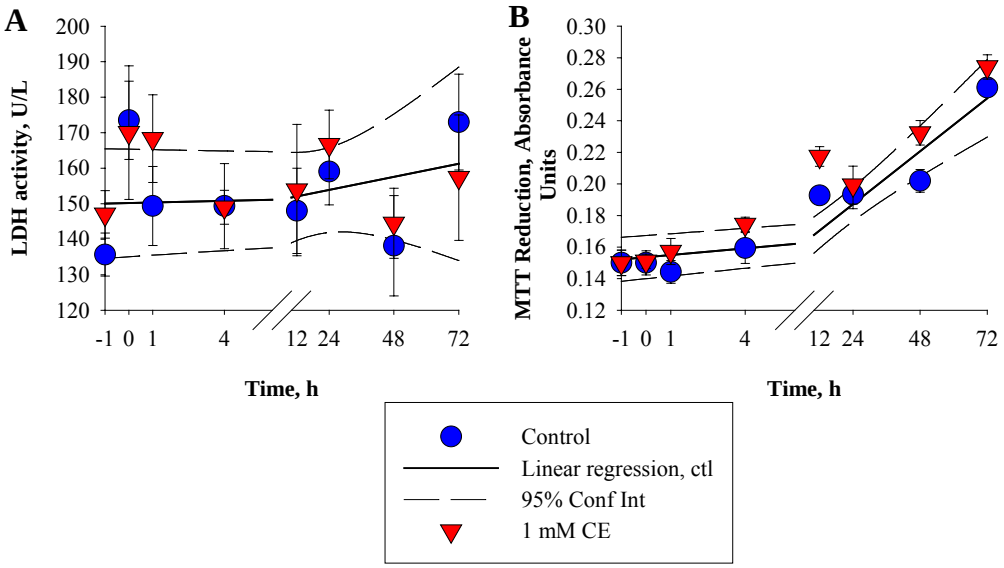

Figure 8: Results of cytotoxicity assays

LDH (A) and MTT reduction (B) were analyzed in HMEC-1 cell monolayers after control (blue circles) or 1 mM CE (red inverted triangles) treatment. On both graphs, the solid line represents the control linear regression, and the dashed lines represent the upper and lower limits of the 95% confidence interval for controls. Error bars represent standard error of mean.

control HMEC-1. However, the time "zero" results show a transient increase in both groups, which could either be due to sampling error, or a cell membrane response to the addition of media (control or CE-containing) that took place at time "zero". Since this change was equal between controls and CE-treated HMEC-1, the conclusion made from the LDH analysis was that the HMEC-1 cell membrane was not irreversibly damaged by the CE exposure [56, 113, 116].

The second assay that was performed was an MTT reduction assay. MTT is converted to a spectral formazan product by mitochondrial oxidases, and as a result this assay has been used as an indicator of growth in proliferating cultures [161, 162], and as a cytotoxicity assay in confluent culture systems [163].

Figure 8B shows the results of the MTT assays. From time-point to time-point, there were two instances where MTT reduction activity was increased in the CE-treated group. At 12 hours, the average control MTT reduction was 0.19 ± 0.004 OD, and treated values averaged 0.22 ± 0.006 OD ($n = 3$, $p<0.001$). However, when comparing these values to the others in the graph, the 12-hour time point data for both treatment groups appear to be outliers. Thus, the change shown at 12 hours is not likely to have physiological significance. At 48 hours, a statistically significant change was observed, with control OD averaging 0.20 ± 0.007, and an average treated OD of 0.27 ± 0.007 ($n = 3$, $p = 0.003$). However, considering that the mean for the CE-treated HMEC-1 cells is contained within the 95% confidence interval for control HMEC-1, it can be concluded that there was no significant change in MTT reduction over time between groups.

3.1.7 Summary of Aim One studies

To summarize the Aim One studies, exposure to CE did not injure HMEC-1 cells for up to 72 hours of continuous exposure. Three indices of viability and cytotoxicity (trypan blue staining, LDH release, MTT reduction) demonstrated that no cytotoxicity occurred when HMEC-1 were exposed to a 1 mM concentration of CE for up to 72 hours. Also, though analysis of culture media taken from CE-treated and control HMEC-1 monolayers indicated shifts in culture pH and buffering/HCO_3^-, no alterations in culture

medium consistent with altered cellular metabolism were observed. This was a positive finding, since it demonstrated that the HMEC-1 cell/CE exposure model would sustain CE exposure long enough for morphological and mechanistic evaluation.

3.2 AIM TWO (MORPHOLOGY & BARRIER) RESULTS

3.2.1 Overview

To fully address the first aspect of the overall hypothesis, which was that CE exposure would affect endothelial morphology and barrier integrity, Aim Two studies were designed with focus on whether morphological change was linked to functional changes in barrier integrity in control and CE-treated HMEC-1 cells. Morphological analyses (transmission electron microscopy and silver staining) and kinetic analysis (resistance monitoring) were used.

3.2.2 Transmission electron microscopy (TEM)

The high magnifications of TEM provided ultrastructural information about the structures of organelles and their membranes and are summarized in Figure 9. Time points up to 24 hours were chosen. [Note: Due to the changes in cellular metabolism observed after 24 hours in the Aim One experiments, most of the remaining studies are conducted with a 24-hour or shorter time frame. The only exception is the electrical resistance study, which was 72 hours long.] Control HMEC-1 (Figure 9A) showed numerous, round or bean-shaped mitochondria († in all sections), large, normal nuclei (asterisks in all sections), numerous lysosomes (√ in all sections) with minimal inclusions, abundant cell-to-cell contacts (‡ in A, B, and E), and visible rough endoplasmic reticulum (§ in all sections).

As early as 1 hour after CE was added to the culture media (Figure 9B), lysosomes became larger (scale bar provided for comparison), and contained inclusions that appeared to contain digested cellular components. Since the digestion of lipids and proteins is most common in lysosomes, it may be assumed that the inclusions observed in Figure 9 contain proteins and/or lipids. Primary lysosomes (those that have not fused with

phagosomes or late endosomes) *appear* as small, empty, vesicular bodies (they actually contain enzymes and some lipids). Thus, the increasing complexity/inclusions of the lysosomes noted in Figure 9 (B through E) suggests an increase in lysosomal activity that occurs when endocytosis or autophagy processes have been increased.

Endocytosis is a process of cell membrane internalization normal cells use to degrade and replace surface proteins, or to remove proteins or organisms that may be bound to the cell membrane [159]. Autophagy is an internal process involving the lysosome that results in the removal of damaged or non-functional cellular organelles [159]. Both processes are important to normal cellular homeostasis. However, both processes are commonly increased in cells that are injured or adapting to environmental change, as cellular organelles are damaged and replaced, and cell membrane surface expression (e.g., of adhesion molecules or receptors) changes [159, 181]. Thus, one role of the lysosome compartment is damage control. These facts suggest that the increased numbers and complexity/inclusions of lysosomes in CE-treated HMEC-1 are the result of cellular injury, and attempts to control the damage for cell survival.

The endoplasmic reticulum (ER) of CE-treated cells was enlarged in some of the images (Figure 8C, D, E). Since the ER of normal cells enlarges when protein turnover takes place, as when the cell responds to an external stimulus or injury, this enlargement in CE-treated HMEC-1 is probably associated with a cellular response to the exposure that requires increased production of protein. Most notably, secretory and integral proteins associated with endothelial communication to other cells, as well as the maintenance of cell-to-cell contact and responsiveness to the external environment, are produced in the ER. Thus, the change in HMEC-1 cell ER size, paired with the increased activity of lysosomes within the cells, suggests that HMEC-1 cells are changing in response to the CE exposure.

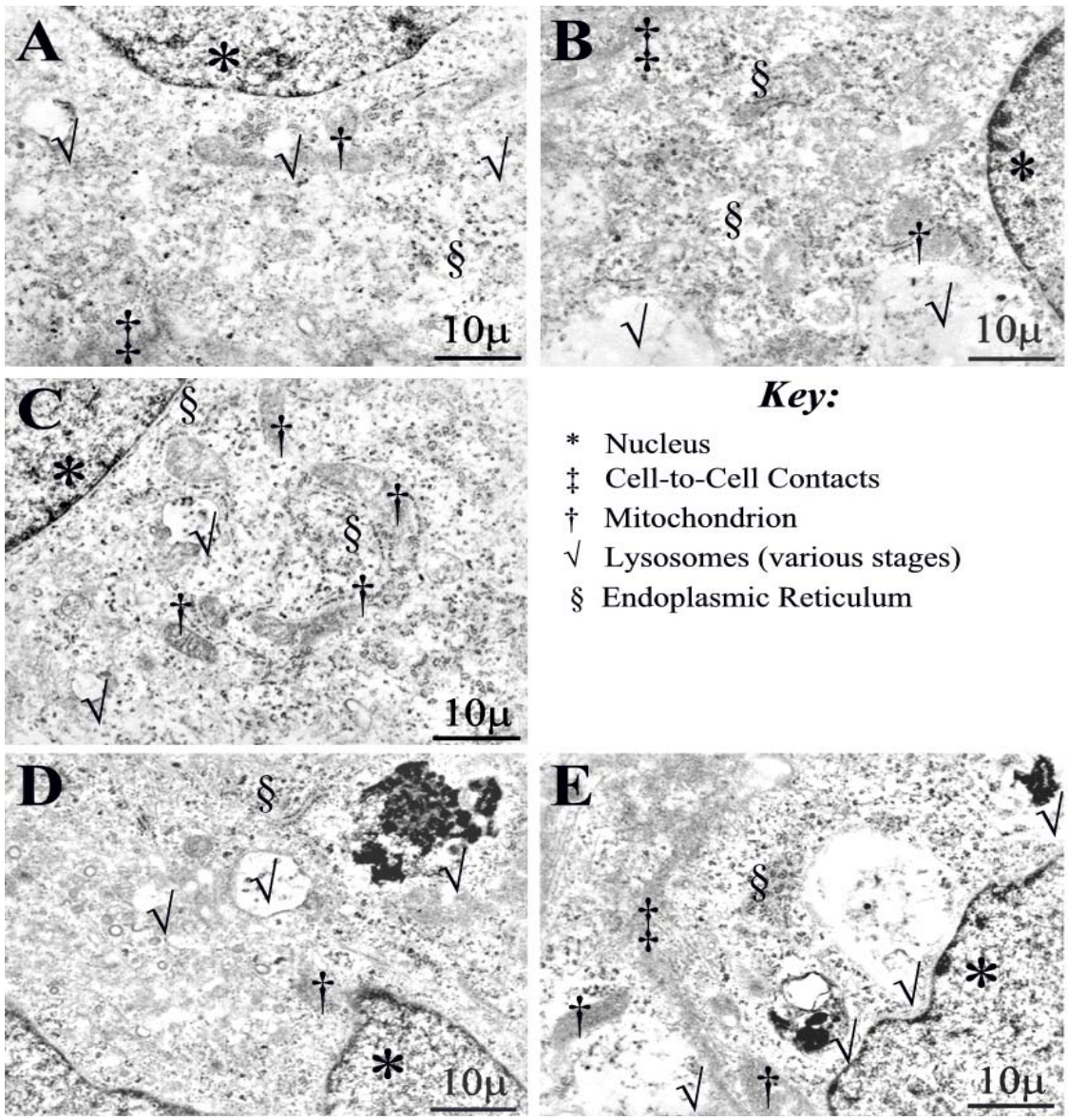

Figure 9: Representative transmission electron microscopy (TEM) results

Representative images of HMEC-1 controls (A), and 1 mM CE-treated HMEC-1 after 1 (B), 4 (C), 12 (D), and 24 (E) hours of exposure. Scale bar equals 10 µm. Symbols: * - nucleus, ‡ - cell-to-cell contacts, † - mitochondrion, √ - lysosomes (various stages), § - endoplasmic reticulum.

Mitochondria and cell-to-cell contacts appeared to be unaffected by CE treatment at all time points (Figure 8 B-D). The lack of change in these two locations reinforces the findings from Aim One that demonstrated a lack of cytotoxicity, since the LDH release assay tests for severe damage to the cell membrane, and the MTT reduction assay tests for severe damage to the mitochondrial oxidative machinery.

Two blinded observers confirmed the TEM results. The first observer was blinded to treatment group and the other was blinded to anticipated outcome. In summary, the crucial finding in the TEM images (Figure 9) that suggested non-lethal HMEC-1 cellular response to CE exposure was the lack of effect on HMEC-1 nuclei and mitochondria for up to 24 hours of constant CE exposure. Apoptotic/necrotic changes are usually first apparent in the nuclei, with segmentation and marginal condensation in the early stages of cell death, and mitochondria, which show widespread swelling and increased water content (that looks like vesicles within the mitochondrion) [159]. These changes were not observed in the majority of the fields viewed when HMEC-1 were imaged. Thus, the TEM study provided the first visual confirmation of cellular change, and support for the suggestion that HMEC-1 response to CE was non-lethal as presented by the biochemical (Figures 5 through 7) and cytotoxicity (Figure 8) data from Aim One (Section 3.1).

3.2.3 Silver staining

Silver staining, the second mode of morphological analysis, was conducted for two reasons. First, confirming the findings of Kolodgie and associates [17] using the HMEC-1/CE exposure model would lend credence to the hypothesis that CE is capable of direct interaction with the microvascular endothelium, and that this interaction results in altered endothleial function. Since emphasis was placed on the temporal association of CE treatment and pathology, the general experimental approach was expanded to include time points up to 24 hours of treatment. Again, the Aim One biochemical analysis of media taken from control and CE-treated HMEC-1 cells indicated an increased potential for cellular stress after 72 hours of confluent culture. The decreased media pH and HCO_3^-, decreasing trend for glucose, and increasing lactate concentrations at 48 and 72 hours resulted in shortening of the morphological assays to 24 hours. This would

minimize potential confounding of monolayer morphological effects due to poor culture conditions over time while allowing for continuous exposure to CE in the HMEC-1 cell model.

The second reason for using silver staining was that the method is cost-effective and relatively simple and gives consistent, clear staining of endothelial cell-to-cell borders. This approach has been used by many researchers in the fields of cell biology and inflammation, *in vivo* and *in vitro* [17, 154, 155].

As shown in Figure 10, control HMEC-1 monolayers showed clear, black-staining intercellular borders (Figure 10A, asterisks). However, after 30 minutes of CE treatment, gap formations (Figure 10B, arrows) were visible in some of the fields randomly chosen for viewing. This finding became consistent after 1 hour of CE treatment, when large and numerous intercellular gap formations (Figure 10C, arrows) were seen in every pre-chosen field. Due to the way that the staining experiments were controlled, a control monolayer was always present on the same slide for comparison. Thus, the gaps were not an artifact of the staining process. This result confirms those reported by Kolodgie and co-workers [17], who observed gap formations of similar size and shape in HUVEC monolayers treated with 1 mM cocaine or CE for 1 hour.

Fading of the black staining of the cell-to-cell junctions at all time points after CE exposure coincided with the observance of intercellular gaps, which were consistently viewed after one hour of CE exposure (Figure 10, C-D). Thus, the fading of the stain after CE treatment was not an artifact of the staining process, since the control monolayers on the same slides showed staining much like that shown in Figure 10A. The fading of the stain was probably due to the increased intercellular permeability of the CE-exposed HMEC-1, and the nature of the staining process. To illustrate, the silver nitrate was able to stain intercellular borders by complexing with intercellular junctional proteins (such as cadherins) and oxidizing. Thus, a decrease in cell-to-cell contact would decrease the availability of sites where the silver nitrate could intercalate and oxidize. Consequently, the increase in monolayer permeability was shown not only by a decrease in the intensity of the silver staining, but also the gap formations observed in Figure 10

B-D. Thus, silver staining had the benefit of two indices of increased monolayer "permeability". [Degree of red counterstaining, however, was dependent upon the set of slides stained. Hence, the redness of cell contents and nuclei in Figure 10 fluctuates.]

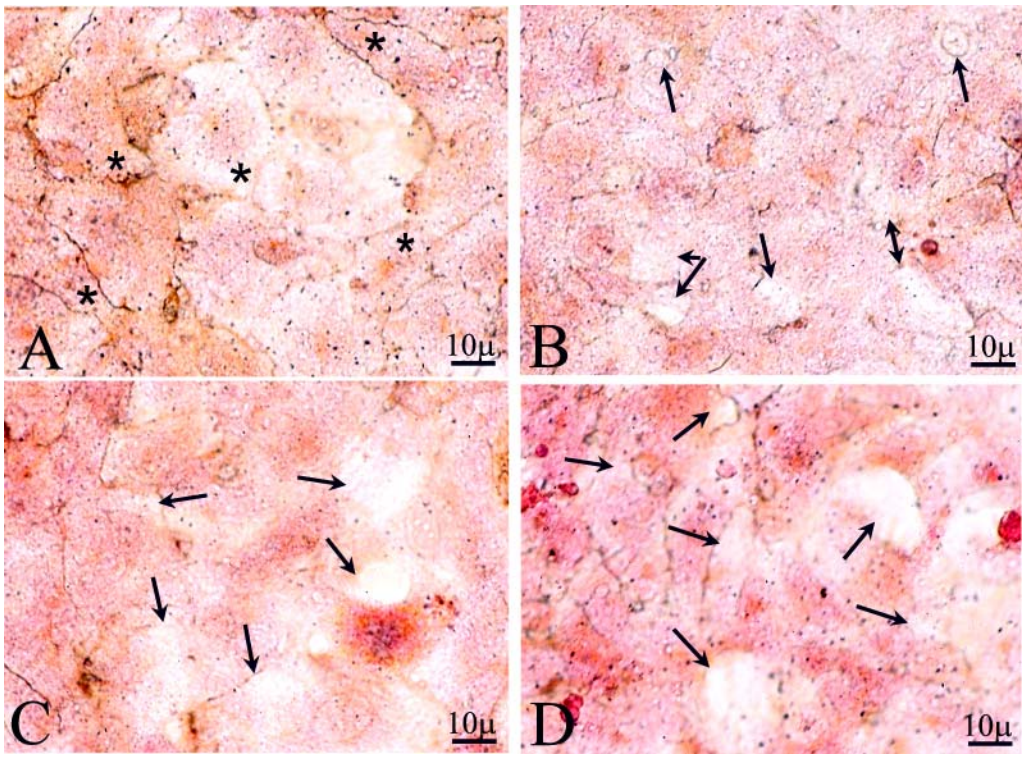

Figure 10: Representative results of silver staining experiments

Representative silver stained control (A) or 1 mM CE-treated (B-D) HMEC-1 monolayers from *n*=10 experiments per time point. Times of exposure were baseline (A), and 30 minutes (B), 1 hour (C), and 24 hours (D) after CE treatment. Asterisks (*) in (A) are placed near cell-to-cell borders stained with silver nitrate. Arrows (B-D) are used to point to gap formations and fading of the silver stain. Note scale bar at bottom right of each frame. Reprinted from *Clinica Chimica Acta*, Vol 345, D. Tacker and A. O. Okorodudu, "Evidence for injurious effect of cocaethylene in human microvascular endothelial cells," pages 69-77, Copyright 2004, with permission from Elsevier (with modifications).

Gap formations were also observed at 4 (not shown), 12 (not shown), and 24 (Figure 9D) hours after CE exposure. Results at 4 and 12 hours were very similar to those shown in Figure 9, C and D. Also, staining at 48 and 72 hours suggested that gap formations would be observed at those time points as well, but these later time points were not repeated. Thus, the reproducibility of gap formations in HMEC-1 cells at 48 and 72 hours is unknown, due to concerns regarding potential morphological effects of the altered media biochemistry observed at these late time points in Aim One.

The potential limitation to using a morphological analysis is that such data are largely qualitative. Qualitative changes were viewed that *seemed* significant, considering the mechanism that was proposed for pathogenesis, but the ultimate goal of Aim Two was to demonstrate that CE exposure was actually increasing the *permeability* (altering the functionality) of the HMEC-1 monolayers. This concern was addressed with a series of trans-endothelial electrical resistance experiments (Section 3.2.4, below), and further discussion will be saved until then.

3.2.4 Resistance measurement using ECIS

The measurement of electrical resistance is often used in studies involving endothelial cells because barrier function of the endothelium is central to tissue homeostasis [17, 117, 119, 120, 144, 156, 165]. Resistance of HMEC-1 monolayers was monitored for 72 hours using electronic cell-substrate impedance sensing (ECIS). A 72-hour exposure was chosen for ECIS monitoring to gauge normal HMEC-1 cell monolayer stability at late (48 and 72-hour) time points. ECIS analysis would allow for evaluation of the function of HMEC-1 at these late time points, and would address concerns that decreasing media quality over 72 hours would compromise the study of the effects of CE in the HMEC-1 model.

ECIS measures the electrical resistance created between the chamber electrodes and the cell culture media. When cells are confluent, resistance is high. However, when morphological changes occur that affect monolayer barrier integrity, resistance decreases (Section 3.2.3). Thus, ECIS provides a functional, quantitative measurement of monolayer integrity that is not provided by the silver stain assay.

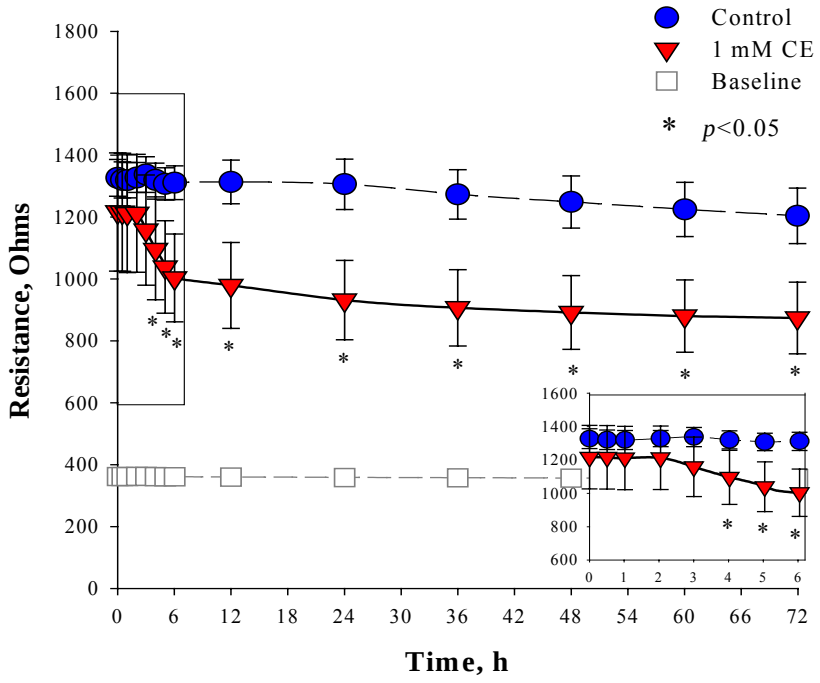

Figure 11: Results of electronic cell substrate impedance sensing (ECIS) experiments

HMEC-1 monolayers in special electrode containing culture wells were controls (blue circles, black dashed line) or treated with 1 mM CE (red inverted triangles, solid black line) for 72 hours. Blank wells (open squares, gray dashed line) were used as background controls. Inset is an enlargement of the boxed area in the main body of the graph. Asterisk represents $p<0.05$ by paired, two-tailed student's t-test. Error bars represent standard error of mean.

ECIS was used for two reasons. First, the even dispersal of ten (10) electrodes in the analysis chamber ensured more consistent results, representing an average of 10 readings taken from each monolayer in each well. The second reason was that a 72-hour experiment using an 8-well chamber allowed for triplicate sampling, duplicate background readings, and over 1,000 data points per well. Both of these benefits of ECIS

vastly increased the statistical power of the results from one set of samples. Thus, the three experiments, performed in triplicate, were more than adequate for determining consistency in the experimental conditions.

Figure 11 shows the results of the ECIS analysis of HMEC-1 under control and CE-treated conditions. A non-cell control (named "Baseline" in Figure 11) provided background resistance data from media alone in duplicate fibronectin-coated wells. The control baseline (time "0", 1327 ± 59.7 Ohm) was not significantly different from the CE-treated baseline (time "0", 1216 ± 190.9 Ohm, $p = 0.316$, Figure 11). As shown in the inset, the CE-treated group showed a significant decrease from its "0"-hour baseline in trans-endothelial resistance within 4 hours of CE exposure (1095 ± 162.5 Ohm, $p = 0.0335$). This trend (Figure 11) continued until the end of the experiment (874.5 ± 116.1 Ohm at 72 hours, $p<0.001$). Since resistance and permeability are inversely related, this result provided clear evidence of a significant increase in endothelial permeability after exposure to CE, and reflects a significant alteration in the physiological barrier function of the HMEC-1 endothelial monolayer by CE.

3.2.5 Summary of Aim Two studies

To summarize Aim Two, HMEC-1 cells exposed to CE undergo morphological changes that result in disruption of barrier integrity. Sub-cellular morphological changes demonstrated by transmission electron microscopy were temporally associated with the permeability change demonstrated by the silver staining and resistance monitoring, and further indicated that cellular injury rather than death was occurring in the exposure model. Silver staining clearly demonstrated intercellular gap formations that indicated an alteration of barrier stability. This finding was confirmed by the observed decrease in monolayer resistance, and demonstrates a functional alteration in the microvascular endothelium, which is central to the regulation of tissue homeostasis in vivo.

3.3 AIM THREE (CATION) RESULTS

3.3.1 Overview

Aim Three was intended to address the question of whether calcium flux was affected in CE-exposed HMEC-1. Two different conditions of ion detection were used. The first is herein called "immediate" exposure, since CE was injected into the quartz cuvette immediately after baseline measurement of cellular ion levels was initiated. This exposure was allowed to run for 5 minutes (300 seconds) after injection, and was performed using CE-naïve HMEC-1. Since permeabilizing the cell with digitonin and chelation with EGTA were required for accurate determination of intracellular ion levels, the total time for the "immediate" analyses was 700 seconds. However, only the first 400 seconds is reported below, since this is the time period where cytosolic calcium was monitored after CE addition.

The second study involved a pre-treatment in which HMEC-1 cells were exposed to control or CE-containing Tyrode buffer for one hour. After the control or CE treatment, baseline cytosolic Ca^{2+} was monitored for 100 seconds, followed by digitonin permeabilization and EGTA chelation. This experiment yielded only the baseline (cytosolic) and total Ca^{2+} content of the cells. Other exposure times (e.g., up to 24, 48, or 72 hours) could have been used for this analysis, but since Ca^{2+} signaling is transient, and the morphological changes in Aim Two began within the first hour of HMEC-1 cell/CE exposure, the early (5 minutes and 1 hour) time points were chosen for this study.

3.3.2 "Immediate exposure" experiments: calcium

The "immediate" analysis of Ca^{2+} in HMEC-1 with a 1 mM CE exposure was performed because Ca^{2+} was often monitored in the first 5 to 10 minutes of drug exposure in the various cocaine/calcium studies reported in the literature [38, 182, 183], and because Ca^{2+} flux is known to compose one of the first phases of cellular response to stimulus and/or injury. Since the existing data varied by treatment concentration, model, and time of analysis, predictions regarding the response of HMEC-1 monolayers to CE

by way of free calcium ion concentration (Ca^{2+}) could not be made. For permeability to change, as observed in the Aim Two studies (Sections 3.2.2 through 3.2.4), Ca^{2+} should increase in the cytosol, as well as in the whole cell. However, given the fact that the morphological and permeability changes were observed at 1 and 4 hours post-exposure, respectively, when this change would occur was unknown. Therefore, previous reports of Ca^{2+} changes after cocaine exposure (since no equivalent studies using CE with regard to exposure model were identified) were implemented in the experimental design, and Ca^{2+} was monitored for 5 minutes (300 seconds) after CE injection in Fura-2-loaded HMEC-1.

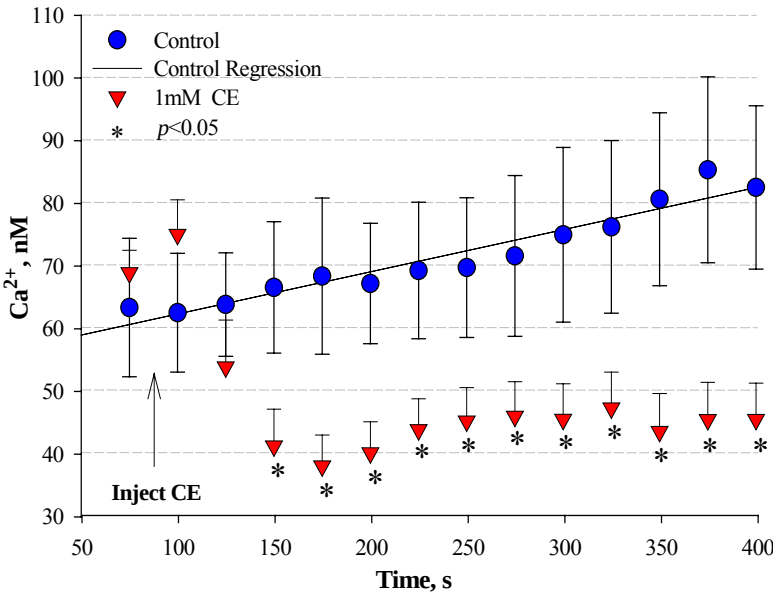

Figure 12: Results of "immediate" cytosolic Ca^{2+} monitoring experiments

Cytosolic Ca^{2+} was monitored in control (blue circles) and 1 mM CE-treated (red inverted triangles) over a 5 minute period. Linear regression for controls (black line) is shown. Error bars represent $p<0.05$ by Aspin-Welch two sample t-test for unequal variance.

In Figure 12, the results of the "immediate" Ca^{2+} monitoring experiments are shown. The baseline point at 75 seconds represented an average baseline value just before treatment with control or CE-containing Tyrode buffer. This was included for reference, and to demonstrate that the control and CE-treated HMEC-1 cells had similar baselines

(63.4 ± 11.0 and 68.9 ± 3.6 nM, respectively) when the experiment began. Between 75 and 100 seconds, CE was injected and the sample was allowed to adjust to the control or CE exposure for another 300 seconds (5 minutes).

Within 25 seconds of CE injection, a discernable but non-significant increase in free cytosolic Ca^{2+} was observed (75.0 ± 5.5 nM, $p>0.05$). This "spike" rapidly returned to baseline levels, and then decreased significantly. The decrease in free Ca^{2+} (41.3 ± 5.8 nM) after CE injection was rapid (Figure 11), reaching statistical significance ($p = 0.009$) at 50 seconds post-injection, and persisted until the end of the 300-second CE exposure (45.5 ± 5.8 nM, $p<0.001$). A linear regression of the control trend was included, which showed a steady increase in Ca^{2+} over time. This increasing trend in the control group was probably due to the calcium present in the buffer injected during ion monitoring, and compromised integrity of the cell membrane over time in the Tyrode buffer in the cuvette. As the cell membrane was compromised (a product of indicator loading and incubations at room temperature, Fura-2 AM literature, Molecular Probes and [167]), Ca^{2+} was able to steadily leak into the cell, thus causing the general rise in free cytosolic Ca^{2+} over time. This was one reason that the study was limited to 5 minutes. The potential mechanism(s) underlying the persistent decrease in free cytosolic Ca^{2+} are discussed in Chapter 4.

3.3.3 Pre-treatment experiments: calcium

Since emphasis was placed on the sequelae of events regarding toxicity and alteration of morphology and permeability in the CE exposure model in Aims One (Section 3.1) and Two (Section 3.2), a later time point (1 hour) for Ca^{2+} was included to coincide temporally with events observed in Aims One and Two. The 1-hour pre-treatment study was designed that would address a longer-term exposure of the HMEC-1 model to CE that would still have an impact on early cellular changes (e.g., gap formations and the decrease in monolayer resistance) in the HMEC-1 cell response to CE.

HMEC-1 cells were treated with Tyrode buffer or CE-Tyrode buffer for one hour, and then baseline (free cytosolic) Ca^{2+} was monitored for 100 seconds. Samples were

permeabilized with digitonin to determine maximal cellular free ionized calcium concentration. After 200 seconds, EGTA was added to chelate the calcium, so that ratiometric calculation of Ca^{2+} would be possible. Illustration 9 in Section 2.4.8 provides a mock-up of a typical experiment, which is detailed in Section 2.4.7.

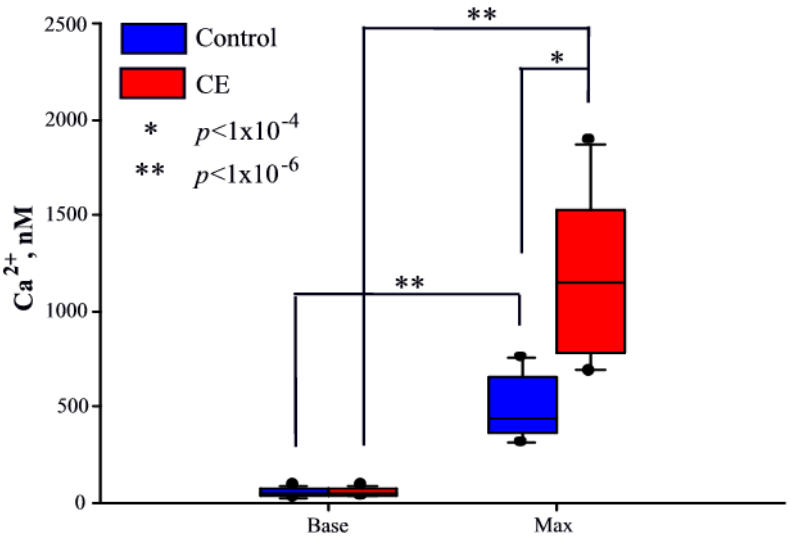

Figure 13: Results of cytosolic and total Ca^{2+} monitoring 1 hour after CE treatment

Control (blue box) and 1 mM CE-treated (red box) HMEC-1 monolayers were loaded with Fura-2 and the Ca^{2+} monitored after a 1-hour CE treatment. Base – cytosolic Ca^{2+} after treatment; Max – total cellular Ca^{2+} after permeabilization with digitonin. Whiskers (with dots) represent range of results, including high and low values. Single asterisk (*) represents p<1x10-4 between groups, double asterisk (**) represents $p<1x10^{-6}$ within groups. For both, significance was established by Aspin-Welch two-sample t-test for unequal variance.

Figure 13 shows the results of the pre-treatment experiments. Baseline free cytosolic Ca^{2+} concentration was unaffected by the 1-hour pre-treatment with CE (54.7 ± 8.6 nM) relative to controls (50.8 ± 7.3 nM, p = 0.694). Addition of digitonin caused a

highly significant increase in the total cellular free ionized calcium concentrations in both groups ($p = 1x10^{-6}$, Figure 12). Since this was the reason digitonin was added in the experiment, the increase was not unexpected.

The significant finding in this experiment was that the total cellular free Ca^{2+} concentration in the samples pre-treated with CE ("Max", 1179 ± 179.7 nM) was nearly three-fold higher than controls ("Max", 486.1 ± 49.3 nM, $p<0.001$, Figure 12). Since the calcium concentration of the Tyrode buffer in the cuvette was identical in both groups, the total cellular Ca^{2+} (cytosolic + sequestered/complexed) in the CE-treated HMEC-1 samples placed in the cuvettes had to be greater than controls before the analysis began. With a 1-hour treatment of the cells with CE, the cellular morphological changes observed (disruption/loosening of intercellular junctions, Aim Two, Figure 9) may have played a role in altering the permeability of the cell membrane, thus enhancing the effect of the digitonin in the CE-treated samples relative to controls, and producing the 1:1 ratio of intracellular to extracellular Ca^{2+}. More discussion of this finding will continue in the Discussion chapter (Section 4.1.3).

3.3.4 Summary of Aim Three studies

To summarize the Aim Three studies, CE exposure was associated with alterations in cytosolic and total cellular Ca^{2+} content. "Immediate" exposure of naïve HMEC-1 to CE resulted in a transient but significant increase in cytosolic Ca^{2+} (Figure 11), followed by a significant decrease for the remaining minutes of the analysis. However, a 1-hour CE treatment of HMEC-1 monolayers before monitoring of baseline and maximal Ca^{2+} resulted in a marked increase in maximal cellular Ca^{2+} (Figure 12).

3.4 AIM FOUR (SIGNALING) RESULTS

3.4.1 Overview

The Aim Three studies of intracellular ions marked the beginning of attempts to characterize mechanism(s) underlying changes observed in the Aim Two studies of morphology and permeability in HMEC-1 cells. In Aim Four, several assays were used to

address calcium-dependent second messenger and signaling cascades related to cellular mobilization and monolayer permeability change, and possible later pro-inflammatory action/protein expression. Due to the transient nature of signaling, and the instability and tight control of signaling molecules such as kinases and transcription factors, shorter time points (1 minute to 4 hours) were used for the Aim Four studies.

Inositol-1,4,5-trisphosphate (IP_3) was the first signaling molecule studied. IP_3 is a lipid-derived second messenger that is generated by activated PLC. Its generation is stimulated by the influence of calcium on the activity of PLC, and since IP_3 is the second messenger responsible for sarcoplasmic reticular release of calcium in the initial phases of cellular response (Section 1.5) [117, 120, 129, 132]. After monitoring IP_3 production during a limited time frame (up to 450 seconds/7.5 minutes) post-CE exposure, phosphorylation of p38 MAPK was measured, because kinase activity in general is stimulated by Ca^{2+}, and because activation of p38 MAPK-related signal cascades results in increased gene expression for pro-inflammatory molecules such as surface adhesion molecules and cytokines/chemokines (Section 1.5). Finally, the DNA binding activity of NF-κB transcription factor family proteins was evaluated using electrophoretic mobility shift assay (EMSA), cold competition EMSA, and supershift analysis. Since NF-κB activation in endothelial cells is typically associated with cell survival and inflammation, alterations in the DNA binding activity of NF-κB in HMEC-1 cells after exposure to CE would be associated with outcomes of survival and HMEC-1 cell "activation" (e.g., the expression of pro-inflammatory surface adhesion molecules, cytokines, and other secreted pro-inflammatory factors such as endothelin-1).

Many other important signaling molecules, such as PKC (directly activated by DAG) and other members of the MAPK family, could have been included in this study. However, due to the placement of p38 MAPK and NF-κB at the end of signaling processes, these two molecules were included in Aim Four to determine whether CE exposure would affect nuclear/DNA-binding activity of transcription factors. Such end points were chosen, because altered p38 MAPK and/or NF-κB would be associated with

activation of intermediate signaling molecules that could be included in future studies. This way, Aim Four would encompass general primary (IP_3) and specific terminal (p38 MAPK and NF-κB) pathways utilized by HMEC-1 cells during response to CE exposure.

3.4.2 Inositol 1,4,5 trisphosphate (IP_3) assays

Increases in cellular IP_3 levels open sarcoplasmic reticular surface calcium channels, which modulate cellular events such as actin-myosin mobilization and kinase signaling activation [117, 120, 129, 132, 144]. Since the Ca^{2+} concentrations monitored in Sections 3.3.2 and 3.3.3 showed a rapid decrease after 50 seconds, which was sustained for 5 minutes (Figure 11), concentration was placed on the effects of CE on IP_3 generation within the first 7.5 minutes of exposure (to allow for a short lag time between cytosolic Ca^{2+} and potential IP_3 changes). CE-exposed HMEC-1 should show a temporal association between IP_3 production and the Ca^{2+} flux that was observed (Section 3.3). This prediction was made based on knowledge of how IP_3 is generated, since an increase in cytosolic calcium (like that observed in Figure 12) within 25 seconds of CE injection results in the activation of PLC and the generation of IP_3. The IP_3 generated then amplifies the calcium signal through SR calcium release, thus perpetuating the calcium signal [117, 120, 129, 144, 145]. This process, however, is also auto-regulatory, since elevations in Ca^{2+} content of the cytosol also serves to block IP_3 generation, and the activity of the IP_3/Ca channel on the SR surface [117, 129].

Figure 14 shows that IP_3 levels increased 39% ± 2.4% from controls (p = 0.004, n=4) in the treated group after 60 seconds/1 minute of CE exposure. IP_3 accumulation was still elevated (25% ± 2.1% from controls, p = 0.030) at 150 seconds/2.5 minutes, but steadily decreased until IP_3 accumulation was significantly lower (-43.8% ± 1.1% from controls, p<0.001) at 450 seconds/7.5 minutes of CE exposure. These results point to an association between IP_3 and the calcium flux observed in Aim Three (Section 3.3). The massive increase in IP_3 accumulation within the first 60 seconds of CE exposure correlated with the significant decrease (Figure 12) in cytosolic Ca^{2+} after 50 seconds of CE exposure. These findings together suggest that cytosolic Ca^{2+} concentration decreased

enough in the initial period after CE exposure to initiate IP_3 generation in an attempt to regulate cytosolic Ca^{2+} concentrations. However, this effect was transient, since IP_3 levels decreased to levels much lower than controls at 450 seconds. This too pointed to an attempt to regulate Ca^{2+} in the cytosol, but it was likely to be one of negative regulation, as discussed in Chapter 4.

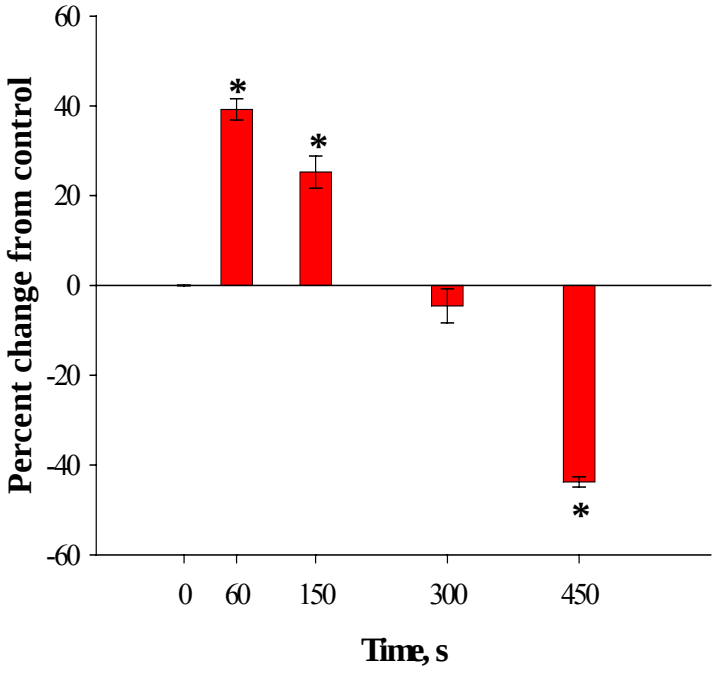

Figure 14: Results of IP_3 experiments

IP_3 was extracted from HMEC-1 after control or 1 mM CE treatment. Data are expressed as percent change from control for the CE-treated (red bars) group. Solid line represents normalized controls. Error bars represent standard error of mean. Asterisk (*) denotes $p<0.05$ by one-way ANOVA between control and CE-treated samples at each time point.

3.4.3 p38 MAPK phosphorylation assays

It is possible that many signaling pathways influenced by calcium would be affected in the experimental model. Due to the involvement of the MAPK signaling pathway in cellular cytoskeletal mobilization/altered permeability, and gene activation of pro-inflammatory proteins such as surface adhesion molecules and cytokines/chemokines [168], a p38 MAPK phosphorylation assay was included in the Aim Four experimental design. The p38 isoform was chosen because of the association between p38 MAPK with

pro-inflammatory response in endothelial cells and the influence of p38 MAPK phosphorylation and activation on NF-κB activation and transcriptional activity [124, 138, 168].

Previously, p38 MAPK phosphorylation assays were conducted on HMEC-1 cells to characterize their response to lipopolysaccharide (LPS) [168]. An LPS positive control was included to determine the maximal p38 MAPK phosphorylation of the model. Phosphorylation of p38 MAPK was measured in picograms/107 cells (pg/10^7 cells) at 0, 1, 2, and 4 hours post-exposure.

Figure 15 shows a maximal response (395.1 ± 63.7 pg/10^7 cells) from the LPS control group at 2 hours post-exposure, which remained high (394.9 ± 52.8 pg/10^7 cells) at 4 hours. This was a highly significant increase (p<0.001, one-way ANOVA) from baseline (14.7 ± 8.6 pg/10^7 cells at 0 h), and demonstrates that HMEC-1 cells increase phosphorylation of p38 MAPK in response to pro-inflammatory stimuli.

Control phospho-p38 levels increased over time from a baseline of 14.7 ± 8.6 pg/10^7 cells to a maximum of 84.0 ± 35.0 pg/10^7 cells at 4 hours post-CE exposure (Figure 15, p<0.001). This increase was probably due to a background response to the PBS, which was used as the vehicle for all groups. Comparing between groups, time points in the LPS group were elevated versus the negative control group (Figure 15, p<0.001), and represented a useful range with which to gauge effect for the CE group.

When CE was added to the HMEC-1 cultures, a response was observed that was immediate (occurring within 5 minutes/0.08 hours), and intermediate when compared to the positive LPS and negative 0 mM CE controls (Figure 15). After one hour of CE exposure, phospho-p38 levels averaged 109.6 ± 30.4 pg/10^7 cells (versus a baseline of 14.7 ± 8.6 pg/mL, p<0.001). Phospho-p38 levels further increased over time, reaching 162.2 ± 37.1 pg/10^7 cells at 4 hours (p<0.001).

Though levels of phospho-p38 were lower than those observed for the LPS positive control group, the difference between the CE-treated group and the control group was significant (Figure 14, p<0.001 by one-way ANOVA). This result demonstrates that CE exposure in microvascular endothelium activates p38 MAPK, which could be

involved in alteration of endothelial permeability as well as pro-inflammatory cellular responses such as alteration of surface adhesion molecules and cytokines [124, 138, 168]. Such responses underlie the promotion of inflammation in blood vessels and tissues, and thus demonstrate a link between the morphological and functional responses that were observed in the Aim Two studies (permeability and gap formations), and intracellular mechanism-of-effect.

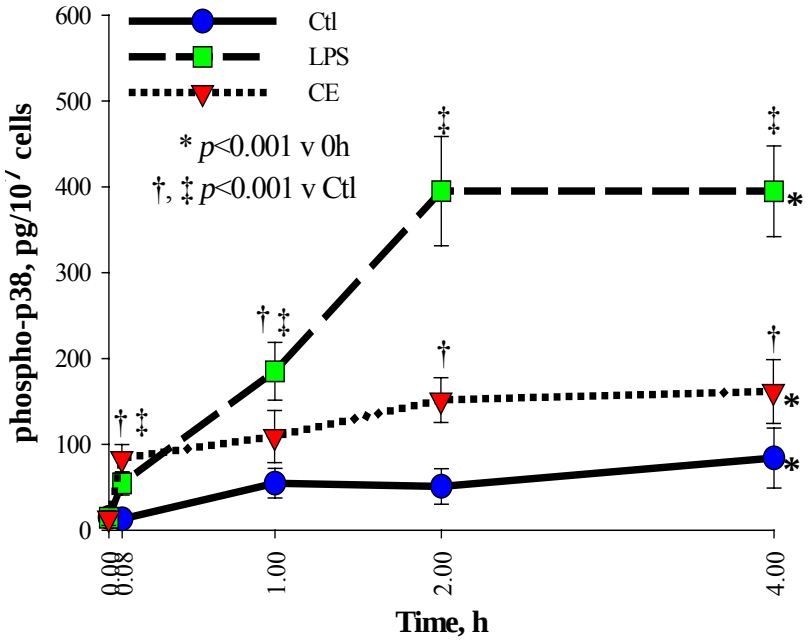

Figure 15: Results of phospho-p38 MAPK assays

Phosphorylated p38 MAPK was extracted from control (blue circles), 1 mM CE-treated (red inverted triangles), or LPS-treated (green squares). HMEC-1 Error bars represent standard error of mean. Asterisk (*) denotes $p<0.05$ by one-way ANOVA within groups (time as factor). Significance of $p<0.05$ for CE (†) or LPS (‡) result versus control by one-way ANOVA.

3.4.4 DNA binding activity (EMSA) assays

The goal of the Aim Four experiments was to incorporate several molecular methods that would address different levels of the HMEC-1 intracellular response to CE, ranging from the cytosol to the nucleus. Since an effect on morphology is only one component of pathological investigation, EMSA was performed to determine the DNA binding activity of NF-κB in control and CE-treated HMEC-1 to thus extend the study of cellular responses to CE to the nucleus. Though no studies were conducted to assess transcripts that would result from transcription factor activation (such as microarray analysis or Northern blot), these assays were designed as a prelude to genomic or proteomic questions that could be addressed in future experiments.

The same three groups used in the phospho-p38 determination were used for DNA binding assays: control (0 mM CE); positive (LPS) control; and 1 mM CE-treated. The LPS positive control was employed in this study because LPS exposure in endothelium is known to result in activation and increased DNA binding activity of NF-κB, as well as up-regulation of adhesion molecule targets of NF-κB [184, 185]. Time points used were baseline (no treatment), 1, and 4 hours post-treatment, because transcription factor activation is usually transient, and takes place within the first few hours of cellular response to stimulus or injury. As a result of the previous findings, and because p38 MAPK activation is linked to stress responses and NF-κB activation [186], this seemed a good preliminary study of DNA binding activity for the HMEC-1/CE exposure model.

Preliminary EMSA Experiments

The first step in analyzing NF-κB activation in the HMEC-1/CE exposure model was a preliminary EMSA of nuclear extracts with the Igκ oligonucleotide. This NF-κB site was originally identified in the mouse kappa light-chain promoter that binds all proteins in the NF-κB family [137, 170, 177]. Optimization of EMSA analysis in HMEC-1 cell extracts (Figure 16) demonstrated six (6) potential bands of interest, but non-

specific oligonucleotide/protein interaction would yield bands that may contain proteins other than the various dimers of NF-κB family proteins such as RelA(p65) and p50.

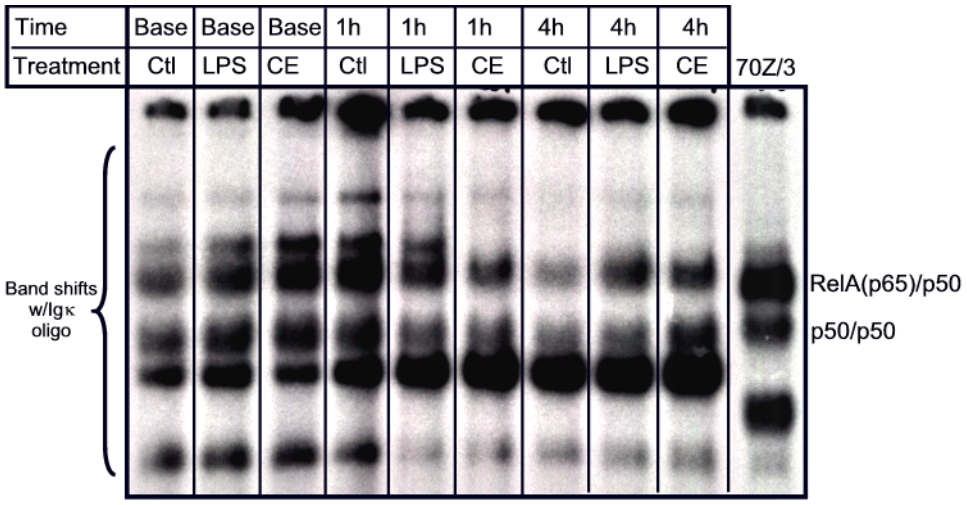

Figure 16: Early EMSA results

EMSA showing bands (shifts) that result when the Igκ oligonucleotide binds protein dimers of the NF-κB family in nuclear extracts taken from HMEC-1 cells when un-treated (baseline, Base), or under control (Ctl), LPS (LPS), and CE (CE) treatment conditions for 1 (1h) or 4 (4h) hours. 70Z/3 cells are pre-B cells that express NF-κB and were used as a positive control. Negative control (not shown) was free oligonucleotide, which produced no bands.

Cold competition assays

In order to identify which of the 6 bands in Figure 16 represented specific NF-κB dimer/oligonucleotide complexes, cold competition assays were conducted. The cold competition EMSAs were conducted in the same manner as the preliminary EMSAs. However, in this assay, the LPS-treated HMEC-1 extracts were used as a presumptive NF-κB-positive control. Thus, standard LPS-treated extract was placed next to an LPS-

treated extract containing 50-fold molar excess of non-radioactive Igκ oligonucleotide in the loading wells of the polyacrylamide gel. The result of the cold competition was the identification of two bands of interest for characterization in later experiments.

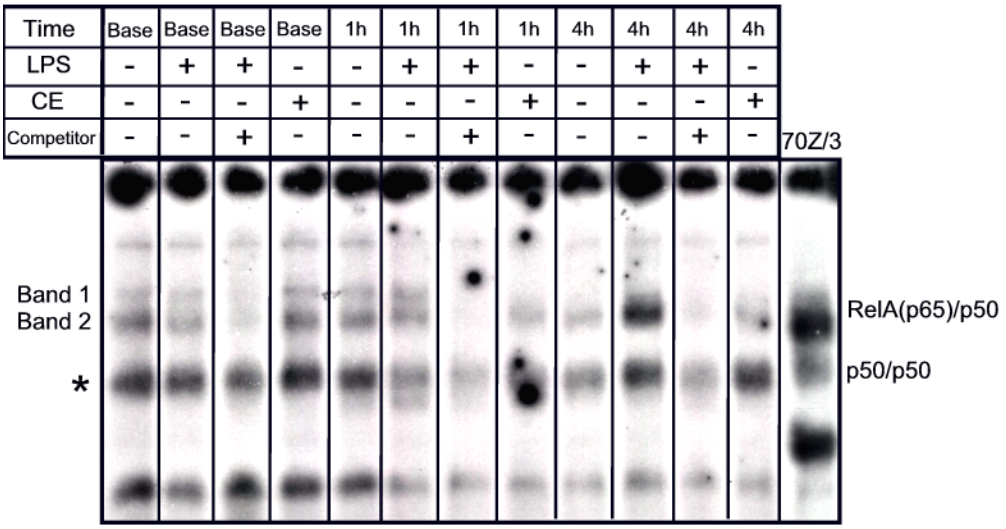

Figure 17: Results of the cold competition assays

LPS = LPS treatment of HMEC-1 cells. CE = CE treatment. Competitor = 50-fold molar excess of unlabeled oligonucleotide. Base = no-treatment baselines. 1h = 1 hour of treatment with CE or LPS. 4h = 4 hours of treatment with CE or LPS. 70Z/3 is the positive control for NF-κB. Known dimers for 70Z/3 are identified on the right. HMEC-1 bands (1 and 2) are labeled on the left. Asterisk (*) represents a third band with specific and non-specific complexes.

As shown in Figure 17, two bands (Bands 1 and 2) of interest were identified based on their elimination by excess unlabeled Igκ oligonucleotide. Complexes specifically bound to unlabeled oligonucleotide could not be bound by the ^{32}P-labeled oligonucleotide. Thus, the specifically bound bands in the EMSA were eliminated, and bands that resulted from non-specific binding remained visible. Since the EMSA patterns for all samples contained similar bands, cold competition was not necessary for all of the

samples. A third band (* in Figure 17) under Band 2 appeared to decrease in density with competition, but given the decrease in band elimination in the competition lanes relative to Band 1 and Band 2, this third band was not studied further because it represented a combination of specific and non-specific binding of the Igκ oligonucleotide. Using the 70Z/3 lanes as a comparison, it is likely that p50/p50 homodimers may have been present. However, the presence of non-specific binding in Band * precluded its use in any quantitative analysis. Thus, the two bands that showed the most elimination after competition with unlabeled oligonucleotide were designated "Band 1" and "Band 2" until they could be further characterized. EMSA analyses including antibodies directed against specific NF-κB proteins to either supershift or eliminate various bands would determine identify which NF-κB proteins were present in each band. This approach would also characterize any changes in NF-κB dimer composition that may occur as a result of the treatment conditions presented to the HMEC-1 cultures (LPS and CE).

Time course of NF-κB band density

Regarding NF-κB dimer DNA binding activity, Figure 18 shows a comparison of the radio-densities of samples not treated with antibody during the supershift assays. Controls were set to 100% at all time points, so that changes in NF-κB could be compared between groups. Baseline LPS and CE band radiodensity (Figure 18) were not different from controls.

When the average density of Band 1 from LPS-treated samples was compared to controls, no significant change was observed after 1 hour of treatment. However, a significant increase in Band 1 density was observed at the 4-hour time point (185% ± 9% of control, $p = 0.013$). This result contrasts sharply with the significant decrease observed in Band 2 density (54% ± 3% of control, $p<0.001$) in LPS-treated samples at the 1-hour time point relative to controls. At 4 hours of LPS treatment, Band 2 density was greater than 100% of controls, but failed to reach significance. Thus, LPS treatment of HMEC-1 increased NF-κB DNA binding activity of Band 1 by 4 hours, and decreased NF-κB DNA binding activity of Band 2 by 1 hour.

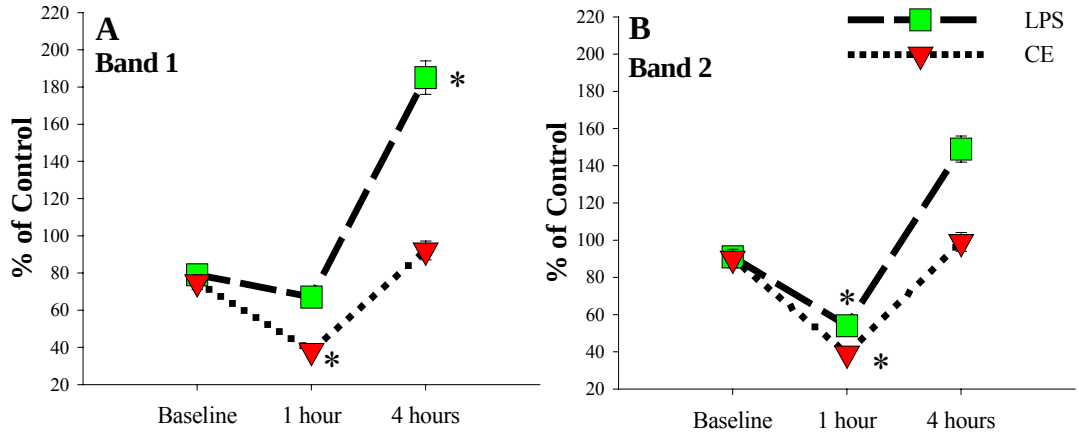

Figure 18: Alterations in NF-κB Bands 1 and 2 in HMEC-1 after treatment with LPS or CE

LPS- (green squares) and CE- (red inverted triangles) treated HMEC-1 band densities expressed as a percentage of control band density at each time point. A = Band 1, B = Band 2. Asterisk (*) represents $p<0.05$ by paired, two-tailed student's t-test.

CE treatment resulted in decreases in NF-κB DNA binding relative to control (Figure 18). Bands 1 and 2 were both significantly decreased (38% ± 2% of control, p = 0.03 and 39% ± 2% of control, p = 0.005, respectively) after 1 hour of CE treatment. However, by 4 hours of treatment, the density of Bands 1 and 2 were nearly equivalent (92% ± 5% of control, and 99% ± 5% of control, respectively, Figure 17) to controls. Thus, CE treatment of HMEC-1 results in a transient decrease in NF-κB DNA binding activity after 1 hour, which recovers by 4 hours of CE exposure. This decrease in DNA binding activity implies a stabilization of NF-κB dimers in the cytosol, which is contrary to the predicted outcome of this experiment. The prediction was that since MAPK phosphorylation increased (Figure 14), NF-κB DNA binding would also increase. Further

discussion of the relevance of this observation can be found in the Discussion (Section 4.1.4).

Supershift assays I: RelA(p65)

Since NF-κB RelA(p65) is ubiquitous and exhibits a strong supershift in the 70Z/3 pre-B cell line, 70Z/3 extracts were used as a positive control throughout this experimentation. Adding antibodies to EMSA reactions increases the molecular weight of bands containing the protein of interest (in this case RelA), moving the supershift band upwards in the gel with proper binding of radiolabeled Igκ oligonucleotide, and the density of the regular band should decrease. Alternatively, if a band contains RelA and the antibody either competes with the Igκ oligonucleotide for binding sites or alters protein conformation, thereby altering the ability of the oligonucleotide to bind DNA. Thus, the entire regular band could disappear rather than be visibly supershifted.

No supershifted bands were observed in any of the samples containing the anti-RelA antibody (Figure 19) as opposed to the supershift observed using the mouse pre-B cell line 70Z/3. This may be due to differences in the antibody binding to human RelA as opposed to mouse RelA. For example, the human HMEC-1 samples could have presented competing binding sites for the antibody and the oligonucleotide or otherwise altered the ability of Igκ to bind DNA, and the mouse 70Z/3 samples did not. Despite this difference, however, both Bands 1 and 2 were decreased in intensity in the presence of antibody against RelA, thereby indicating that RelA is one member of the NF-κB dimer in each band. The decline in any additional bands (particularly the third band, *, at 1 hour, Figure 17) may be the result of proteolytic cleavage of RelA protein. Proteolytic cleavage produces artifacts of nuclear extraction that are often observed in some cell lines despite the liberal use of protease and phosphatase inhibitors during sample preparation. Such could be the case in the later (Figures 20-22) supershift assays as well.

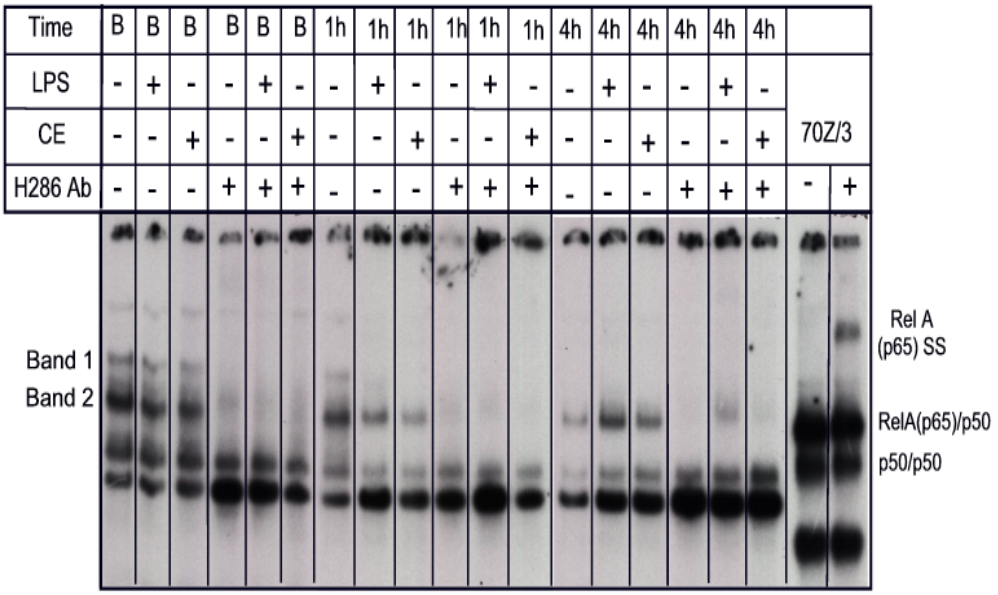

Figure 19: Results of the RelA(p65) supershift assays

Supershift analysis of HMEC-1 cells for RelA(p65). LPS = LPS (0.1 μg/mL) treatment; CE = CE (1 mM) treatment. Base = no-treatment baselines. 1h = 1 hour of treatment with CE or LPS. 4h = 4 hours of treatment with CE or LPS. H286 = anti-RelA antibody. 70Z/3 is the positive control for NF-κB. Known dimers and RelA(p65) supershift for 70Z/3 are identified on the right. HMEC-1 bands (1 and 2) are labeled on the left. Note the lack of supershifting in the HMEC-1 samples, which resulted from antibody competition with the Igκ oligonucleotide

Regarding RelA (p65, Figure 19), a 75% loss of Band 1 density in all groups at baseline was observed. Band 1 at 1 and 4 hours was completely eliminated by anti-RelA(p65). Thus, RelA(p65) appears to be a major component of Band 1 in all three groups, and, assuming that none of the other antibodies affect Band 1, it is plausible that Band 1 is composed solely of RelA(p65) homodimers in control, LPS-, and CE-treated HMEC-1 after 1 to 4 hours of drug exposure (Figure 19).

RelA(p65) was also a major component of Band 2 in the HMEC-1 extracts analyzed (Figure 19). Baseline HMEC-1 extracts from all groups showed a decrease in Band 2 density (~60%). By 1 hour of treatment in all groups of cells, the intensity of Band 2 had declined by 75%. The difference in Band 2 density after antibody treatment was most noticeable at the 4-hour time point, where control and CE-treated extracts showed decreases in Band 2 intensity exceeding 75%. However, LPS-treated HMEC-1 extracts lost less Band 2 density (~50%, Figure 19). This demonstrates that a non-RelA-containing protein complex is present in Band 2 after 4 hours of LPS treatment in HMEC-1 cells.

Overall, RelA(p65) appears to be a component of Band 2 in HMEC-1 extracts, and the level of RelA(p65) in dimers composing this band is not affected by CE treatment (relative to the changes observed in the control group). LPS, however, decreases the amount of RelA(p65) in Band 2 over time. RelA could be a component of both bands due to different dimerization patterns of RelA (with itself, or another NF-κB protein). Since different NF-κB proteins have different molecular weights, a RelA homodimer would migrate differently through a polyacrylamide gel than a RelA/p50 heterodimer. Thus, it is plausible that both bands could contain RelA. Determinations of other proteins in the band complexes (e.g., p50, c-Rel, or p52) would confirm this reasoning.

Supershift assays I: p50

A supershift assay using an anti-p50 antibody also yielded interesting results (Figure 20). First, two supershifted bands were observed that migrated similarly to the 70Z/3 control supershift for p50. Thus, these supershifted bands are probably specific to p50 and are likely to indicate p50 homodimers (from Band *) and p50/RelA(p65) heterodimers. Band 1 showed the same decrease in density over time, disappearing in all treatment groups by 4 hours. However, the 1-hour sample for LPS-treated cell extracts showed two strong bands that cannot be explained at this time (Figure 20).

Second, patterns of p50 supershifting changed depending on the time and treatment group. All three groups showed supershifting of p50 at baseline, with complete

elimination of Band 1 and supershifting of approximately 25-30% for Band 2. At the 1-hour time point, the control group showed elimination of Band 1, and a Band 2 supershift of approximately 30%. However, supershifting in this group was significantly less at 4 hours (approximately 20% for Band 2), and Band 1 was undetectable in both regular EMSA and supershifted samples. Thus, control HMEC-1 samples showed p50 content in both Bands 1 and 2 at baseline and 1 hour, and in Band 2 only at 4 hours.

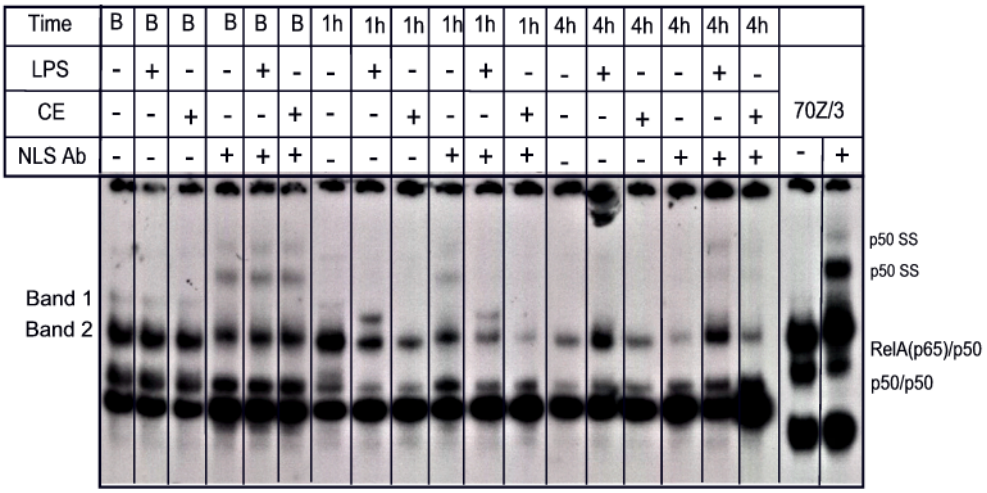

Figure 20: Results of p50 supershift assay

Supershift analysis of HMEC-1 cells for p50. LPS = LPS (0.1 μg/mL) treatment; CE = CE (1 mM) treatment. Base = no-treatment baselines. Base = no-treatment baselines. 1h = 1 hour of treatment with CE or LPS. 4h = 4 hours of treatment with CE or LPS. NLS = anti-p50 antibody. 70Z/3 is the positive control for NF-κB. Known dimers and p50 supershifts for 70Z/3 are identified on the right. HMEC-1 bands (1 and 2) are labeled on the left. Note the two supershifted bands in the HMEC-1 samples.

LPS-treated lanes showed a different pattern of p50 supershifting at 1 and 4 hours. At the 1-hour time point, both Bands 1 and 2 showed a marginal change in band density, but no supershifted bands were detectable. At 4 hours, Band 1 was undetectable in both regular EMSA and supershifted lanes, and Band 2 showed minimal (10-20%) change in

density. However, two faint supershifted bands are visible at 4 hours, suggesting that the supershifted p50 observed came from Band 1, which was probably completely supershifted by treatment with anti-p50 antibody, and not detectable in the regular EMSA lane. Consequently, p50 content of Band 1 increased, and decreased in Band 2, after LPS treatment in HMEC-1.

CE-treated lanes showed no detectable Band 1 at the 1- and 4- hour time points. However, Band 2 density was strong with EMSA at both 1 and 4 hours. At 1 hour, Band 2 density decreased by 50% upon supershifting, but no supershifted band was detectable. At 4 hours, Band 2 density was not altered by Supershift assay, but two faint supershifted bands were observed. Since this is the same pattern that was observed for LPS-treated HMEC-1 at 4 hours, it is probable that the source of the supershifted bands after CE treatment at 4 hours is Band 1, even though the regular EMSA lane shows no detectable Band 1 density. Thus, p50 content of Band 2 decreased, and increased in Band 1, over time with CE treatment, a pattern that matches that of the LPS exposure.

Overall, it appeared that p50 was a component of the NF-κB complexes in Bands 1 and 2, but the amount of p50 that was present in the nucleus declined over time in Band 2, while Band 1 p50 content increased over time. Thus, at the end of p50 supershift analysis, Band 1 appeared to be composed of a RelA/p50 heterodimer because of the complete elimination of Band 1 at baseline and 4 hours when antibody to either protein was added. Band 2 appeared to contain both RelA(p65) and p50, and potentially other NF-κB family proteins, due to the lack of complete elimination of the band when antibody to either protein was added.

Supershift assays III: c-Rel

The third NF-κB family protein assessed using supershifts was c-Rel (Figure 21). As with RelA, c-Rel did not supershift. Instead, bands containing c-Rel were eliminated when anti-c-Rel antibody was added to EMSA samples. Addition of c-Rel antibody to 70Z/3 extracts also resulted in reductions in band intensities, rather than supershifting.

In Figure 21, significant change in Band 1 density (>75%) was observed when supershift lanes were compared to regular EMSA lanes at baseline. At baseline, a reduction in Band 2 density (of approximately 50%) was also observed when anti-c-Rel was added to HMEC-1 samples.

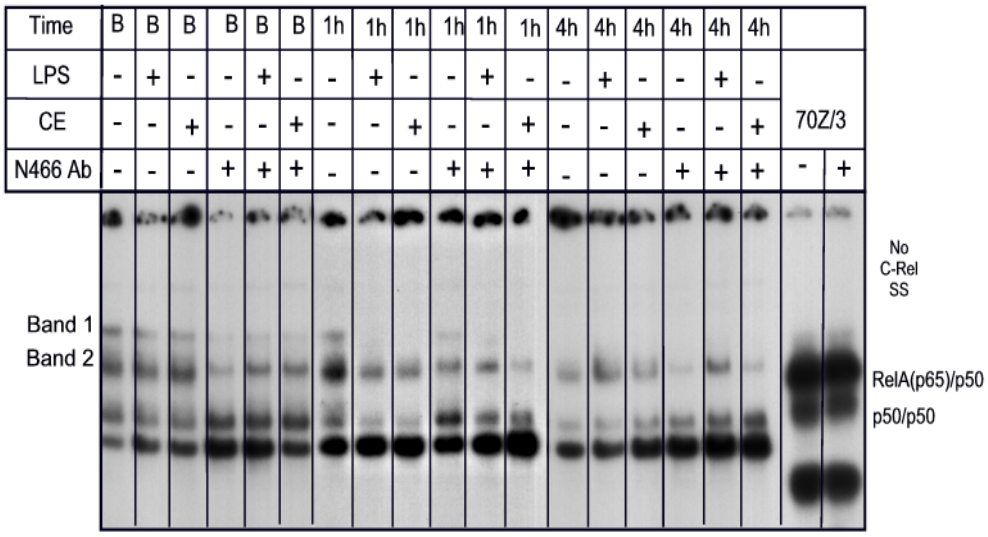

Figure 21: Results of c-Rel supershift assay

Supershift analysis of HMEC-1 cells for c-Rel. LPS = LPS (0.1 μg/mL) treatment; CE = CE (1 mM) treatment. Base = no-treatment baselines. Base = no-treatment baselines. 1h = 1 hour of treatment with CE or LPS. 4h = 4 hours of treatment with CE or LPS. N466 = anti-c-Rel antibody. 70Z/3 is the positive control for NF-κB. Known dimers for 70Z/3 are identified on the right. HMEC-1 bands (1 and 2) are labeled on the left. Note the lack of supershifting in both 70Z/3 positive control and HMEC-1 samples.

Control HMEC-1 showed no Band 1 or 2 density changes at 1 hour, but Band 2 density decreased again at 4 hours. LPS-treated extracts showed no change in Band 1 or 2 densities at 1 or 4 hours. This suggests that c-Rel is not a component of either band after HMEC-1 exposure to LPS. This lack of response is not unexpected, since c-Rel expression is low in 70Z/3 cells, as well as other kinds of cells [137]. CE-treated HMEC-

1 nuclear extracts showed a strong decrease (>75%) in Band 2 density after 1 and 4 hours of treatment (Band 2 was not detected in either sample). Thus, c-Rel is a potential component of Bands 1 and 2 in HMEC-1 cells under baseline conditions. LPS treatment appears to decrease c-Rel in Bands 1 and 2, but not CE treatment. The effects of these treatments on Band 1 c-Rel composition at 4 hours are unknown.

Supershift assays IV: p52

Performing EMSA on HMEC-1 extracts using anti-p52 antibody had a minimal effect on the densities of Bands 1 and 2 (Figure 22) at baseline. Neither band showed a significant change in density in the supershift lane relative to the regular EMSA lane, despite the presence of a very faint p52 supershifted band near the loading well. This faint supershift was only observed at baseline. Thus, the supershifted band could have originated from another band on the gel, such as the third (*) band from Figure16.

At 1 hour, however, some change in band densities were observed. Control samples showed a slight change in Band 2 density. Band 1 density was variable, with no Band 1 visible in the regular EMSA lane, but a visible Band 1 was present in the supershifted lane. The conclusion was made that Band 1 density was not altered in the 1-hour control samples. LPS treatment showed a noticeable reduction in Band 2 density. Also, LPS-treated samples showed variability in Band 1 density. The conclusion was that Band 1 density was not altered by LPS Treatment. No changes were observed in Band 1 or 2 densities in the 1- or 4-hour CE-treated samples. At 4 hours, no supershifting was observed. Also, no discernable change in band density was observed at 4 hours.

Thus, it appears that p52 is not a component of Band 1, and may be a component in Band 2 complexes. LPS treatment appeared to decrease p52 content at 1 hour, comparable to controls. CE treatment does not appear to affect the p52 content of HMEC-1.

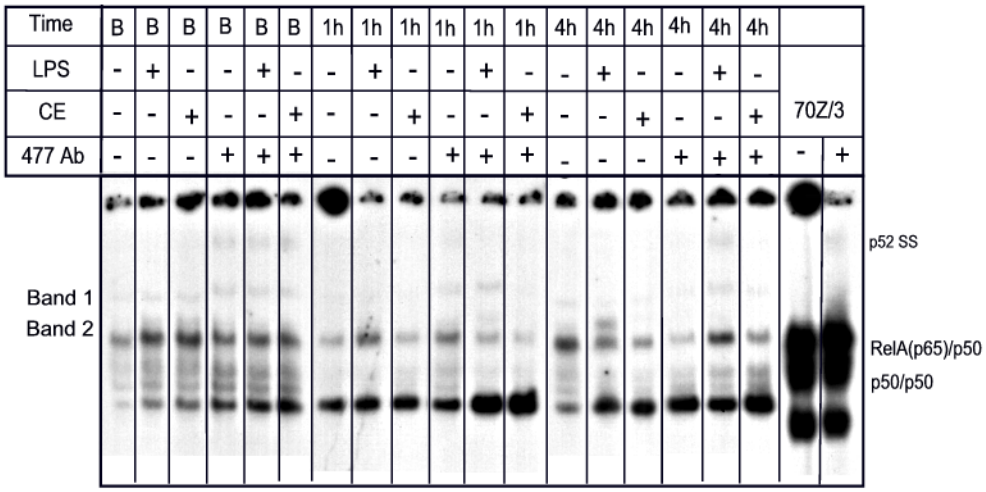

Figure 22: Results of p52 supershift assays.

Supershift analysis of HMEC-1 cells for p52. LPS = LPS (0.1 μg/mL) treatment; CE = CE (1 mM) treatment. Base = no-treatment baselines. Base = no-treatment baselines. 1h = 1 hour of treatment with CE or LPS. 4h = 4 hours of treatment with CE or LPS. 477 = anti-p50 antibody. 70Z/3 is the positive control for NF-κB. Known dimers and p52 supershift for 70Z/3 are identified on the right. HMEC-1 bands (1 and 2) are labeled on the left. Note the faint supershifting in both 70Z/3 positive control and HMEC-1 samples.

Supershift assays V: Band composition

From these supershifts, the presence of the four NF-κB family proteins in the nucleus at various times and treatments could be characterized. First, Band 1 appears to contain RelA(p65), p50, and to a lesser degree c-Rel. Thus, Band 1 is probably composed of RelA(p65)/p50 heterodimers (Table 3). This is reasonable considering that the upper band seen on 70Z/3 control samples is known to be a RelA(p65)/p50 dimer, and that the RelA/p50 heterodimer is the most common NF-κB complex detected in cells. This complex typically acts as an activator of gene transcription in response to endothelial cell

stimulus and/or stress. Also, in resting or untreated HMEC-1, these complexes are present, and they diminish with CE or LPS treatment rapidly (within 1 to 4 hours). This is consistent with the transient nature of transcription factor activation and regulation.

The composition of Band 2 was more complex than Band 1, potentially containing all four NF-κB proteins at any given time. Based on the degree of supershifting (or elimination) observed in the Aim Four experiments, the predominant NF-κB proteins in Band 2 are RelA (p65) and p50, with lesser amounts of c-Rel, and potentially p52. Since p52 activity was low in the EMSA analysis in this study (Figure 22), and p52 activity is almost exclusively observed in lymphatic tissues [137, 187], p52 is not considered to be a component of Band 2 NF-κB complexes (observed activity could have resulted from cross-reactivity between the p52 antibody and the p50 subunit present in Band 2). Thus, Band 2 is composed of RelA-, p50-, and c-Rel-containing complexes for the following reasons.

Table 3: Composition of Bands 1 and 2, EMSA analysis

	RelA (p65)	p50	c-Rel	p52	LPS		CE	
					1 h	4 h	1 h	4 h
Band 1	✓	✓	×	×	↔	↑	↓	↔
Band 2	✓	✓	✓	?	↓	↔	↓	↔
Symbols: ✓ = present, × = not detected, ? = inconclusive, ↔ = no change, ↑ = increase, ↓ = decrease								

First, given that the second band observed in 70Z/3 control samples is known to contain p50 homodimers, the major component of HMEC-1 Band 2 is probably a p50 homodimer. This is probable because the p50 homodimer is one of the three dominant NF-κB complexes in most cells, and since the RelA/p50 homodimer (Band 1) migrated in

a similar pattern relative to the known banding patterns of the 70Z/3 controls, Band 2 is the most likely location for the p50 homodimer.

Second, since RelA/p50 dimers containing a truncated form of RelA(p65) are known to migrate immediately below the p50 homodimer [188], this explains the presence of RelA in both bands (1 and 2). The truncation of the RelA subunit occurs at the C-terminal end of the protein, and is an artifact of the purification method. Despite the addition of copious amounts of protease inhibitors to the lysis buffers used in this method, it appears that some truncated RelA(p65) resulted from the nuclear extraction, hence creating a smaller RelA/p50 dimer that migrated similar to the p50 homodimer.

Finally, c-Rel is an NF-κB protein that is constitutively localized to the nucleus, and provides NF-κB activity in quiescent cells [137, 187]. Since the c-Rel/p50 homodimer is most common in the nucleus [187], it is reasonable to conclude that the c-Rel activity noted in Band 2 is due to the presence of this complex.

Thus, the three most probable dimers composing Band 2 are: 1) p50 homodimers; 2) truncated RelA/p50 heterodimers; and 3) p50/c-Rel heterodimers (in order of abundance). One final observation made about Band 2 is that its composition seems to change with CE or LPS treatment and time (consistent with activation of RelA/p50 and/or p50 homodimers, and the potential down-regulation of c-Rel/p50), as demonstrated in Figures 19-22.

3.4.5 Summary of Aim Four studies

To summarize the results of Aim Four, CE exposure to HMEC-1 resulted in an initial increase, and then steady and significant decrease, in the generation of IP_3 (Figure 13). Also, CE-treated HMEC-1 showed increased amounts of phospho-p38 MAPK (Figure 14) relative to controls. Nuclear localization of NF-κB fluctuated after exposure to CE or LPS, with CE treatment tending to decrease NF-κB DNA binding activity transiently (at 1 hour but not 4 hours, Figure 17), and LPS treatment tending to decrease (1 hour), then increase (4 hours) NF-κB DNA binding activity. Two NFκB-containing

bands were identified in all HMEC-1 extracts (Figures 18-21). The composition of Band 1 was predicted to be a RelA(p65)/ p50 heterodimer. Band 2 had a more complex composition, and was probably composed of p50/p50 homodimers, truncated RelA dimerized with p50, and c-Rel/p50 dimers.

CHAPTER 4: SUMMARY AND DISCUSSION

4.1 SUMMARY OF MAJOR RESEARCH FINDINGS

There were four major findings in this study. First, HMEC-1 exposure to CE did not alter cellular viability or induce cytotoxicity. Second, CE exposure in HMEC-1 cultures resulted in increased monolayer permeability, as evidenced by the formation of intercellular gaps noted one (1) to 24 hours after CE exposure, and a decrease in trans-endothelial resistance. Third, intracellular calcium concentration was altered in HMEC-1 exposed to CE, as shown when HMEC-1 cytosolic free Ca^{2+} concentrations fluctuated immediately after CE exposure, and when total cellular Ca^{2+} increased markedly after a 1-hour CE treatment prior to monitoring. Finally, CE exposure in HMEC-1 was associated with increased p38 MAPK phosphorylation and decreased DNA binding of NF-κB dimers in the nucleus. Similar changes would be expected in an HMEC-1/cocaine exposure model, since cocaine and CE have similar pharmacological profiles, and were previously reported to affect HUVEC permeability equally [17].

4.1.1 HMEC-1 exposure to CE is not cytotoxic, but may alter cellular function

Several general indices of cellular viability were used in the Aim One experiments to determine whether the HMEC-1/CE exposure model would be suitable for investigation of the central hypothesis that CE induces morphological and functional changes in microvascular endothelium. Aside from directly causing vasculitis, these changes could promote ischemia and inflammation in surrounding tissues via alterations in second messengers and signal transduction, which are partially mediated by cation flux. The growth curve (Figure 1) results showed that exposure to HMEC-1 cells to 1 mM CE was sufficient to alter HMEC-1 cell function as indicated by the affects on growth and viability of proliferating HMEC-1 (Figures 1 and 2, Table 2). CE was demonstrated to persist in cell culture media for up to 72 hours (Figure 3). Viability testing in confluent monolayers showed no overt lethality (Figure 4) resulting from 1 mM CE exposure, and biochemical analysis of media samples from control and CE-treated

HMEC-1 (Figures 5 and 6) showed that the treated HMEC-1 had increased media acid concentrations, and a concomitant decrease in HCO_3^-, but no other indication that cellular change had occurred as a result of the CE exposure. Cytotoxicity analysis by LDH release and MTT reduction assays (Figure 7) showed no overt cytotoxicity.

There are no reports of organized cell culture or human studies of the biochemical effects of cocaine or CE on media (or blood) pH, gases, glucose, and lactate. Only case reports mention acidosis or hypokalemia as incidental findings [85, 189, 190], but conclusions regarding incidence, prevalence, or risk cannot be drawn until such studies are performed. Thus, the results of this study cannot be compared with those of other research groups. The ^{51}Cr release assay used by Kolodgie and colleagues [17] also showed a lack of cytotoxicity in HUVEC exposed to cocaine (1 mM). Thus, the lack of cell injury observed in Aim One of this study is in agreement with that demonstrated by Kolodgie and colleagues [17], and peripherally, that observed in case studies [85, 189, 190].

Overall, it is unclear how the CE treatment in HMEC-1 caused the disruption in pO_2/pCO_2 balance (Figure 5). Speculation points to a *decrease* in the oxidative capacity of the cells, but the lack significant alteration of the rate of HMEC-1 cell glucose consumption from media and lactate formation suggests that the increase in media O_2 may have been associated with the decreased media pH observed in the CE-treated group. Cocaine has been reported to affect mitochondrial integrity [164, 191] in various cell culture systems. Consequently, an assumption of mitochondrial damage as a result of CE exposure is plausible. However, since no alteration of general mitochondrial function was observed (MTT reduction assay, Figure 8B), more definite experimentation focused on the mitochondria would be required in order to determine whether impairment of oxidative phosphorylation was the cause of the alterations in pO_2 observed in the CE-treated group. Thus, the Aim One studies demonstrate that even a high/lethal exposure to CE *in vivo* does not cause microvascular endothelial cell death.

A. Welder [163] performed an *in vitro* experiment on a cardiomyocyte-cocaine exposure model that used both MTT reduction and LDH release assays as measures of cytotoxicity, and observed no significant decreases in MTT reduction over a 1 to 24-hour time period using cocaine concentrations in a 1 nM to 1 mM range on spontaneously-beating cardiomyocytes. However, morphological changes and LDH release alterations were observed in the 10 μM and 1 mM treatment groups, which were increased at all time points analyzed. This result is logical given the reported cardiac complications of cocaine abuse, and the high nutritional and energy demands of cardiomyocytes, which are compromised by exposure to cocaine [163]. Also, these results show the importance of using more than one cytotoxicity assay in model development, since different toxicants may affect a cell using different mechanisms (e.g., cell membrane destabilization v. mitochondrial toxicity).

During the design of the Aim One experiments in this study, the results reported by Welder [163] were used to predict that the HMEC-1 model would show a similar pattern of toxicity, but to a lesser degree due to the functional "quiescence" of endothelial cells compared to cardiomyocytes. All three cytotoxicity assays (LDH and MTT assays, Figure 8, and media biochemical analysis, Figures 5 through 7) performed in this study showed that no cytotoxicity resulted from CE exposure to HMEC-1 cells. The only notable changes demonstrated were decreased pH and HCO_3^- (CE-dependent), and an increase in media pO_2 that is not fully explained by the other biochemical results obtained. Since endothelial monolayers are more quiescent than myocardial cells, the differences in the results of the Aim One experiments *versus* the Welder study [163] are not unexpected. Thus, the conclusion made from the Aim One studies is that CE was not cytotoxic to HMEC-1 cells.

The Aim Two experiments demonstrated that CE exposure may alter HMEC-1 cell function, in that transmission electron microscopy (TEM) of control and CE-treated HMEC-1 showed that the cells were responding to the CE exposure, but that the response was not lethal (Figure 9). This conclusion was made based on the lack of nuclear and

mitochondrial morphological change observed in the CE-treated HMEC-1 monolayers viewed for each time-point of analysis, paired with the increase in numbers and inclusions in the lysosomes within CE-treated HMEC-1. Since there is no presentation or description of TEM performed on cocaine- or CE- treated endothelial cells in the literature, there is no published data with which to compare the results of this study. However, there is agreement of the visual results from the TEM experiment with the biochemical results of the Aim One, in that no mitochondrial or cell border morphological changes were noted that would coincide with severe damage of cellular oxidative capacity or the ability of the HMEC-1 cells to retain cytoplasmic enzymes such as LDH. The increase in lysosomal activity may account for some increase in media acidity if exportation of digested lysosomal contents were to occur as part of a cellular response to CE exposure. Though these data denote cellular change or alteration after CE exposure, they do not appear to demonstrate cellular injury.

4.1.2 CE exposure in HMEC-1 cultures results in increased monolayer permeability

The Aim Two experiments involving silver staining (Figure 10) and trans-endothelial electrical resistance (Figure 11) provided strong support for one aspect of the overall hypothesis, namely that CE alters HMEC-1 morphology and permeability. The silver stains and the electrical resistance data indicate that CE exposure in humans may be a greater problem than previously thought. These data agree with the observations made by Kolodgie and associates [17], which included increased intercellular gaps and decreased monolayer electrical resistance within 30 minutes of exposure to cocaine. CE and cocaine were reported to have equivalent effects, but the actual result for CE was only reported with regards to resistance. The prolonged morphological response (persistence of gaps for up to 24 hours, Figure 10) suggests great potential for vascular toxicity in those chronically exposed to CE, such as cocaine abusers that “binge”, or chronic users that may ingest smaller doses of cocaine frequently.

One disparity in the comparison of these data with data presented by Kolodgie and co-workers [17] is that the HMEC-1 cell model showed significant increase in

permeability (e.g., decreased resistance) only after several hours, whereas Kolodgie and co-workers reported an increase within 30 minutes. We have no explanation for why the small-vessel HMEC-1 cells, which are typically more reactive to stimuli than macrovascular cells, responded more slowly. It is conceivable that differences in the source and type of cells used account for the difference, since the HUVEC cells were a primary cell isolate from umbilici, whereas the HMEC-1 cell line was an immortalized dermal cell line (both of human origin) [156]. Since a direct comparison of the two cell lines cannot be found in the literature with regards to electrical resistance and pro-inflammatory stimuli, the mechanism of the discrepancy remains to be described.

However, it can be concluded from these two separate studies that CE can affect the function of the endothelial barrier in both large and small blood vessels, thereby providing evidence that the endothelial barrier plays a role in cocaine/CE toxicity that may be of great mechanistic importance. This is because demonstration of a direct effect of CE on the endothelium provides evidence that cocaine/CE is capable of promoting the development of vasculitis, which could be an additional pathogenic mechanism underlying systemic disease in cocaine abusers. Since cocaine abusers present an array of organ and tissue diseases to clinical practitioners that appear to have vascular origin (edema, rashes, ulcerative lesions, and others described in Section 1.2), a direct link between the vascular compartment and resulting tissue disease would strengthen the relevance of such a mechanism. Thus, knowledge of the mechanism of this response is necessary to determine the degree of endothelial involvement in CE-associated pathology, including potential therapeutic targets for cocaine/CE-associated pathologies.

4.1.3 Cytosolic and total cellular calcium content is altered in HMEC-1 exposed to CE

The results of the Aim Three studies indicated that calcium was involved in the cellular response of HMEC-1 to CE. The first major finding was a slight increase, then rapid and significant decrease in Ca^{2+} within 60-75 seconds of CE exposure (Figure 12), which is in accordance with cocaine/calcium studies conducted in other cell models [38, 182, 183]. However, the sustained depression of intracellular calcium concentration for 5

minutes after CE addition to Fura-2-loaded HMEC-1 cells was a novel finding, since previous studies showed a steady recovery of Ca^{2+} after removal of cocaine from Fura-2-loaded cells. Since removal of CE from the quartz cuvette was precluded by our experimental design and equipment, determination of whether recovery would occur when CE was removed from the cuvette was not possible. Consequently, only a comparison of the initial "peak" response of the cytosolic calcium after exposure to CE is possible at this point in time.

The second major observation in Aim Three was the large (nearly 3-fold) increase in the total cellular Ca^{2+} when HMEC-1 cells were treated with CE for 1 hour before ion monitoring (Figure 13). This change occurred without a significant alteration of the baseline Ca^{2+} concentration, which was unexpected given the results of the "immediate" exposure experiments, where the presence of CE resulted in lower cytosolic Ca^{2+} concentrations for 5 minutes. Thus, a significantly lower baseline (cytosolic Ca^{2+}) was expected at the end of the 1-hour incubation, but this did not occur. Such results suggest that the first hour of CE exposure is deserving of more detailed study with regards to endothelial calcium content, cell membrane permeability (fluidity), and the localization of Ca^{2+} in endothelial cell compartments.

The rapid increase in the cytosolic Ca^{2+} concentration in CE-exposed HMEC-1 (Figure 11) is typical of a cellular response to insult or stimulus [117, 120, 128, 129, 144, 146, 166]. Since calcium signaling is involved in so many cellular functions, the use of calcium by the cell is brief but capable of sustained effects on cellular function. However, just as increases in cytosolic calcium are capable of altering cellular morphology and function, so are decreases in the Ca^{2+} concentration [117, 132]. In fact, sustained alterations in cytosolic calcium can have cytotoxic effects, due to over- or under-signaling to cellular targets such as the cytoskeleton, signaling molecules, and even the nucleus [117, 120, 121, 128-130, 132, 144, 146, 166]. Sustained alterations in calcium have several etiologies, each of which should be considered when studying mechanisms of pathogenesis of any disease in any cell type. However, given the array of calcium-altering mechanisms within a cell, elucidation of such mechanisms exceeds the scope of

this study. Thus, mechanisms considered to be involved in the microvascular response to CE will be discussed with the reservation that such a discussion is speculative.

One possible cause of the sustained decline in cytosolic Ca^{2+} (Figure 11) is the disruption of cellular structure caused by the CE exposure. As evidenced by the results of the silver staining (Section 3.2.3) and the resistance experiment (Section 3.2.4), HMEC-1 barrier integrity was compromised by CE exposure, and this alteration resulted in cellular morphological changes within the first hour of exposure. Mobilization of the cytoskeleton is often fairly rapid (minutes) [121, 124, 126], followed by reorganization in the following minutes to hours. Since such drastic alterations in cellular morphology and monolayer integrity involve mobilization of the actin-myosin cytoskeleton [17, 155, 165], and cytoskeletal components (actin and associated proteins) bind calcium when un-complexed [117, 120, 129, 144], the decline may be due to a sequestration of calcium *from* the indicator, which binds only free calcium ions. Thus, though calcium may have been present in the cytosol, it is possible that much of it was complexed to cytoskeletal proteins or kinases being mobilized or activated as part of the cellular response to CE and thus inaccessible to the indicator. However, to demonstrate this conclusively, actin staining and other analyses would be required.

The first question presented by this possible mechanism, that calcium may have been complexed in the cytosol and was thus undetectable by the Fura indicator, is: When did calcium levels return to baseline? If one were to examine the two experiments in series, the immediate exposure lasted 5 minutes, and the baselines for the 1-hour CE pre-treatment experiments were obtained 55 minutes later. Results from previous (Aim Two, Section 3.2) experiments demonstrated that the morphological alterations persisted for much longer than 1 hour. However, after reorganization of the cytoskeleton in the first hour, calcium may have been made available once again, demonstrating the “normal” baseline levels that were observed after the 1-hour incubation. If this is true, and if cytosolic calcium was only complexed in the immediate phases of exposure, then why was such a marked increase in total cellular/sample calcium seen after a 1-hour pre-treatment with CE?

Two potential mechanisms might be operating to account for this effect. The first mechanism could involve regulation of calcium signaling by sequestration. Calcium signaling in cells typically originates from the release of calcium from intracellular stores such as the endoplasmic reticulum (ER, or sarcoplasmic reticulum, SR, in the case of the endothelium), due to second messenger systems that are discussed in the Aim Four experiments (Section 3.4). After the signal has reached a threshold, which may vary from cell-to-cell, the calcium is sequestered by re-uptake into these stores, or "sinks". If CE were to affect calcium channels in HMEC-1, then the ability of these cells to release and sequester calcium would be impaired.

Increased total cellular Ca^{2+} occurring in the model after 1 hour of CE exposure (Figure 12) may be related to a block of one or many HMEC-1 calcium channels, particularly on the SR [117, 120, 128, 129, 144, 146]. Qui and Morgan [183] demonstrated that cocaine and CE caused negative inotropic effect in cardiomyocytes using intracellular calcium monitoring and antagonists such as noradrenaline and calcium. The concentrations of cocaine and CE used were 100 μM to 10 mM, placing the CE exposure concentration of 1 mM used in this study within the range used by Qui and Morgan [128, 129, 146]. The chief finding of their study was that CE had a lower ED_{50} than cocaine (nearly ten-fold lower) with regards to cellular contraction and action potential peak shortening. The authors concluded that both agents had a negative inotropic effect on spontaneously beating cardiomyocytes, but CE appeared to have greater potency than cocaine, and that this potency was based on CE's ability to decrease the availability of intracellular free calcium. The authors suggested that an SR blockade could be the cause of the alteration in free calcium levels in the cardiomyocyte model [183].

Though my study was conducted in microvascular endothelium, many of my observations parallel with the findings of Qui and Morgan [183]. First, Qui and Morgan demonstrated a morphological and functional effect on their cell model as a result of CE exposure. The Aim Two finding of altered permeability is comparable due to the

involvement of the actin-myosin cytoskeleton in both cardiomyocyte beating and endothelial morphological change. Second, CE exposure in both models resulted in a decrease in available cytosolic Ca^{2+}, which is important to the continuance of cellular stability in both cases. Thus, the evidence from my studies supports Qui and Morgan's hypothesis that CE may also be capable of SR calcium channel blockade [183]. Such activity would add to CE's repertoire of cocaine-like activity. However, this evidence needs definition, since true confirmation can only come from inhibitor studies and specific study of the channels themselves.

The second phase of Ca^{2+} increase, which was observed in the 1-hour CE pre-treatment experiments, could be a consequence of such a blockade. If the SR is unable to release calcium, but other channels responsible for sequestration are still operable, then permeabilization of the SR membrane (as with digitonin treatment) in such a cell would provide greater quantities of calcium than a cell with functioning SR calcium channels and normal calcium flux prior to analysis [128, 129, 146].

A second calcium "sink" present in cells is the mitochondrion, which can take up excess Ca^{2+} when SR channels are not functioning, or the cell is flooded with calcium [128, 129, 146]. Thus, if an SR blockade occurs as a result of CE exposure in microvascular endothelium, and mitochondria are flooded with calcium in an attempt to regulate cytosolic Ca^{2+} content, then release of calcium with the injection of digitonin during calcium monitoring would yield a higher total cellular Ca^{2+} concentration than that observed in control cells (as well as mitochondrial dysfunction).

Another source of calcium that could cause a cellular "overload" would be the extracellular environment [128, 129, 146]. If SR channels are not functional, then store-operated channels on the cell surface could be recruited by an as-yet unknown signal or chaperone to open, allowing calcium to be pumped in from the extracellular compartment. This is could have resulted in the high Ca^{2+} levels in the CE-pretreatment group, since the cell would essentially be hypocalcaemic in the event of an SR channel block and would rely on calcium from the extracellular space for its signaling needs.

Also, since the calcium concentration in the Tyrode solution was constant during analysis, buildup of Ca^{2+} in cellular sinks would have to take place *before* analysis (e.g., during the 1-hour pre-treatment period).

The second, and more likely mechanism that could have affected total cellular calcium in the pre-treatment experiment involves the cell membrane itself. If CE affects cell membrane stability, this could be one cause of the alteration in barrier function (Section 3.2, Permeability studies), as well as provide a way for calcium to bypass channels and gain entrance to the cells. Thus, the model presented in this dissertation may represent a two-step method of permeabilizing HMEC-1 cells. CE could have destabilized the HMEC-1 cell membrane, resulting in Ca^{2+} leakage into the cell and organelles. Then, when digitonin was added as a permeabilizing agent for obtaining total cellular calcium, the membranes of CE-treated HMEC-1 were fluidic relative to control cells, thus yielding additional Ca^{2+} and the several-fold increase in cellular Ca^{2+} versus controls.

The proposed theory of increased membrane fluidity is supported by the findings of Kunze *et al* [147]. The authors reported an increase in membrane fluidity, and an inhibition of phospholipase A_2 (possibly important in the next section) by high (1 mM and greater) concentrations of cocaine. Increasing (0.5 – 1 mM) concentrations of calcium in the reaction buffer used abrogated the inhibitory effect, but calcium concentrations above 1 mM potentiated the anesthetic inhibition. Finally, in each case, the ability of the anesthetic to affect PLA_2 activity was parallel to its lipophilicity [147]. Thus, cells exposed to high concentrations of cocaine (or CE) would display increased membrane fluidity, opening the cytosol to ion/particle leakage. Since CE is slightly more lipophilic than cocaine (due to the ethyl ester), the results of my study and the study conducted by Kunze *et al* are in agreement. However, to demonstrate the mechanism of increased membrane fluidity conclusively, future studies focused on cell membrane composition should be conducted.

From these findings, it can be concluded that calcium plays an important role in the cellular response to CE, as evidenced by the significant alterations that were observed in a relatively short sampling period. Several mechanisms could be operating that affect the calcium flux, but no clear conclusions can be drawn from the data. Future studies employing specific calcium channel blockers and calcium-free Tyrode solution (or calcium concentration curves) would be of benefit in further characterization of calcium-modulated signaling in our HMEC-1/CE exposure model.

4.1.4 CE exposure in HMEC-1 is associated with altered signaling

Second messengers

The Aim Four studies served to further test the proposed mechanism of cellular response following CE exposure in the microvascular endothelial cell line, HMEC-1. Since this project was largely exploratory due to a lack of pre-existing data regarding the cellular effect of CE, many intracellular targets were evaluated that could potentially be involved in the morphological and barrier function alterations that were observed in Aim Two (Section 3.2). Thus, this Aim was composed of several preliminary molecular analyses.

The results of the IP_3 accumulation assays (Figure 14) showed a drastic increase, followed by a gradual but significant decrease, in IP_3 in CE-treated HMEC-1. This result reflected an attempt to regulate cytosolic Ca^{2+}, which was decreased in the CE treatment group within seconds of drug injection (Figure 12). This part of the IP_3 generation data was clear-cut, requiring little interpretation. Cytosolic Ca^{2+} decreased, and the cell was making an attempt to bring it back to baseline levels.

The data that resulted in the biggest question from the IP_3 experiments was the gradual and significant decrease in IP_3 (Figure 14), which appeared to begin just after the 60-second time point, and continued until the 450-second time point was reached. If cytosolic Ca^{2+} (Figure 12) had returned to control levels, this depression would not be compelling – the fact that IP_3 levels were decreased in Figure 14 despite the lack of free Ca^{2+} concentration recovery (Figure 12) points to negative regulation of IP_3 generation

mediated by Ca^{2+}. Considering the question generated in Section 4.1.3 regarding the status of Ca^{2+} in the cytosol (was it sequestered in sinks, or still in the cytosol, but complexed to various targets?), this IP_3 data suggests that the Ca^{2+} was indeed present in the cytosol, but not available to the indicator due to complexation with various targets. Since two targets of Ca^{2+} in the cytosolic compartment are the SR surface IP_3 receptor, and PLC [117, 128, 146], it is entirely plausible that this is true.

The idea that Ca^{2+} could have been complexed to PLC is supported by the findings of Kunze *et al*, who demonstrated that high concentrations of cocaine, paired with high concentrations of Ca^{2+}, were capable of inhibiting PLA_2 activity [147]. A similar scenario may be present in the current study, in that inhibition by CE of PLC would be potentiated by high cytosolic Ca^{2+}, which is a co-factor and regulator PLC activity [117, 129]. Thus, not only could there be inhibition of PLC activity over time by CE, but there is also the possibility that Ca^{2+} is complexed and unavailable to the Fura-2 indicator. The inhibition of IP_3 generation indicates that this is a possible mechanism of CE's effect on the microvascular endothelium that should be investigated further.

Repetition of this assay could provide additional information regarding the temporal associations between Ca^{2+} and IP_3 in CE exposure scenarios, and should include: 1) positive and negative controls; 2) calcium channel inhibitors; 3) possibly an extended time of analysis; and 3) varying concentrations of CE. A positive control that was previously used in an endothelial-IP_3 experiment [168], bacterial lipopolysaccharide (LPS, which was used in the p38 phosphorylation and EMSA assays), should be included to determine the potential for maximal IP_3 generation in the model. This will be necessary so that determination of the degree of physiological significance of changes due to CE exposure could be made in reference to a positive control. Negative controls should include a no-CE media treatment like the one used, and potentially an inactive homolog of CE and/or cocaine, if one can be identified.

There are no studies in the literature that describe the effects of CE on phosphoinositide production or metabolism. Cocaine's effects on IP_3 have been tested in

a chronic cocaine treatment model of rat aorta [192]. The authors noted a doubling of IP_3 generation in this model shortly (seconds) after 30 μM cocaine was added to norepinephrine-stimulated aortic rings taken from rats chronically exposed to cocaine. The results observed in Aim Four support this finding, despite the differences in model, drug, and treatment concentration. Consequently, the Aim Four IP_3 results have been corroborated by limited studies in different models, and should be further expanded and tested for greater depth of understanding concerning the time course and influence of IP_3 generation in HMEC-1 after CE exposure.

Kinase phosphorylation

A clear increase in p38 MAPK phosphorylation (Figure 15) was observed in the HMEC-1/CE exposure model. This suggests that the calcium signals indicated by the Aim Three results were affecting kinases as soon as 5 minutes after CE exposure, and reaching maximal levels at 2 hours. Also, the effect was sustained for the additional 2 hours of CE treatment (the 4-hour time point). Because activated p38 MAPK affects endothelial morphological change, this increase in phosphorylation supports the findings of increased endothelial permeability in Aim Two [128, 130, 146]. Thus, it would appear that even a transient changes in cytosolic calcium and IP_3 generation can result in kinase activation in CE-exposed HMEC-1 cells, and that continued exposure results in the alteration of barrier function.

Again, there are no studies in the literature describing the effects of CE exposure in endothelial cells with regard to p38 MAPK. However, one report of the effects of cocaine on fetal rat myocardial cells that demonstrated increased p38 MAPK *activity* (not phosphorylation) after cultured cells were exposed to 0.1 mM cocaine for 15 minutes [191]. This increase was transient, and p38 MAPK activity returned to control levels after 30 minutes of cocaine treatment.

A second cardiac study utilizing cocaine (0.01 to 1 μM) exposures in adult rat cardiomyocytes [193] reported no change in phosphorylation of p38 MAPK when the cardiomyocyte cultures were exposed to cocaine. Also, no change in the other two major

forms of MAPK, ERK and SAPK/JNK, was observed. However, the low doses of cocaine did increase PKCα activity in the model. Given the difference between the HMEC-1 cells and cardiomyocyte models, and the levels of drug exposure in each, it is not surprising that a change was seen in one model (HMEC-1) and not the other (cardiomyocytes) regarding MAPK phosphorylation.

There are many differences between the HMEC-1/CE exposure model and the myocyte models used in these two studies [191, 193] that would account for the drastic differences between the results observed. As stated previously, cardiomyocytes have higher energy demands than endothelial cells, thus making them more susceptible to damage and death (which was seen in [191]) or hypertrophy (which was seen in [193]). Second, the drug (cocaine) and drug concentrations used (ranging from 0.01 to 100 μM cocaine) were different than the 1 mM CE concentration used in this study. Though distinctly toxic to the cardiomyocyte cell model, the 0.1 mM exposure showed no overt effect on HMEC-1 during early viability studies in this study, and was not further tested. Third, the authors of [191] used a p38 MAPK activity assay, whereas the analysis used in this study was a phosphorylation assay. Though phosphorylation indicates signaling molecule activation, the two assay results cannot be directly compared. Thus, while the p38 MAPK data presented in Aim Four demonstrate a direct effect of CE exposure on HMEC-1 cell signaling, this analysis should be expanded and further tested using related models and drug concentrations.

DNA binding activity

The Aim Four studies showed that DNA binding of RelA(p65)/p50 heterodimers and other NF-κB complexes present in HMEC-1 decreased transiently (1 hour) after CE treatment (Figures 17-22), and then returned to control levels. Since RelA(p65)/p50 activation is believed to be an important component of normal cellular function [137, 176], the decline in DNA binding activity of this complex after CE treatment could indicate a rapid and transient alteration of cellular status by the NF-κB signaling pathway. This result was not predicted for two reasons. First, NF-κB DNA binding

activity was expected to be similar to that of the positive control LPS, which increased DNA binding activity of NF-κB dimers over time, reaching maximal levels at 4 hours in the HMEC-1 model. Second, a report from 2001 [194] showed that human brain microvascular endothelial cells exposed to cocaine (up to 200 μM) for 3 hours exhibited increased levels of DNA binding of NF-κB proteins p65 and p50 (more below).

The relevance of NF-κB DNA binding activity in HMEC-1 cells exposed to CE relies on the gene targets of NF-κB, and their resulting protein expression [132, 137, 140, 187]. Activated NF-κB binds the promoters of genes encoding surface adhesion molecules (such as VCAM-1 and ICAM-1), pro-inflammatory cytokines (such as IL-8), and NF-κB and IκB family genes. Thus, NF-κB is auto-regulatory, and its activation results in the transcription of genes that, when transcribed and expressed in protein form, promote inflammation [140]. Regarding the pathogenesis of vasculitis in cocaine abusers, a finding that CE is capable of altering the expression of these genes (and proteins) through NF-κB would provide a mechanistic link to vasculitic pathogenesis. Thus, it was assumed that the HMEC-1/CE exposure model would produce similar results. The fact that the assumed outcomes did not occur raises two questions at this time.

First, would CE treatment ever elevate NF-κB DNA binding activity in HMEC-1, or is CE somehow preventing NF-κB activation? Given the activation of p38 MAPK by CE (Aim Four), it appears that intersecting signaling pathways are activated. However, NF-κB signaling intersects with a number of signaling pathways, and only one of them (p38 MAPK) was analyzed in this study. Thus, the question of whether CE exposure to HMEC-1 cells would alter NF-κB activity is complex and could only be answered with the addition of time points to the existing models, as well as analysis of the activities of other intersecting signaling pathways that modulate NF-κB activation. Also, varying CE concentrations should be added in case differential results are seen with regard to dose.

Second, why did CE affect RelA(p65) and p50 content in the nucleus, but not c-Rel? The answer to this question is likely to be tied to the first question, in that the DNA

binding activities of various dimers affected by CE treatment may be influenced by the effects of CE on intersecting or NF-κB modulating pathways. However, since c-Rel is constitutively expressed in the nucleus and has no nuclear export sequence [137, 187], low levels of c-Rel should be found in the endothelium at baseline sampling. Thus, due to c-Rel's status as a constitutively expressed transcription factor [137, 187], and RelA's status as an inducible NF-κB protein (and hence differences in cellular localization/accessibility by other signaling molecules), it is logical that HMEC-1 cell stimulation with LPS or CE would increase DNA binding activity of RelA and not c-Rel.

Again, there is no information available in the literature regarding the effect of CE exposure on the DNA binding activity of transcription factors in any cell line or model. However, some data are available regarding the effects of cocaine on NF-κB activation in human brain microvascular endothelial cells, and the mouse brain [194, 195] that may answer the above questions.

Lee et al [194] reported induction of NF-κB in human brain endothelial cells after treatment with 50 to 200 μM cocaine for 2 hours. This is one instance where cell model is comparable to the HMEC-1 model, since two bands containing NF-κB were identified using EMSA. The first band appeared to contain p50 and RelA(p65), and the second band appeared to contain a p50 homodimer. DNA binding of NF-κB increased with increasing cocaine concentrations, a finding that contradicts the results of the present study.

The fact that the HMEC-1/CE model did not show the same activity as the human brain endothelial model can derive from several factors. First, the concentration of cocaine used in the human brain endothelial model was $1/5^{th}$ that of the HMEC-1 model. Thus, the high concentration of CE in this study could have caused a decrease in NF-κB binding activity as a result of toxicity. Second, it is possible that the endothelial cell models are different enough to show different responses to cocaine/CE. Though the endothelium in the periphery is highly dynamic, it is possible that there is a true difference between peripheral and brain endothelial cells regarding the sensitivity of NF-

κB activating pathways. Third, the difference in time of sampling (3 hours in the brain endothelial cell model of Lee *et al* versus the 1- and 4-hour time points in the HMEC-1 model of the present study) could present a problem. Since NF-κB signaling is transient, 1 hour can make a large difference in the DNA binding activity detected. Thus, perhaps a peak occurred at 2 or 3 hours post-CE-treatment that was not detected because no sampling occurred at those time points.

Consequently, the results of the study conducted by Lee *et al* are not supported by this study, but they do provide useful information that should be considered in future experimental design, in that the study by Lee [194] presents different concentration and time ranges that could be evaluated in the HMEC-1 model. Thus, an interesting future study could involve a concentration curve for CE that would begin near 50 μM and end at the 1 mM concentration. Such use of varying drug concentrations may determine whether the difference between the two models was cell origin or drug concentration.

A study performed by Ang *et al* [195] was conducted using a mouse model of cocaine exposure, which included a single-dose group and what the authors referred to as a "chronic" dose group, which was actually sub-chronic: cocaine concentration was 20 mg/kg daily for 14 days for the sub-chronic group, and 4 hours on one day for the single dose group. Microarray analysis of the nucleus accumbens of mice exposed to cocaine for 14 days showed a 9-fold increase in the mRNA expression of NF-κB family protein p105 (the precursor to p50). Subsequent Western blots of nucleus accumbens from mice chronically exposed to cocaine showed an increase in p105 content, as well as a 40% increase both in RelA(p65) and IκBγ [195]. Single exposure to cocaine, however, did not affect NF-κB protein in the mouse nucleus accumbens. Thus, NF-κB was concluded to be a target of signaling mechanisms related to addiction and reinforcement in the mouse model after chronic cocaine abuse only.

Since protein analysis in the mouse included Western blots (thus indicating protein *content* rather than activity), and this study included EMSA for DNA binding activity of NF-κB, the results from the two studies cannot be directly compared. Because

protein concentration does not equate to protein activity, it would be interesting to repeat the study with the mouse model, including EMSA analysis of NF-κB DNA binding activity. Also, analysis for more NF-κB proteins and their targets would be warranted, since the authors of the mouse study [195] reported 2.5- to 9- fold up-regulation of 77 different genes in their model – p105 was the only one to which further study was dedicated. At this time, however, the main benefit that the mouse study presents is knowledge that cocaine (and potentially CE) targets NF-κB transcriptional and translational activation, and thus increases the likelihood that the presence and activation of this important cell regulator will occur. Also, this report points to NF-κB as a major effector of neuronal function in chronic drug abuse scenarios, emphasizing the need for more study in this area.

From the findings of Ang and colleagues [195], future experiments in the HMEC-1 model should include microarray analysis to identify families of molecules that may be up- or down- regulated by CE exposure. Given the activation of p38 MAPK (Figure 15), and the reduction in NF-κB DNA binding activity by CE exposure in HMEC-1 cells (Figures 17-22), such analysis is warranted. Additionally, the EMSA analysis of HMEC-1 nuclear extracts could be extended to determine what effects CE has on the cell model after 6, 12, or 24 hours of treatment. It is possible that activation of NF-κB binding activity by CE is delayed in the more quiescent HMEC-1 cell line, and thus CE's potential as an activator should not be ruled out. Conversely, it is possible that CE has a stabilizing effect on NF-κB/IκB complexes, thus preventing NF-κB dimers from reaching the nuclear compartment. An interesting way to test this concept would be to combine CE and LPS treatments in the HMEC-1 exposure model to see if CE has an inhibitory effect on the 4-hour activation observed in the LPS-treated group (Figure 18).

A paper presented by Gan *et al* [185] highlights the importance of understanding the effects of drugs-of-abuse on cellular signaling. The authors reported that Brain MicroVascular Endothelial Cells (BMVEC) isolated from human biopsies and exposed to cocaine (1 nM to 10 μM range) showed increased monocyte and neutrophil adhesion and

monocyte transmigration that resulted from upregulation of BMVEC expression of VCAM-1, ICAM-1, and ELAM-1 (endothelial-leukocyte adhesion molecule-1). Demonstration of increased levels of ICAM-1 mRNA in cellular extracts pointed to transcriptional upregulation [185]. Since NF-κB is a prime activator of cellular adhesion molecules, knowledge of NF-κB activation and suppression patterns in this and other models would be key to predicting inflammatory outcomes, as well as the design of potential drugs to prevent inflammation and vasculitis resulting from cocaine/CE exposure.

4.1.5 Closing remarks, discussion

The data presented in this dissertation reflect the complicated and dynamic cellular response to CE, which requires further investigation. Since the study of the effects of CE on endothelial cells is a new area of research, there is little existing data to which the results in this dissertation can be compared. The one existing cocaine-endothelial study that included CE supports the current findings herein, in that a morphological and permeability change was observed that was not associated with cell death [17]. Other studies that focused on cocaine effects on cellular ion levels [38, 182, 183, 196] also agree with the Aim Three calcium data, despite the difference in the models used. Consequently, it is assumed that the data presented herein represent a true and significant alteration in the function of the vascular endothelium, which could result in systemic toxicity and disease. The microvascular/CE exposure model appears to be a suitable one for toxicological analysis, and could prove useful in other areas of toxicological research.

4.2 BENEFITS & LIMITATIONS OF THIS MODEL/STUDY

Several potential benefits and limitations of the HMEC-1/CE exposure model have been identified as this project has developed. Below is a summary of those considered to be the most important.

4.2.1 Benefits

Containment of exposure and response

One benefit to using a cell culture model for mechanistic research is that the model is usually composed of a single cell type, and is free from outside influences that may alter the cellular response to the agent in question. For example, despite the ultimate goal to fully describe the whole-body effect of CE from a mechanistic standpoint, such description would be impossible unless the mechanism could be compartmentalized, and then integrated back into the whole body. Such was the idea for the use of the microvascular cell line HMEC-1 as a representative of the entire microvascular endothelium. Thus, there were no blood-borne immune cells, tissue-derived factors, or neurotransmitters present to complicate the response of the CE exposure. Response was clearly a product of interaction between the endothelium and CE, which was a major question that provided the impetus for this study. Also, the uniformity of the cultures yielded much lower variability, thus making determination of significance easier during data analysis, especially in this early phase of researching endothelial-CE interactions.

Resource consumption and ethics

Use of the cell culture model is more flexible and less costly than any animal or whole-human model available. Human and animal protocols require more resources overall, and give results with much higher variability than those yielded by cell models. Also, the ethics of performing the studies conducted herein on a human population would be inadmissible in an IRB protocol, especially since highly invasive or surgical procedures (e.g., to obtain skin for tissue studies) would be required to obtain materials suitable for such study. Designing such studies for an animal model, with no previous data, would also not be favorable for acceptance of an animal use protocol. Thus, gathering data for future use in such models is often left to *in vitro* experimentation.

Relevance to humans

The HMEC-1 cell line was derived from human dermis. Thus, the endothelial cell model presented in this study is directly relevant to humans, as well as the effects of

cocaine/CE on humans, since the skin is often a target of cocaine-associated pathology (Section 1.2). Also, the dermal microvascular endothelium has been noted to be generally applicable to endothelium in other organs [156]. As such, this model provided the most universal results possible at this early phase of experimentation.

Approach

This study was exploratory, since there is limited information in the literature regarding the vascular endothelial effects of cocaine and/or CE in the periphery. As such, the approach used in this study provided a survey of different types and levels of the effects of CE on HMEC-1 cells, using a number of different methods with varying detection sensitivities to evaluate the scope and degree of effect that CE had on the HMEC-1 cell model. To focus on only one type or level of response would have limited this study, since any negative result in a more specific study may have ended the project prematurely. Certainly, the general approach in Aim One, and increasingly specific studies in later Aims, should stimulate interest in the model, as well as prove its worth as an appropriate model for toxicological assessment.

4.2.2 Limitations

CE concentration used

The CE concentration (1 mM) used in this study was high. As discussed in Section 1.1, serum CE concentrations observed in emergency room admissions often range from low nanomolar to high micromolar concentrations [12, 13, 43, 46]. Since cocaine and CE are both metabolized post-mortem (due to residual serum cholinesterase activity) to benzoylecgonine, the upper limit of serum cocaine and/or CE concentrations is currently unknown. However, it is thought that millimolar serum concentrations of CE are possible in severe overdoses and lethal cases, but the ability to detect cocaine or CE intact is dependent on the time elapsed from death to autopsy/blood sampling [19, 21, 22].

Though intermediate effects of 0.1 and 0.5 mM concentrations of CE were observed in the HMEC-1 cell growth studies of Aim One (Section 3.1), it was decided

that the higher concentration should be used for the characterization of the model, due to its clear and consistent effects on cell growth and viability in proliferating HMEC-1 (Section 3.1.2). In the future, these and other, lower concentrations of CE should be tested in the HMEC-1 cell model, so that a characterization of dose-response would be possible.

Non-inclusion of cocaine and/or cocaine + ethanol groups

Since the goal of this study was to survey endothelial response to CE, and a previous study [17] had shown some effect of cocaine equivalent to that of CE, cocaine and cocaine + ethanol groups were not included. This decision was made to make experiments more manageable, since testing CE alone (and later, the LPS positive control group) resulted in the operation of the laboratory at full capacity.

Cocaine and CE have been reported to share most of cocaine's molecular targets, including the dopamine transporter [18, 20], serotonin and norepinephrine receptors[19, 22, 32], sodium channels in excitable cells such as neurons and the myocardium[29, 32, 35, 36, 38, 40, 42], and potentially sarcoplasmic reticular calcium ATPases [182, 183]. In the future, expansion of the HMEC-1 cell model to include cocaine and cocaine + ethanol groups should be considered for direct comparison of the effects of cocaine and CE on the HMEC-1 model.

Time limitations of the HMEC-1 model

Since the endothelial model is comprised of a confluent monolayer, and cultured endothelial cells have a limited "window" for viability and normal operation in culture at confluence, the upper limit of analysis in the HMEC-1 model is 72 hours. After that, issues can develop regarding cellular changes as a result of death in an increasing population of the culture. It was apparent during the Aim One biochemistry studies (Section 3.1.5, Figures 5 and 6) and Aim Two electrical resistance studies (Section 3.2.4, Figure 10) that cellular metabolism was being altered by 72 hours even in control cells. As a result, later studies of morphology, calcium monitoring, and signaling were restricted to the first 24 hours of CE exposure. Thus, in future studies seeking to expand

the timeline of CE exposure and effect, or address chronic low-dose exposures of CE, another model (e.g., animal, or bioengineered or perfused tissue) may be necessary. However, for preliminary studies including shorter exposures (such as the ones contained in this dissertation), the HMEC-1 model was suitable and should be further characterized.

Lack of rescue analysis and negative controls

Several *in vitro* studies utilizing techniques such as resistance monitoring and calcium ion determination employ drug removal from culture or analysis buffers and subsequent observation for potential recovery of the cell culture to control conditions [17, 29, 182, 183, 196]. During this study, this strategy was not employed in the ECIS experiments, and was not possible in the calcium ion monitoring experiments. Future studies would greatly benefit from inclusion of such an approach, so that reversibility of the effects observed herein may be estimated.

Regarding the lack of negative controls, there are no known metabolites of CE that are completely inactive. Benzoylecgonine (BZE) does not share the local anesthetic properties of cocaine and CE, and was shown not to affect HUVEC monolayer resistance by Kolodgie *et al* [17]. Thus, it would appear that BZE is a good candidate as a negative control for endothelial permeability and ion channel evaluations. However, since BZE is capable of inducing seizures in animal models, it is unlikely that BZE would be considered an ideal negative control for cocaine and CE. Currently, data on the effects of this and other cocaine and CE metabolites on peripheral targets, such as the vascular endothelium, are lacking. As such, testing similar to that performed in this study would need to be conducted before BZE, or any other candidate molecule, could be used as a negative control in the HMEC-1 cell model.

4.3 IMPLICATIONS & THE FORMATION OF A MECHANISM

The data herein strongly suggest that cocaine abusers could have an increased risk for systemic disease of vascular origin, due to the effects of CE on the microvascular endothelium. This conclusion was made because of the frequency of cocaine and ethanol

co-abuse, the prevalence of cocaine and ethanol double-positive results in toxicological testing of emergency room admissions associated with traumatic and tissue failure emergencies, the confirmed presence of CE in a majority of cocaine and ethanol double-positive clinical toxicology samples, and the case history records of systemic disease in cocaine abusers. These associations suggest a high risk for sudden death, and vascular origins of life-threatening illness in this population.

The demonstration that CE is capable of interaction with human microvascular endothelium *in vitro*, isolated from other factors that could exacerbate endothelial dysfunction, suggests that CE is an effector in cocaine-associated systemic disease pathogenesis. Though the CE concentration used is on the high end of the clinical scale, observed in overdoses and lethal cases, it is possible that chronic exposure to low levels of CE could elicit an effect on the endothelium. However, due to the potential for differential effects of CE depending on dose, as seen in cocaine studies, speculation as to what those effects would be is too far-reaching. This study highlights the necessity for more extensive research before this suggestion can be validated, using *in vitro* and *in vivo* studies in a variety of exposure scenarios.

The major result from this work is a mechanism that is beginning to take form (Illustration 12), which incorporates a vascular endothelial origin into the tissue disease pathogenesis observed in cocaine abusers. CE, through an as-yet unidentified interaction with the endothelial cell, alters the free cytosolic calcium concentration of the endothelial cell.

Since calcium in the cytosol has a role in the regulation of metabolism and stress response, feedback regulation of second messenger generation, and kinase and channel stability, as well as cytoskeletal mobilization, the decrease in free cytosolic calcium results in multiple cellular responses that culminate in cellular dysfunction and the loss of endothelial barrier integrity. These changes may trigger the tissue changes and inflammation underlying vasculitis, which causes the same tissue-damaging diseases observed in cocaine abusers (Section 1.2).

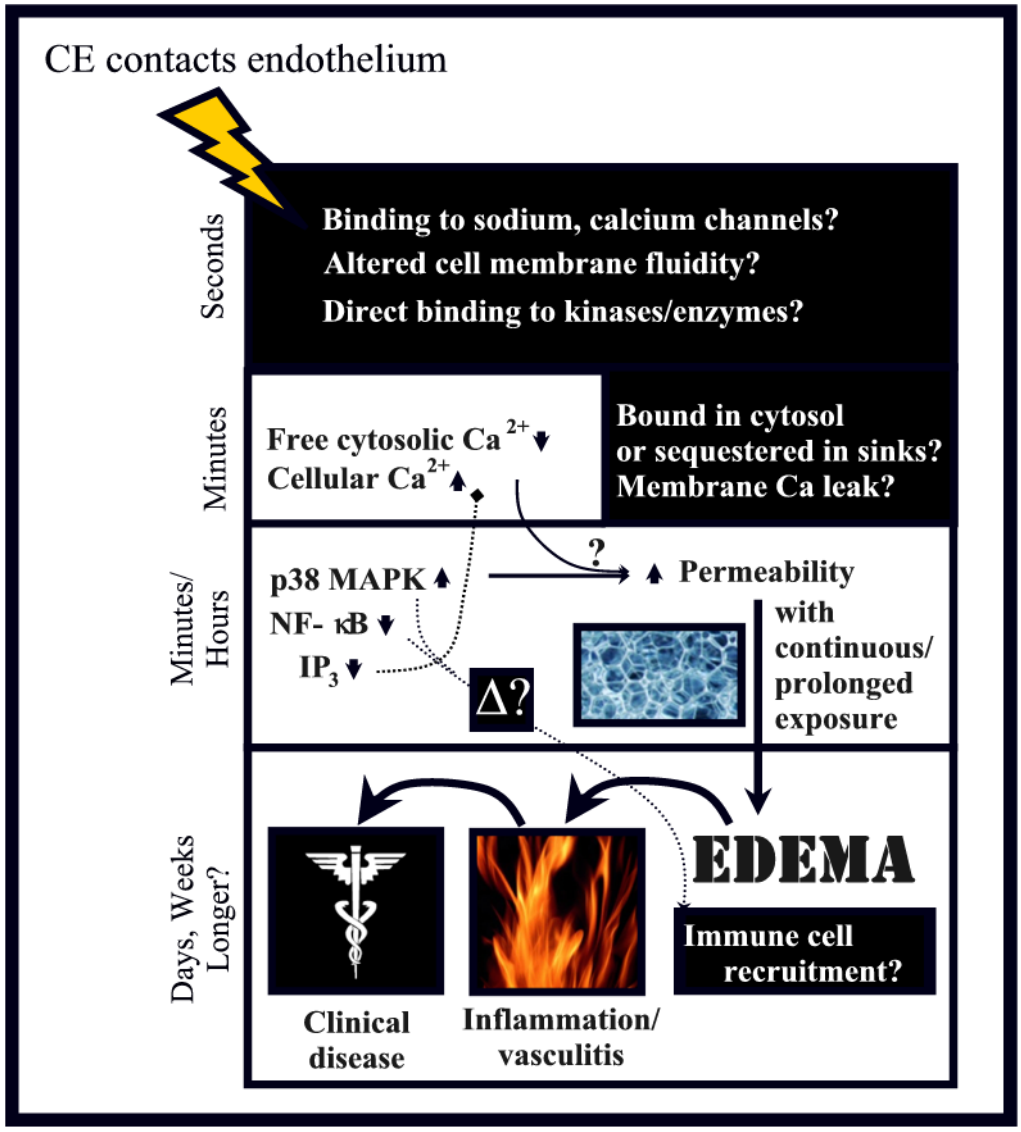

Illustration 12: Proposed mechanism of CE effect on microvascular endothelial cells

Incorporation of this mechanism with existing cocaine/CE mechanisms of toxicity provides a better, though incomplete, understanding of the pathogenesis of tissue pathology in cocaine abusers. It also provides a better explanation of the chronic nature of some of the diseases observed in the case literature (e.g., kidney failure, gastrointestinal ischemia, panarteritis, progressive mucosal destruction, and vasculitic lesions, as discussed in Section 1.2).

Though specific questions arise from the individual studies performed herein, a large remaining question is: How does CE interact with the endothelium? Does it bind/block ion channels on the surface or interior of the endothelial cell? Can CE interact with signaling molecules directly? This is represented by the black box in Illustration 12, and symbolizes the need for more thorough mechanistic knowledge of drug-associated pathological outcomes in general. Discovering the route of endothelial/CE interaction would be of great benefit to researchers who are attempting to identify effective therapies that extend beyond cocaine addiction itself, and target physiological effects of cocaine and CE.

4.4 FUTURE STUDIES

The studies conducted in this dissertation project were exploratory. Each Aim asked general questions, and resulted in the generation of new questions that could easily be expanded into stand-alone research projects. Below are examples of future studies that could be generated from the findings of this study.

In general, incorporation of available negative and positive controls, and cocaine and cocaine + ethanol groups, into this model would greatly contribute to the characterization of CE as an endothelial effector in relation to its parent compounds, cocaine and ethanol. These controls and additional experimental groups would aid in delineation of the mechanism of CE's (and potentially cocaine's) effects on endothelial cells, and identification of existing or unique molecular targets of the drug(s) in endothelial tissue. Identification of the molecular targets of cocaine/CE would be

valuable in the development of potential drugs that could be used to treat the systemic effects of cocaine abuse until a cure for addiction is found.

The questions generated by the studies of Aim One regarding toxicity could be further addressed with studies focused on the mitochondrion, placing particular emphasis on the status of cellular oxidative phosphorylation and the potential for oxidative stress in CE-exposed endothelium. Since oxidative stress is a source of endothelial dysfunction that does not always lead to cell death (and is associated with signaling pathways such as MAPK and NF-κB), this topic warrants further investigation despite the lack of cytotoxicity observed in Aim One. Oxidative phosphorylation and mitochondrial membrane potential should be monitored after HMEC-1 exposure to varying concentrations of CE. Isolated mitochondria could be used for a number of specific toxicity assays, such as cytochrome c release.

The permeability studies of Aim Two could (and should) be expanded to include rescue analysis, whereby CE is removed from culture media or assay buffer, and serum-free media or assay buffer replacement is incorporated into the method. Such a study would address the potential for recovery from the exposure to CE once it is removed from the system, and would more accurately represent an *in vivo* condition of CE production and clearance. Electron microscopy analysis could be made more specific with immuno-EM, with the purpose of targeting protein metabolism, cell membrane turnover, and/or lysosomal changes. Also, using immuno-EM, specific cell-surface receptors (i.e., junctional proteins) could be used to define events linked with the observed change in permeability reported in Aim Two.

Cation studies of Aim Three could be made more specific with channel blocking inhibitors, and calcium concentration curves. Also, since the source of the increased calcium in the 1-hour CE exposure experiment (Section 3.3.3) is unknown, organelle specific indicators (if available) could be used to track calcium accumulation within cellular calcium sinks (the SR and the mitochondrion, and potentially the nuclear compartment). Such studies would better characterize the observed cytosolic and cellular Ca^{2+} concentration changes, and may be useful for clinical purposes.

Aim Four could be expanded into a full proteomic and/or genomic analysis of CE exposure in the endothelial model, or be limited to expanded analysis of one or more pathways represented by the Aim Four experiments. Such information would be useful in drug discovery for the purposes of preventing pathology and/or lethality in the clinics, and expand the known mechanism of cocaine- and CE-associated pathogenesis, with particular focus on non-neuronal and –cardiac targets.

This project could be translated back to an animal model, so that an *in vivo* response could be studied without the inclusion of human patients. However, such an involved series of studies should only be conducted after extensive *in vitro* characterization clearly points to defined cellular targets or biomarkers that could be employed in the animal model.

In the distant future, various human studies could be designed from these data. The possibilities for such studies range from emergency room observation for signs of vasculitis in presenting human cases, to carefully executed human exposure and effect studies that examine more than just blood pressure and heart rate, or psychological measurements of "high" and mood.

REFERENCES

1. Karch SB: **A brief history of cocaine**. Boca Raton: CRC Press; 1998.

2. **Results from the 2002 National Survey on Drug Use and Health** [http://www.samhsa.gov/oas/nhsda/2k2nsduh/Results/2k2Results.htm]

3. **The DAWN report** [http://dawninfo.samhsa.gov]

4. **US Population: The basics** [http://www.census.gov/]

5. **DEA drug seizures** [http://www.dea.gov/statistics.html]

6. **State Factsheets, Texas** [http://www.dea.gov/pubs/states/texasp.html]

7. Lester BM, LaGasse LL, Seifer R: **DRUG ABUSE:Cocaine Exposure and Children: The Meaning of Subtle Effects**. *Science* 1998, **282**(5389):633-634.

8. **Prenatal cocaine exposure costs at least $352 million per year.** [http://www.nida.nih.gov/NIDA_Notes?NNVol113N5/BBoard.html]

9. Pennings EJ, Leccese AP, Wolff FA: **Effects of concurrent use of alcohol and cocaine**. *Addiction* 2002, **97**(7):773-783.

10. Hearn WL, Rose S, Wagner J, Ciarleglio A, Mash DC: **Cocaethylene is more potent than cocaine in mediating lethality**. *Pharmacol Biochem Behav* 1991, **39**(2):531-533.

11. Andrews P: **Cocaethylene toxicity**. *J Addict Dis* 1997, **16**(3):75-84.

12. Blaho K, Logan B, Winbery S, Park L, Schwilke E: **Blood cocaine and metabolite concentrations, clinical findings, and outcome of patients presenting to an ED**. *Am J Emerg Med* 2000, **18**(5):593-598.

13. Signs SA, Dickey-White HI, Vanek VW, Perch S, Schechter MD, Kulics AT: **The formation of cocaethylene and clinical presentation of ED patients testing positive for the use of cocaine and ethanol**. *Am J Emerg Med* 1996, **14**(7):665-670.

14. Kolodgie FD, Farb A, Virmani R: **Pathobiological determinants of cocaine-associated cardiovascular syndromes**. *Hum Pathol* 1995, **26**(6):583-586.

15. McCance-Katz EF, Price LH, McDougle CJ, Kosten TR, Black JE, Jatlow PI: **Concurrent cocaine-ethanol ingestion in humans: pharmacology, physiology, behavior, and the role of cocaethylene**. *Psychopharmacology (Berl)* 1993, **111**(1):39-46.

16. McCance EF, Price LH, Kosten TR, Jatlow PI: **Cocaethylene: pharmacology, physiology and behavioral effects in humans**. *J Pharmacol Exp Ther* 1995, **274**(1):215-223.

17. Kolodgie FD, Wilson PS, Mergner WJ, Virmani R: **Cocaine-induced increase in the permeability function of human vascular endothelial cell monolayers**. *Exp Mol Pathol* 1999, **66**(2):109-122.

18. Landry MJ: **An overview of cocaethylene, an alcohol-derived, psychoactive, cocaine metabolite**. *J Psychoactive Drugs* 1992, **24**(3):273-276.

19. Jatlow P: **Cocaethylene: pharmacologic activity and clinical significance**. *Ther Drug Monit* 1993, **15**(6):533-536.

20. Hearn WL, Flynn DD, Hime GW, Rose S, Cofino JC, Mantero-Atienza E, Wetli CV, Mash DC: **Cocaethylene: a unique cocaine metabolite displays high affinity for the dopamine transporter**. *J Neurochem* 1991, **56**(2):698-701.

21. Jatlow P, Hearn WL, Elsworth JD, Roth RH, Bradberry CW, Taylor JR: **Cocaethylene inhibits uptake of dopamine and can reach high plasma concentrations following combined cocaine and ethanol use**. *NIDA Res Monogr* 1991, **105**:572-573.

22. Jatlow P, McCance EF, Bradberry CW, Elsworth JD, Taylor JR, Roth RH: **Alcohol plus cocaine: the whole is more than the sum of its parts**. *Ther Drug Monit* 1996, **18**(4):460-464.

23. McCance-Katz EF, Kosten TR, Jatlow P: **Concurrent use of cocaine and alcohol is more potent and potentially more toxic than use of either alone--a multiple-dose study**. *Biol Psychiatry* 1998, **44**(4):250-259.

24. Woodward JJ, Mansbach R, Carroll FI, Balster RL: **Cocaethylene inhibits dopamine uptake and produces cocaine-like actions in drug discrimination studies**. *Eur J Pharmacol* 1991, **197**(2-3):235-236.

25. Brzezinski MR, Abraham TL, Stone CL, Dean RA, Bosron WF: **Purification and characterization of a human liver cocaine carboxylesterase that catalyzes the production of benzoylecgonine and the formation of cocaethylene from alcohol and cocaine**. *Biochem Pharmacol* 1994, **48**(9):1747-1755.

26. Brzezinski MR, Spink BJ, Dean RA, Berkman CE, Cashman JR, Bosron WF: **Human liver carboxylesterase hCE-1: binding specificity for cocaine, heroin, and their metabolites and analogs**. *Drug Metab Dispos* 1997, **25**(9):1089-1096.

27. Hart CL, Jatlow P, Sevarino KA, McCance-Katz EF: **Comparison of intravenous cocaethylene and cocaine in humans**. *Psychopharmacology (Berl)* 2000, **149**(2):153-162.

28. Baumann MH, Horowitz JM, Kristal MB, Torres G: **Effects of cocaethylene on dopamine and serotonin synthesis in Long-Evans and Sprague-Dawley brains**. *Brain Res* 1998, **804**(2):316-319.

29. Xu YQ, Crumb WJ, Jr., Clarkson CW: **Cocaethylene, a metabolite of cocaine and ethanol, is a potent blocker of cardiac sodium channels**. *J Pharmacol Exp Ther* 1994, **271**(1):319-325.

30. Henning RJ, Wilson LD: **Cocaethylene is as cardiotoxic as cocaine but is less toxic than cocaine plus ethanol**. *Life Sci* 1996, **59**(8):615-627.

31. Gilloteaux J, Dalbec JP: **Transplacental cardiotoxicity of cocaine: atrial damage following treatment in early pregnancy**. *Scanning Microsc* 1991, **5**(2):519-529; discussion 529-531.

32. Tella SR, Goldberg SR: **Monoamine transporter and sodium channel mechanisms in the rapid pressor response to cocaine**. *Pharmacol Biochem Behav* 1998, **59**(2):305-312.

33. Parker RB, Williams CL, Laizure SC, Mandrell TD, LaBranche GS, Lima JJ: **Effects of ethanol and cocaethylene on cocaine pharmacokinetics in conscious dogs**. *Drug Metab Dispos* 1996, **24**(8):850-853.

34. Schindler CW, Zheng JW, Goldberg SR: **Effects of cocaine and cocaine metabolites on cardiovascular function in squirrel monkeys**. *Eur J Pharmacol* 2001, **431**(1):53-59.

35. Pradhan L, Dabisch PA, Liles JT, Agrawal KC, Kadowitz PJ: **Effect of acute intravenous cocaine administration on endothelium-dependent vasodepressor responses to acetylcholine**. *J Cardiovasc Pharmacol Ther* 2003, **8**(1):43-51.

36. Erzouki HK, Baum I, Goldberg SR, Schindler CW: **Comparison of the effects of cocaine and its metabolites on cardiovascular function in anesthetized rats**. *J Cardiovasc Pharmacol* 1993, **22**(4):557-563.

37. Wilson LD, Jeromin J, Garvey L, Dorbandt A: **Cocaine, ethanol, and cocaethylene cardiotoxity in an animal model of cocaine and ethanol abuse**. *Acad Emerg Med* 2001, **8**(3):211-222.

38. Togna GI, Graziani M, Russo P, Caprino L: **Cocaine toxic effect on endothelium-dependent vasorelaxation: an in vitro study on rabbit aorta**. *Toxicol Lett* 2001, **123**(1):43-50.

39. Kuhn FE, Gillis RA, Virmani R, Visner MS, Schaer GL: **Cocaine produces coronary artery vasoconstriction independent of an intact endothelium**. *Chest* 1992, **102**(2):581-585.

40. Wang SY, Nunez BD, Morgan JP, Dai HB, Ross JN, Sellke FW: **Cocaine and the porcine coronary microcirculation: effects of chronic cocaine exposure and hypercholesterolemia**. *J Cardiothorac Vasc Anesth* 1995, **9**(3):290-296.

41. Wilson LD, French S: **Cocaethylene's effects on coronary artery blood flow and cardiac function in a canine model**. *J Toxicol Clin Toxicol* 2002, **40**(5):535-546.

42. Jain AK, Carpentier RG: **Cardiac electrophysiological actions and interactions of ethanol, cocaine, and the metabolite ethylcocaine**. *J Electrocardiol* 1998, **31**(4):293-302.

43. Bailey DN: **Serial plasma concentrations of cocaethylene, cocaine, and ethanol in trauma victims**. *J Anal Toxicol* 1993, **17**(2):79-83.

44. Bailey DN: **Cocaethylene (ethylcocaine) detection during toxicological screening of a university medical center patient population**. *J Anal Toxicol* 1995, **19**(4):247-250.

45. Bailey DN: **Comprehensive review of cocaethylene and cocaine concentrations in patients**. *Am J Clin Pathol* 1996, **106**(6):701-704.

46. Brookoff D, Rotondo MF, Shaw LM, Campbell EA, Fields L: **Coacaethylene levels in patients who test positive for cocaine**. *Ann Emerg Med* 1996, **27**(3):316-320.

47. Wu AH, Onigbinde TA, Johnson KG, Wimbish GH: **Alcohol-specific cocaine metabolites in serum and urine of hospitalized patients**. *J Anal Toxicol* 1992, **16**(2):132-136.

48. Meehan SM, Schechter MD: **Cocaethylene-induced lethality in mice is potentiated by alcohol**. *Alcohol* 1995, **12**(4):383-385.

49. Aguila-Mansilla N, Little BB, Ho RH, Barnea A: **Differential potencies of cocaine and its metabolites, cocaethylene and benzoylecgonine, in suppressing the functional expression of somatostatin and neuropeptide Y producing neurons in cultures of fetal cortical cells**. *Biochem Pharmacol* 1997, **54**(4):491-500.

50. Morishima HO, Whittington RA, Iso A, Cooper TB: **The comparative toxicity of cocaine and its metabolites in conscious rats**. *Anesthesiology* 1999, **90**(6):1684-1690.

51. Schechter MD, Meehan SM: **The lethal effects of ethanol and cocaine and their combination in mice: implications for cocaethylene formation**. *Pharmacol Biochem Behav* 1995, **52**(1):245-248.

52. Sobel BF, Hutchinson AC, Diamond HF, Etkind SA, Ziervogel SD, Ferrari CM, Riley AL: **Assessment of cocaethylene lethality in Long-Evans female and male rats**. *Neurotoxicol Teratol* 1998, **20**(4):459-463.

53. Perez-Reyes M, Jeffcoat AR, Myers M, Sihler K, Cook CE: **Comparison in humans of the potency and pharmacokinetics of intravenously injected cocaethylene and cocaine**. *Psychopharmacology (Berl)* 1994, **116**(4):428-432.

54. Redinbo MR, Bencharit S, Potter PM: **Human carboxylesterase 1: from drug metabolism to drug discovery**. *Biochem Soc Trans* 2003, **31**(Pt 3):620-624.

55. Cami J, Farre M, Gonzalez ML, Segura J, de la Torre R: **Cocaine metabolism in humans after use of alcohol. Clinical and research implications**. *Recent Dev Alcohol* 1998, **14**:437-455.

56. Klaassen CD: **Casarett & Doull's Toxicology: The basic science of poisons**, 6th edition edn. New York: McGraw; 2001.

57. Gillams AR, Allen E, Hrieb K, Venna N, Craven D, Carter AP: **Cerebral infarction in patients with AIDS**. *AJNR Am J Neuroradiol* 1997, **18**(8):1581-1585.

58. Golbe LI, Merkin MD: **Cerebral infarction in a user of free-base cocaine ("crack")**. *Neurology* 1986, **36**(12):1602-1604.

59. Green RM, Kelly KM, Gabrielsen T, Levine SR, Vanderzant C: **Multiple intracerebral hemorrhages after smoking "crack" cocaine**. *Stroke* 1990, **21**(6):957-962.

60. Kase CS: **Intracerebral haemorrhage**. *Baillieres Clin Neurol* 1995, **4**(2):247-278.

61. Keller TM, Chappell ET: **Spontaneous acute subdural hematoma precipitated by cocaine abuse: case report**. *Surg Neurol* 1997, **47**(1):12-14; discussion 14-15.

62. Kibayashi K, Mastri AR, Hirsch CS: **Cocaine induced intracerebral hemorrhage: analysis of predisposing factors and mechanisms causing hemorrhagic strokes**. *Hum Pathol* 1995, **26**(6):659-663.

63. Kloner RA, Rezkalla SH: **Cocaine and the heart**. *N Engl J Med* 2003, **348**(6):487-488.

64. Klonoff DC, Andrews BT, Obana WG: **Stroke associated with cocaine use**. *Arch Neurol* 1989, **46**(9):989-993.

65. Kokkinos J, Levine SR: **Stroke**. *Neurol Clin* 1993, **11**(3):577-590.

66. Levine SR, Brust JC, Futrell N, Ho KL, Blake D, Millikan CH, Brass LM, Fayad P, Schultz LR, Selwa JF *et al*: **Cerebrovascular complications of the use of the "crack" form of alkaloidal cocaine**. *N Engl J Med* 1990, **323**(11):699-704.

67. Martinez N, Diez-Tejedor E, Frank A: **Vasospasm/thrombus in cerebral ischemia related to cocaine abuse**. *Stroke* 1996, **27**(1):147-148.

68. Neiman J, Haapaniemi HM, Hillbom M: **Neurological complications of drug abuse: pathophysiological mechanisms**. *Eur J Neurol* 2000, **7**(6):595-606.

69. Nolte KB, Brass LM, Fletterick CF: **Intracranial hemorrhage associated with cocaine abuse: a prospective autopsy study**. *Neurology* 1996, **46**(5):1291-1296.

70. Perrone J, Hollander JE, De Roos F: **Cardiovascular risk factors and atherosclerosis in children and young adults**. *N Engl J Med* 1998, **339**(15):1083-1084.

71. Peterson PL, Roszler M, Jacobs I, Wilner HI: **Neurovascular complications of cocaine abuse**. *J Neuropsychiatry Clin Neurosci* 1991, **3**(2):143-149.

72. Tolat RD, MW OD, Golamco-Estrella SP, Avella H: **Cocaine-associated stroke: three cases and rehabilitation considerations**. *Brain Inj* 2000, **14**(4):383-391.

73. Tun A, Khan IA: **Myocardial infarction with normal coronary arteries: the pathologic and clinical perspectives**. *Angiology* 2001, **52**(5):299-304.

74. Turnicky RP, Goodin J, Smialek JE, Herskowitz A, Beschorner WE: **Incidental myocarditis with intravenous drug abuse: the pathology, immunopathology, and potential implications for human immunodeficiency virus-associated myocarditis**. *Hum Pathol* 1992, **23**(2):138-143.

75. Waller BF, Fry ET, Hermiller JB, Peters T, Slack JD: **Nonatherosclerotic causes of coronary artery narrowing--Part III**. *Clin Cardiol* 1996, **19**(8):656-661.

76. Steinhauer JR, Caulfield JB: **Spontaneous coronary artery dissection associated with cocaine use: a case report and brief review**. *Cardiovasc Pathol* 2001, **10**(3):141-145.

77. Chen JC, Hsiang YN, Morris DC, Benny WB: **Cocaine-induced multiple vascular occlusions: a case report**. *J Vasc Surg* 1996, **23**(4):719-723.

78. Ford PV, Parker HG: **Unsuspected deep venous thrombophlebitis detected by gallium-67 imaging**. *Clin Nucl Med* 1987, **12**(7):556-557.

79. Fortier S, Demaria RG, Pelletier GB, Carrier M, Perrault LP: **Left ventricular thrombectomy in a cocaine user with normal coronary arteries**. *J Thorac Cardiovasc Surg* 2003, **125**(1):204-205.

80. Keung YK, Morgan D, Cobos E: **Cocaine-induced microangiopathic hemolytic anemia and thrombocytopenia simulating thrombotic thrombocytopenia purpura**. *Ann Hematol* 1996, **72**(3):155-156.

81. Lisse JR, Davis CP, Thurmond-Anderle ME: **Upper extremity deep venous thrombosis: increased prevalence due to cocaine abuse**. *Am J Med* 1989, **87**(4):457-458.

82. Lisse JR, Thurmond-Anderle M, Davis CP: **Deep venous thrombosis in intravenous cocaine abuse mimicking septic arthritis of the shoulder**. *South Med J* 1991, **84**(2):278-279.

83. Stuck RM, Doyle D: **Superficial thrombophlebitis following parenteral cocaine abuse. A case report**. *J Am Podiatr Med Assoc* 1987, **77**(7):351-353.

84. Nolte KB: **Rhabdomyolysis associated with cocaine abuse**. *Hum Pathol* 1991, **22**(11):1141-1145.

85. Enriquez R, Palacios FO, Gonzalez CM, Amoros FA, Cabezuelo JB, Hernandez F: **Skin vasculitis, hypokalemia and acute renal failure in rhabdomyolysis associated with cocaine**. *Nephron* 1991, **59**(2):336-337.

86. Garcia-Rostan y Perez GM, Garcia Bragado F, Puras Gil AM: **Pulmonary hemorrhage and antiglomerular basement membrane antibody-mediated glomerulonephritis after exposure to smoked cocaine (crack): a case report and review of the literature**. *Pathol Int* 1997, **47**(10):692-697.

87. Peces R, Navascues RA, Baltar J, Seco M, Alvarez J: **Antiglomerular basement membrane antibody-mediated glomerulonephritis after intranasal cocaine use**. *Nephron* 1999, **81**(4):434-438.

88. Orser B: **Thrombocytopenia and cocaine abuse**. *Anesthesiology* 1991, **74**(1):195-196.

89. Tumlin JA, Sands JM, Someren A: **Hemolytic-uremic syndrome following "crack" cocaine inhalation**. *Am J Med Sci* 1990, **299**(6):366-371.

90. Volcy J, Nzerue CM, Oderinde A, Hewan-Iowe K: **Cocaine-induced acute renal failure, hemolysis, and thrombocytopenia mimicking thrombotic thrombocytopenic purpura**. *Am J Kidney Dis* 2000, **35**(1):E3.

91. Daggett RB, Haghighi P, Terkeltaub RA: **Nasal cocaine abuse causing an aggressive midline intranasal and pharyngeal destructive process mimicking midline reticulosis and limited Wegener's granulomatosis**. *J Rheumatol* 1990, **17**(6):838-840.

92. Deutsch HL, Millard DR, Jr.: **A new cocaine abuse complex. Involvement of nose, septum, palate, and pharynx**. *Arch Otolaryngol Head Neck Surg* 1989, **115**(2):235-237.

93. Hofbauer GF, Burg G, Nestle FO: **Cocaine-related Stevens-Johnson syndrome**. *Dermatology* 2000, **201**(3):258-260.

94. Chevalier X, Rostoker G, Larget-Piet B, Gherardi R: **Schoenlein-Henoch purpura with necrotizing vasculitis after cocaine snorting**. *Clin Nephrol* 1995, **43**(5):348-349.

95. Mockel M, Kampf D, Lobeck H, Frei U: **Severe panarteritis associated with drug abuse**. *Intensive Care Med* 1999, **25**(1):113-117.

96. Seyer BA, Grist W, Muller S: **Aggressive destructive midfacial lesion from cocaine abuse**. *Oral Surg Oral Med Oral Pathol Oral Radiol Endod* 2002, **94**(4):465-470.

97. Sittel C, Eckel HE: **Nasal cocaine abuse presenting as a central facial destructive granuloma**. *Eur Arch Otorhinolaryngol* 1998, **255**(9):446-447.

98. Alexandrakis G, Tse DT, Rosa RH, Jr., Johnson TE: **Nasolacrimal duct obstruction and orbital cellulitis associated with chronic intranasal cocaine abuse**. *Arch Ophthalmol* 1999, **117**(12):1617-1622.

99. Armstrong M, Jr., Shikani AH: **Nasal septal necrosis mimicking Wegener's granulomatosis in a cocaine abuser**. *Ear Nose Throat J* 1996, **75**(9):623-626.

100. Dirkx CA, Gerscovich EO: **Sonographic findings in methamphetamine-induced ischemic colitis**. *J Clin Ultrasound* 1998, **26**(9):479-482.

101. Fredericks RK, Lefkowitz DS, Challa VR, Troost BT: **Cerebral vasculitis associated with cocaine abuse**. *Stroke* 1991, **22**(11):1437-1439.

102. Gertner E, Hamlar D: **Necrotizing granulomatous vasculitis associated with cocaine use**. *J Rheumatol* 2002, **29**(8):1795-1797.

103. Gradon JD, Wityk R: **Diagnosis of probable cocaine-induced cerebral vasculitis by magnetic resonance angiography**. *South Med J* 1995, **88**(12):1264-1266.

104. Herrine SK, Park PK, Wechsler RJ: **Acute mesenteric ischemia following intranasal cocaine use**. *Dig Dis Sci* 1998, **43**(3):586-589.

105. Sercarz JA, Strasnick B, Newman A, Dodd LG: **Midline nasal destruction in cocaine abusers**. *Otolaryngol Head Neck Surg* 1991, **105**(5):694-701.

106. Orriols R, Munoz X, Ferrer J, Huget P, Morell F: **Cocaine-induced Churg-Strauss vasculitis**. *Eur Respir J* 1996, **9**(1):175-177.

107. Marder VJ, Mellinghoff IK: **Cocaine and Buerger disease: is there a pathogenetic association?** *Arch Intern Med* 2000, **160**(13):2057-2060.

108. Bonkovsky HL, Mehta S: **Hepatitis C: a review and update**. *J Am Acad Dermatol* 2001, **44**(2):159-182.

109. Frazier SK: **Diagnosing and treating primary pulmonary hypertension**. *Nurse Pract* 1999, **24**(9):18, 21-12, 25-16 passim; quiz 42-13.

110. Keung YK, Morgan D, Cobos E: **Cocaine-contaminated allogeneic bone marrow transplantation**. *Acta Haematol* 2001, **106**(3):136-137.

111. Fritsma GA, Leikin JB, Maturen AJ, Froelich CJ, Hryhorczuk DO: **Detection of anticardiolipin antibody in patients with cocaine abuse**. *J Emerg Med* 1991, **9 Suppl 1**:37-43.

112. Asherson RA, Cervera R: **Vascular Manifestations of Systemic Autoimmune Diseases**. Boca Raton: CRC Press; 2001.

113. Burtis CA, Ashwood ER, Tietz NW: **Tietz textbook of clinical chemistry**, 3rd edn. Philadelphia: W.B. Saunders; 1998.

114. Tapia JF, Schumacher JM: **Case records of the Massachusetts General Hospital. Weekly clinicopathological exercises. Case 27-1993. A 32-year-old man with the sudden onset of a right-sided headache and left hemiplegia and hemianesthesia**. *N Engl J Med* 1993, **329**(2):117-124.

115. Schnittler H-J: **Structural and functional aspects of intercellular junctions in vascular endothelium**. *Basic Research in Cardiology* 1998, **93**(Sup 3):30-39.

116. Cotran RS, Kumar V, Collins T, Robbins SL: **Robbins' pathologic basis of disease**, 6th edn. Philadelphia: Saunders; 1999.

117. Tiruppathi C, Minshall RD, Paria BC, Vogel SM, Malik AB: **Role of Ca2+ signaling in the regulation of endothelial permeability**. *Vascul Pharmacol* 2003, **39**(4-5):173-185.

118. Suzuki Y, Ruiz-Ortega M, Lorenzo O, Ruperez M, Esteban V, Egido J: **Inflammation and angiotensin II**. *Int J Biochem Cell Biol* 2003, **35**(6):881-900.

119. Sandoval R, Malik AB, Minshall RD, Kouklis P, Ellis CA, Tiruppathi C: **Ca(2+) signalling and PKCalpha activate increased endothelial permeability by disassembly of VE-cadherin junctions**. *J Physiol* 2001, **533**(Pt 2):433-445.

120. Sandoval R, Malik AB, Naqvi T, Mehta D, Tiruppathi C: **Requirement for Ca2+ signaling in the mechanism of thrombin-induced increase in endothelial permeability**. *Am J Physiol Lung Cell Mol Physiol* 2001, **280**(2):L239-247.

121. Vuong PT, Malik AB, Nagpala PG, Lum H: **Protein kinase C beta modulates thrombin-induced Ca2+ signaling and endothelial permeability increase**. *J Cell Physiol* 1998, **175**(3):379-387.

122. Ueda N, Wise LM, Stacker SA, Fleming SB, Mercer AA: **Pseudocowpox virus encodes a homolog of vascular endothelial growth factor**. *Virology* 2003, **305**(2):298-309.

123. Messmer UK, Briner VA, Pfeilschifter J: **Tumor necrosis factor-alpha and lipopolysaccharide induce apoptotic cell death in bovine glomerular endothelial cells**. *Kidney Int* 1999, **55**(6):2322-2337.

124. Zhao Y, Davis HW: **Endotoxin causes phosphorylation of MARCKS in pulmonary vascular endothelial cells**. *J Cell Biochem* 2000, **79**(3):496-505.

125. Schaeffer RC, Jr., Bitrick MS, Jr.: **Death after Pichinde virus infection in large and small strain 13 guinea pigs**. *J Infect Dis* 1993, **167**(5):1059-1064.

126. Zhao Y, Davis HW: **Hydrogen peroxide-induced cytoskeletal rearrangement in cultured pulmonary endothelial cells**. *J Cell Physiol* 1998, **174**(3):370-379.

127. Torres G, Horowitz JM: **Individual and combined effects of ethanol and cocaine on intracellular signals and gene expression**. *Prog Neuropsychopharmacol Biol Psychiatry* 1996, **20**(4):561-596.

128. Nilius B, Droogmans G: **Ion channels and their functional role in vascular endothelium**. *Physiol Rev* 2001, **81**(4):1415-1459.

129. Bootman MD, Collins TJ, Peppiatt CM, Prothero LS, MacKenzie L, De Smet P, Travers M, Tovey SC, Seo JT, Berridge MJ *et al*: **Calcium signalling - an overview**. *Cell Devel Biol* 2001, **12**:3-10.

130. Yuan SY: **Protein kinase signaling in the modulation of microvascular permeability**. *Vascul Pharmacol* 2002, **39**(4-5):213-223.

131. Lum H, Podolski JL, Gurnack ME, Schulz IT, Huang F, Holian O: **Protein phosphatase 2B inhibitor potentiates endothelial PKC activity and barrier dysfunction**. *Am J Physiol Lung Cell Mol Physiol* 2001, **281**(3):L546-555.

132. Yuan SY: **Signal transduction pathways in enhanced microvascular permeability**. *Microcirculation* 2000, **7**(6 Pt 1):395-403.

133. Dejana E, Spagnuolo R, Bazzoni G: **Interendothelial junctions and their role in the control of angiogenesis, vascular permeability and leukocyte transmigration**. *Thromb Haemost* 2001, **86**(1):308-315.

134. Telo P, Breviario F, Huber P, Panzeri C, Dejana E: **Identification of a novel cadherin (vascular endothelial cadherin-2) located at intercellular junctions in endothelial cells**. *J Biol Chem* 1998, **273**(28):17565-17572.

135. Pearlstein DP, Ali MH, Mungai PT, Hynes KL, Gewertz BL, Schumacker PT: **Role of mitochondrial oxidant generation in endothelial cell responses to hypoxia**. *Arterioscler Thromb Vasc Biol* 2002, **22**(4):566-573.

136. Lum H, Roebuck KA: **Oxidant stress and endothelial cell dysfunction**. *Am J Physiol Cell Physiol* 2001, **280**(4):C719-741.

137. Caamano J, Hunter CA: **NF-κB family of transcription factors: central regulators of innate and adaptive immune functions**. *Clin Microbiol Rev* 2002, **15**(3):414-429.

138. Roux PP, Blenis J: **ERK and p38 MAPK-activated protein kinases: A family of protein kinases with diverse biological functions.** *Microbiol Molec Biol Rev* 2004, **68**(2):320-344.

139. Wagner M, Klein CL, Kleinert H, Euchenhofer C, Forstermann U, Kirkpatrick CJ: **Heavy metal ion induction of adhesion molecules and cytokines in human endothelial cells: the role of NF-κB, IκB-α, and AP-1**. *Pathobiol* 1997, **65**(5):241-252.

140. de Martin R, Hoeth M, Hofer-Warbinek R, Schmid JA: **The transcription factor NF-kB and the regulation of vascular cell function**. *Arterioscler Thromb Vasc Biol* 2000, **20**:e83-e88.

141. Zhang A, Cheng TP-O, Altura BT, Altura BM: **Acute cocaine results in rapid rises in intracellular free calcium concentration in canine cerebral vascular smooth muscle cells: Possible relation to etiology of stroke**. *Neurosci Letters* 1996, **215**:57-59.

142. Oztezcan S, Dogru-Abbasoglu S, Mutlu-Turkoglu U, Calay Z, Aykac-Toker G, Uysal M: **The role of stimulated lipid peroxidation and impaired calcium sequestration in the enhancement of cocaine induced hepatotoxicity by ethanol**. *Drug Alcohol Dependence* 2000, **58**(1-2):77-83.

143. Marie-Claire C, Laurendeau I, Canestrelli C, Courtin C, Vidaud M, Roques B, Noble F: ***Fos* but not *Cart* (cocaine and amphetamine regulated transcript) is**

overexpressed by several drugs of abuse: A comparative study using real-time quantitative polymerase chain reaction in rat brain. *Neurosci Letters* 2003, **345**:77-80.

144. Tiruppathi C, Freichel M, Vogel SM, Paria BC, Mehta D, Flockerzi V, Malik AB: **Impairment of store-operated Ca2+ entry in TRPC4(-/-) mice interferes with increase in lung microvascular permeability**. *Circ Res* 2002, **91**(1):70-76.

145. Nguyen LT, Lum H, Tiruppathi C, Malik AB: **Site-specific thrombin receptor antibodies inhibit Ca2+ signaling and increased endothelial permeability**. *Am J Physiol* 1997, **273**(5 Pt 1):C1756-1763.

146. Nilius B, Viana F, Droogmans G: **Ion channels in vascular endothelium**. *Annu Rev Physiol* 1997, **59**:145-170.

147. Kunze H, Nahas N, Traynor JR, Wurl M: **Effects of local anaesthetics on phospholipases**. *Biochim Biophys Acta* 1976, **441**:93-102.

148. Krendel DA, Ditter SM, Frankel MR, Ross WK: **Biopsy-proven cerebral vasculitis associated with cocaine abuse**. *Neurology* 1990, **40**(7):1092-1094.

149. Martin K, Rogers T, Kavanaugh A: **Central nervous system angiopathy associated with cocaine abuse**. *J Rheumatol* 1995, **22**(4):780-782.

150. Merkel PA, Koroshetz WJ, Irizarry MC, Cudkowicz ME: **Cocaine-associated cerebral vasculitis**. *Semin Arthritis Rheum* 1995, **25**(3):172-183.

151. Scott DW, Morrell JI, Vernotica EM: **Focal necrotizing panniculitis and vascular necrosis in rats given subcutaneous injections of cocaine hydrochloride**. *J Cutan Pathol* 1997, **24**(1):25-29.

152. Barroso-Moguel R, Villeda-Hernandez J, Mendez-Armenta M, Rios C: **Brain capillary lesions produced by cocaine in rats**. *Toxicol Lett* 1997, **92**:9-14.

153. Chang SL, Bersig J, Felix B, Fiala M, House SD: **Chronic cocaine alters hemodynamics and leukocyte-endothelial interactions in rat mesenteric venules**. *Life Sci* 2000, **66**(24):2357-2369.

154. Baluk P, Hirata A, Thurston G, Fujiwara T, Neal CR, Michel CC, McDonald DM: **Endothelial gaps: time course of formation and closure in inflamed venules of rats**. *Am J Physiol* 1997, **272**(1 Pt 1):L155-170.

155. McDonald DM, Thurston G, Baluk P: **Endothelial gaps as sites for plasma leakage in inflammation**. *Microcirculation* 1999, **6**(1):7-22.

156. Bouis D, Hospers GA, Meijer C, Molema G, Mulder NH: **Endothelium in vitro: a review of human vascular endothelial cell lines for blood vessel-related research**. *Angiogenesis* 2001, **4**(2):91-102.

157. Ades EW, Candal FJ, Swerlick RA, George VG, Summers S, Bosse DC, Lawley TJ: **HMEC-1: establishment of an immortalized human microvascular endothelial cell line**. *J Invest Dermatol* 1992, **99**(6):683-690.

158. Burdick JD, Boni RL, Fochtman FW: **Quantitation of cocaine and cocaethylene in small volumes of rat whole blood using gas chromatography-mass spectrometry**. *J Pharm Biomed Anal* 1997, **15**(8):1167-1173.

159. Alberts B, Bray D, Lewis J, Raff M, Roberts K, Watson JD: **Molecular Biology of the Cell**, 3rd edn. New York: Garland; 1994.

160. Jiang T, Grant RL, Acosta D: **A digitized fluorescence imaging study of intracellular free calcium, mitochondrial integrity and cytotoxicity in rat renal cells exposed to ionomycin, a calcium ionophore**. *Toxicology* 1993, **85**(1):41-65.

161. Denizot F, Lang R: **Rapid colorimetric assay for cell growth and survival. Modifications to the tetrazolium dye procedure giving improved sensitivity and reliability**. *J Immunol Methods* 1986, **89**(2):271-277.

162. Mosmann T: **Rapid colorimetric assay for cellular growth and survival: application to proliferation and cytotoxicity assays**. *J Immunol Methods* 1983, **65**(1-2):55-63.

163. Welder AA: **A primary culture system of adult rat heart cells for the evaluation of cocaine toxicity**. *Toxicology* 1992, **72**(2):175-187.

164. Grant RL, Acosta D: **Comparative toxicity of tetracaine, proparacaine and cocaine evaluated with primary cultures of rabbit corneal epithelial cells**. *Exp Eye Res* 1994, **58**(4):469-478.

165. Thurston G, Baluk P, Hirata A, McDonald DM: **Permeability-related changes revealed at endothelial cell borders in inflamed venules by lectin binding**. *Am J Physiol* 1996, **271**(6 Pt 2):H2547-2562.

166. Faury G, Garnier S, Weiss AS, Wallach J, Fulop T, Jr., Jacob MP, Mecham RP, Robert L, Verdetti J: **Action of tropoelastin and synthetic elastin sequences on vascular tone and on free Ca2+ level in human vascular endothelial cells**. *Circ Res* 1998, **82**(3):328-336.

167. Okorodudu AO, Yang H, Tarek Elghetany M: **Ionized magnesium in the homeostasis of cells: intracellular threshold for Mg(2+) in human platelets**. *Clin Chim Acta* 2001, **303**(1-2):147-154.

168. Chen JX, Berry LC, Christman BW, Meyrick B: **Glutathione mediates LPS-stimulated COX-2 expression via early transient p42/44 MAPK activation**. *J Cell Physiol* 2003, **197**(1):86-93.

169. Dyer RB, Herzog NK: **Isolation of intact nuclei for nuclear extract preparation from a fragile B-lymphocyte cell line**. *Biotechniques* 1995, **19**(2):192-195.

170. Dyer RB, Herzog NK: **Immunodepletion EMSA: a novel method to identify proteins in a protein-DNA complex**. *Nucleic Acids Res* 1995, **23**(16):3345-3346.

171. Lindsey KQ, Caughman SW, Olerud JE, Bunnett NW, Armstrong CA, Ansel JC: **Neural regulation of endothelial cell-mediated inflammation**. *J Invest Dermatol Symp Proc* 2000, **5**(1):74-78.

172. Bierhaus A, Nawroth PP: **Modulation of the vascular endothelium during infection - the role of NF-κB activation**. *Contrib Microbiol* 2003, **10**:86-105.

173. Collins T, Read MA, Neish AS, Whitley MZ, Thanos D, Maniatis T: **Transcriptional regulation of endothelial cell adhesion molecules: NF-κB and cytokine-inducible enhancers**. *FASEB J* 1995, **9**(10):899-909.

174. Mackman N: **Regulation of tissue factor gene expression in human monocytic and endothelial cells**. *Haemostasis* 1996, **26**(Sup 1):17-19.

175. Rodel F, Hantschel M, Hildebrand G, Schultze-Mosgauss S, Rodel C, Herrmann M, Sauer R, Voll RE: **Dose-dependent biphasic induction and transcriptional activity of nuclear factor kappa B (NF-κB) in EA.hy.926 endothelial cells after low-dose irradiation**. *Int J Radiat Biol* 2004, **80**(2):115-123.

176. De Nigris F, Lerman LO, Condorelli M, Lerman A, Napoli C: **Oxidation-sensitive transcription factors and molecular mechanisms in the arterial wall**. *Antiox Redox Signal* 2001, **3**(6):1119-1130.

177. Bassett SE, Fennewald SM, King DJ, Li X, Herzog NK, Shope R, Aronson JF, Luxon BA, Gorenstein DG: **Combinatorial selection and edited combinatorial selection of phosphorothioate aptamers targeting human nuclear factor-kappaB RelA/p50 and RelA/RelA.** *Biochemistry* 2004, **43**(28):9105-9115.

178. Lowry DR, NJ; Farr, AL; Kandall, KJ: **Protein measurement with the Folin-Phenol reagents.** *J Biol Chem* 1951, **193**:265-275.

179. Smith PK, RI; Hermanson, GT; Mallia, AK; Gartner, FH; Provenzano, MD; Fujimoto, EK; Goeke, NM; Olson, BJ; Klenk, DC: **Measurement of protein using bicinchoninic acid**. *Anal Biochem* 1985, **150**:76-85.

180. Boelsterli UA, Wolf A, Goldlin C: **Oxygen free radical production mediated by cocaine and its ehtanol-derived metabolite, cocaethylene, in rat hepatocytes**. *Hepatology* 1993, **18**:1154-1161.

181. Calle E, Berciano MT, Fernandez R, Lafarga M: **Activation of the autophagy, c-FOS and ubiquitin expression, and nucleolar alterations in Schwann cells precede demyelination in tellurium-induced neuropathy**. *Acta Neuropathol* 1999, **97**:143-155.

182. Yuan C, Acosta D: **Inhibitory effect of cocaine on calcium mobilization in cultured rat myocardial cells**. *J Mol Cell Cardiol* 1994, **26**(11):1415-1419.

183. Qiu Z, Morgan JP: **Differential effects of cocaine and cocaethylene on intracellular Ca2+ and myocardial contraction in cardiac myocytes**. *Br J Pharmacol* 1993, **109**(2):293-298.

184. Thurberg BL, Collins T: **The nuclear factor-kappaB/inhibitor of kapp B autoregulatory system and atherosclerosis**. *Curr Opin Lipidol* 1998, **9**(5):387-396.

185. Gan X, Zhang L, Berger O, Stins MF, Way D, Taub DD, Chang SL, Kim KS, House SD, Weinand M *et al*: **Cocaine enhances brain endothelial adhesion molecules and leukocyte migration**. *Clin Immunol* 1999, **91**(1):68-76.

186. Hoefen RJ, Berk BC: **The role of MAP kinase in endothelial activation**. *Vascul Pharmacol* 2002, **38**:271-273.

187. Gilmore TD: **The Rel/NF-kB signal transduction pathway: introduction**. *Oncogene* 1999, **18**:6842-6844.

188. Bureau F, Bonizzi G, Kirschvink N, Delhalle S, Desmecht D, Merville M-P, Bours V, Lekeux P: **Correlation between nuclear factor-κB activity in bronchial brushing samples and lung dysfunction in an animal model of asthma**. *Am J Resp Crit Care Med* 2000, **161**:1314-1321.

189. Bethke RA, Gratton M, Watson WA: **Severe hyperlactemia and metabolic acidosis following cocaine use and exertion**. *Am J Emerg Med* 1990, **8**(4):369-370.

190. Drake TR, Henry T, Marx J, Gabow PA: **Severe acid-base abnormalities associated with cocaine abuse**. *J Emerg Med* 1990, **8**(3):331-334.

191. Li G, Xiao Y, Zhang L: **Cocaine induces apoptosis in fetal rat myocardial cells through the p38 MAPK and mitochondrial/cytochrome c pathways**. *J Pharm Exp Ther* 2004, **Pre-publication, available online at http://libux.utmb.edu:2338/cgi/reprint/jpet.104.073494v1**.

192. Zavecz JH: **Chronic cocaine administration decreases norepinephrine-induced phosphoinositide hydrolyiss in rat aorta**. *Life Sci* 1992, **51**(21):1675-1681.

193. Henning RJ, Li Y: **Cocaine produces cardiac hypertrophy by protein kinase C dependent mechanisms**. *J Cardiovasc Pharmacol Ther* 2003, **8**(2):149-160.

194. Lee YW, Hennig B, Fiala M, Kim KS, Toborek M: **Cocaine activates redox-regulated transcription factors and induces TNF-α expression in human brain endothelial cells**. *Brain Res* 2001, **920**:125-133.

195. Ang E, Chen J, Zagouras P, Magna H, Holland J, Schaeffer E, Nestler EJ: **Induction of nuclear factor-κB in nucleus accumbens by chronic cocaine administration**. *J Neurochem* 2001, **79**:221-224.

196. Grant RL, Acosta D: **Interactions of intracellular pH and intracellular calcium in primary cultures of rabbit corneal epithelial cells**. *In Vitro Cell Dev Biol Anim* 1996, **32**(1):38-45.

VITA

Danyel Hermes Tacker was born to Sharlene Ann and Russell Clyde Hermes in San Antonio, Texas on August 23, 1975. She has one brother, Jessie Lloyd Hermes. A small scholarship in 1993 (Nancy Groff Memorial Scholarship) started Danyel's college education at Southwest Texas Junior College in 1993. While in attendance at Southwest Texas Junior College, Danyel worked as a general studies tutor, and as the chemistry laboratory assistant. In 1996, Danyel obtained her Associate's degree with high honors and transferred to Texas A&M University-Corpus Christi. There, she double majored in Cell Biology and Chemistry, tutored chemistry and English, and met her husband, Matthew Ernest Tacker. After graduating with honors in 1999, Danyel matriculated to the University of Texas Medical Branch. While at UTMB, Danyel received several awards for her work, including a pre-doctoral training grant from the NIH that was continuously funded for the three years of Danyel's dissertation project, and numerous travel awards that allowed her to present her research at national and international toxicology and chemistry meetings.

Danyel can be reached through her family at 217 River Bluff Road, Castroville, TX 78009.

Education

A.A., May 1996, Southwest Texas Junior College, Uvalde, TX

B.S., May 1999, Texas A&M University – Corpus Christi, Corpus Christi, TX

Publications

Journal Articles

Tacker, DH; Okorodudu, AO. **Evidence for Injurious Effect of Cocaethylene in Human Microvascular Endothelial Cells.** *Clinica Chimica Acta* 2004, **345**(1-2): 69-77.

Tacker, DH; Olano, J; Okorodudu, AO. **Cocaethylene Induced Changes in Endothelial Cell Permeability, Calcium, and Inositol 1,4,5 Trisphosphate.** S*ubmitted.*

Published Abstracts

Tacker, DH; Okorodudu, AO. **Human Microvascular Endothelial Cells and Cocaethylene-Induced Vascular Toxicity: Biochemical and Morphological Determinations.** *Toxicological Sciences* 2003, **72**(S1): 157-158, Abstract #765.

Tacker, DH; Okorodudu, AO. **Toxicity in Human Microvascular Endothelial Cells Induced by Cocaethylene.** *The FASEB Journal* 2003, **17**, Abstract #171.5 [CD-ROM].

Tacker, DH; Okorodudu AO. **Microvascular Biochemical and Morphological Alterations After Exposure to Cocaethylene.** *Clinical Chemistry* 2003, **49**(S6): A77, Abstract #C-51.

Tacker, DH; Okorodudu, AO. **Cocaethylene-Induced Changes in Endothelial Permeability and Cation Flux.** *Toxicological Sciences* 2004, **78**(S1): Abstract #1311 [CD-ROM].

Graduate Honors

Robert L Harrison Award for Clinically Based Research, UTMB Department of Pathology, 2001

Pre-Doctoral Fellowship in Clinical Chemistry, UTMB Clinical Chemistry Division, 2001

Ruth L. Kirschstein National Research Service Award (Pre-Doctoral Fellowship), National Institute on Drug Abuse, 2002 (continuously funded from June 2002 to Present)

Student Travel Award, Society of Toxicology, 2003

Young Pathologist Fellowship, American Society for Investigative Pathology, 2003

Educational Research Award, Society of Forensic Toxicologists, 2004

Danyel Tacker typed this dissertation, and drew all of the illustrations herein.